A&A 674, A114 (2023)
https://doi.org/10.1051/0004-6361/202345874

Astronomy & Astrophysics

The CORALIE survey for southern extrasolar planets

XIX. Brown dwarfs and stellar companions unveiled by radial velocity and astrometry⋆,⋆⋆

D. Barbato[1,2], D. Ségransan[1], S. Udry[1], N. Unger[1], F. Bouchy[1], C. Lovis[1], M. Mayor[1], F. Pepe[1], D. Queloz[5,6], N. C. Santos[7,8], J. B. Delisle[1], P. Figueira[1], M. Marmier[1], E. C. Matthews[3,1], G. Lo Curto[4], J. Venturini[1], G. Chaverot[1], M. Cretignier[1], J. F. Otegi[1], and M. Stalport[1]

[1] Department of Astronomy, University of Geneva, Chemin Pegasi 51, 1290 Versoix, Switzerland
e-mail: domenico.barbato@unige.ch
[2] INAF – Osservatorio Astrofisico di Torino, Via Osservatorio 20, 10025 Pino Torinese, Italy
[3] Max-Planck-Institut für Astronomie, Königstuhl 17, 69117 Heidelberg, Germany
[4] European Southern Observatory, Casilla 19001, Santiago, Chile
[5] ETH Zurich, Department of Physics, Wolfgang-Pauli-Strasse 2, 8093 Zurich, Switzerland
[6] Astrophysics Group, Cavendish Laboratory, JJ Thomson Avenue, CB3 0HE Cambridge, UK
[7] Instituto de Astrofísica e Ciências do Espaço, Universidade do Porto, CAUP, Rua das Estrelas, 4150-762 Porto, Portugal
[8] Departamento de Física e Astronomia, Faculdade de Ciências, Universidade do Porto, Rua do Campo Alegre, 4169-007 Porto, Portugal

Received 9 January 2023 / Accepted 29 March 2023

ABSTRACT

Context. A historical search for exoplanets among a sample of 1647 nearby southern main sequence stars with the CORALIE spectrograph at La Silla Observatory has been underway since 1998, with a backup subprogram dedicated to the monitoring of binary stars.
Aims. We reviewed 25 years of CORALIE measurements and search for Doppler signals consistent with stellar or brown dwarf companions to produce an updated catalog of both known and previously unpublished binary stars in the planet-search sample. We assessed the binarity fraction of the stellar population and survey the prospects for more precise searches for planets in the binary sample.
Methods. We performed a new analysis on the CORALIE planet-search sample's radial velocity measurements, searching for stellar companions and obtaining orbital solutions for both known and new binary systems. We performed simultaneous radial velocity and proper motion anomaly fits on the subset of these systems for which HIPPARCOS and *Gaia* astrometry measurements are available, obtaining accurate estimates of true mass for the companions.
Results. We found 218 stars in the CORALIE sample to have at least one stellar companion, 130 of which are not yet published in the literature and for which we present orbital solutions. The use of the proper motion anomaly allowed us to derive true masses for the stellar companions in 132 systems, which we additionally used to estimate stability regions for possible planetary companions on circumprimary or circumbinary orbits. Finally, we produced detection-limit maps for each star in the sample and obtained occurrence rates of $0.43^{+0.23}_{-0.11}$% and $12.69^{+0.87}_{-0.77}$% for brown dwarf and stellar companions, respectively, in the CORALIE sample.

Key words. astrometry – proper motions – stars: fundamental parameters – binaries: general – techniques: radial velocities – planets and satellites: dynamical evolution and stability

1. Introduction

Since June 1998, the historical CORALIE exoplanet-search survey has been continuously monitoring a southern hemisphere volume-limited sample composed of 1647 main sequence stars located within 50 pc from the Sun, having spectral types ranging from F8 to K0 (Queloz et al. 2000; Udry et al. 2000). At the time of writing, the survey has collected more than 60 000 radial velocity measurements using the CORALIE Echelle spectrograph mounted on the Euler Telescope at La Silla Observatory, with an average measurement precision of ∼5 ms^{-1} and an average timespan of ∼7600 d.

This uniquely long and continuous survey is especially suited to the detection of giant planets with semimajor axes as large as 10 au (Tamuz et al. 2008; Ségransan et al. 2010; Marmier et al. 2013; Rickman et al. 2019) as well as brown dwarfs (Udry et al. 2002; Santos et al. 2002; Rickman et al. 2019). It also contributes data to statistical studies of the frequency of planetary companions and its dependence on stellar properties (see e.g. Santos et al. 2001; Udry & Santos 2007; Mayor et al. 2011), making the almost 25-yr long CORALIE survey an invaluable asset to the field of exoplanetology. Finally, it is worth remarking

⋆ The radial velocity measurements and additional data products discussed in this paper are available on the DACE web platform at https://dace.unige.ch/radialVelocities. A copy of the data and full Tables 1, 2, and 3 are available at the CDS via anonymous ftp to cdsarc.cds.unistra.fr (130.79.128.5) or via https://cdsarc.cds.unistra.fr/viz-bin/cat/J/A+A/674/A114

⋆⋆ Based on observations collected with the CORALIE spectrograph mounted on the 1.2 m Swiss telescope at La Silla Observatory.

that the continuous monitoring of the less-active stars in the volume-limited sample also makes the CORALIE survey a fertile ground in the search for low-mass exoplanetary candidates suitable for follow-up studies with higher precision instruments such as HARPS (Pepe et al. 2000; Mayor et al. 2003) and ESPRESSO (Pepe et al. 2014). This effectively expands its role in the search for exoplanetary bodies toward the realm of terrestrial companions.

During the sample selection process (see Udry et al. 2000), known large-amplitude binary stars were collected in a low-priority subprogram within the planet-search survey, due to the disruptive influence that a close-in stellar companion would have on the stability of the inner region of a planetary system (Holman & Wiegert 1999; Musielak et al. 2005; Turrini et al. 2005; Marzari & Gallina 2016), as well as to limit both the blending effect produced by double-lined spectroscopic binaries (SB2) and the observational effort necessary to disentangle the planetary signal from the higher amplitude stellar contribution. On the other hand, longer period binary companions producing only linear trends in radial velocity have instead been considered adequate candidates for the planet-search survey, both due to the weak gravitational effect that the distant stellar companion would produce on the inner regions of planetary systems and the fact that such linear trends can easily be corrected for (such as Gl86 and HD 41004AB, see Queloz et al. 2000; Santos et al. 2002). This selection strategy also reflected the initial bias against low-separation binaries in favour of stellar environments similar to that of the Solar System (Eggenberger & Udry 2010; Quarles et al. 2020). Still, the large number of measurements collected during almost 25 yr of observations with CORALIE have unveiled the binary nature of a non-negligible portion of the stars selected over a wide range of orbital periods and an updated assessment of the binary population in the sample is a necessary step for advancing the analysis of the CORALIE exoplanet-search survey.

The long-term search for stellar companions within the CORALIE survey represents a key contribution to the current endeavours to further our understanding of stellar formation. Both observational and theoretical studies have now shown that most stars form with at least one stellar companions and, more specifically, that about half of FGK stars are part of a binary system (see e.g. Moe & Di Stefano 2017; Halbwachs et al. 2018; Offner et al. 2022) in which the main sequence companions appear to follow a lognormal separation distribution, peaking around 40 au and roughly uniform mass-ratio distributions (Duquennoy & Mayor 1991; Melo 2003; Raghavan et al. 2010; Tokovinin 2014). It has also been shown that tighter solar-type binaries seem to favor larger mass ratios (Lucy & Ricco 1979; Tokovinin 2000; Moe & Di Stefano 2017), suggesting a common formation and evolution history in a shared circumbinary disc; the fact that wider ($a > 200$ au) binaries also feature a small but significant fraction of high mass ratio systems (El-Badry et al. 2019) is also an indication that at least some wide stellar companions form at intermediate separations and undergo outward migration in later stages of their dynamical evolution. Many different theoretical models have been proposed to explain the formation and observed characteristics of binary systems, such as the fragmentation of filaments and cores in star-forming regions (Könyves et al. 2015; Pineda et al. 2015; Guszejnov & Hopkins 2015; Guszejnov et al. 2017) and of massive accretion discs around individual forming stars (Bonnell 1994; Gammie 2001; Kratter et al. 2010; Harsono et al. 2011), as well as the continuous study of the statistics of binary systems is essential in deepening our understanding of stellar formation.

Considering instead the brown dwarf companion population around solar-type stars, a robust study of its demographics is hindered by the low number of detections at present, as less than 100 brown dwarf companions are currently known to orbit such stars (see e.g. Ma & Ge 2014; Grieves et al. 2017), but recent works have suggested that only ∼4% of solar-type stars have a brown dwarf companion (Offner et al. 2022). However, a notable characteristic is the clear paucity of brown dwarf companions around solar-type primary stars on close-in orbits in what is commonly referred to as the brown dwarf desert and that could be explained by post-formation migration processes (see e.g. Grether & Lineweaver 2006; Sahlmann et al. 2011b; Shahaf & Mazeh 2019; Kiefer et al. 2019).

The importance in the characterisation of binary stellar systems within the scope of a radial velocity survey aimed at the detection of planetary companions is clear given the effect that the presence or absence of an additional stellar companion has on the formation and stability of planetary bodies, which stands as a fundamental theme in exoplanetary science. While works such as that of Roell et al. (2012) have found the binarity rate among planet-hosting stars to be about four times smaller than for single solar-type stars, the high sample heterogeneity and observational bias are still impediments to a full understanding of exoplanet demographics in the binary environment (see e.g. Thebault & Haghighipour 2015; Quarles et al. 2020, and references therein for reviews on the subject). More recently, Ngo et al. (2017) found no evidence that host binarity alters the distribution of planet properties in systems characterised by radial velocity observations, while Su et al. (2021) reported a positive correlation between planetary multiplicity and stellar orbital separations in circumprimary planetary systems.

In this paper, we present the results of a new analysis of the CORALIE measurements of the 1647 stars in the sample, specifically aimed at the search of radial velocity signals comparable with stellar or brown dwarf companions of the target stars. More precisely, in this study, we focus on a specific region of the binary companion parameter space, namely, a region limited both in orbital separation as a result of the 25 yr duration of the CORALIE survey and in mass regimes, as we focus on companions having minimum mass higher then 40 $M_{\rm Jup}$. Companions populating the rest of the parameter space will be the main focus of future papers in this series. We find a total of 218 stars in the sample to have at least one such companion, among which 130 are previously unpublished ones and 88 are instead already known and for which we present updated orbital solutions. Additionally, we present further refined orbital solution for a subset of 132 binary stars in the sample using astrometry constraints provided by proper motion measurements from HIPPARCOS (Perryman et al. 1997) and *Gaia* Early Data Release 3 (*Gaia* EDR3, Gaia Collaboration 2021).

Our paper is organised as follows. In Sect. 2, we describe the physical characteristics of the stars in host stars in our sample. In Sect. 3, we present an overview of the CORALIE observational campaign and of the search for radial velocity signals compatible with brown dwarf and stellar companions, while in Sect. 4, we obtain estimates of dynamical masses for a subset of the presented companions using HIPPARCOS and *Gaia* proper motion measurements. In Sects. 5 and 6, we discuss a few systems especially worthy of note and the prospects for follow-up search for exoplanets in the systems comprising our sample. In Sect. 7, we derive occurrence rate values for brown dwarfs and stellar companion in the CORALIE exoplanetary search sample. We present our discussion and conclusions in Sect. 8.

2. Host star characteristics

Out of the 1647 stars composing the CORALIE exoplanet-search sample, we first excluded known SB2, identified as such either based on archive query or by identifying double peaks in the cross-correlation function (CCF) of the radial velocity spectra. Based on these results, we further identified a subset of 218 stars for which we detect a robust radial velocity signal hinting at the presence of a massive companion having minimum mass $M \sin i \gtrsim 40\ M_{\rm Jup}$; the radial velocity analysis that led to this selection is fully detailed in Sect. 3. For clarity, we refer to this subsample of 218 stars hosting stellar companions that is the main focus of this work simply as the 'binary sample' throughout this paper, while the larger CORALIE exoplanet-search sample is referred to as 'the CORALIE sample'.

In order to have an updated and homogeneous characterisation of the physical properties of every star in the sample, we fit the stellar spectral energy distribution (SED) of each star, using the MESA Isochrones and Stellar Tracks (MIST) (Dotter 2016; Choi et al. 2016) via the `IDL` suite `EXOFASTv2` (Eastman et al. 2019). With this method, the stellar parameters are simultaneously constrained by the SED and the MIST isochrones, since the SED primarily constrains the stellar radius, $R_\star$, and effective temperature, $T_{\rm eff}$, while a penalty for straying from the MIST evolutionary tracks ensures that the resulting star is physical in nature (see Eastman et al. 2019, for more details on the method). For each star, we fitted all available archival magnitudes from *Tycho* B_T and V_T bands (Høg et al. 2000), Johnson's B, V and 2MASS J, H, and K bands from the UCAC4 catalog (Zacharias et al. 2012), WISE bands (Cutri et al. 2021), and *Gaia* G, $G_{\rm BP}$, and $G_{\rm RP}$ bands (Gaia Collaboration 2016), imposing Gaussian priors on each star's effective temperature, $T_{\rm eff}$, and metallicity, [Fe/H], based on their respective values in the Anders et al. (2019) catalog, as well as on the stellar parallax ϖ based on *Gaia* EDR3 astrometric measurement (Gaia Collaboration 2021).

The stellar parameters derived from the SED fitting for the binary sample are listed in Table 1, along with each star's archival spectral type, while the distribution of a few selected parameters for both the binary and CORALIE sample are plotted in Fig. 1. The median value of host star mass in our sample is of 0.94 $M_\odot$, and the average relative error on this parameter is 10%; median values and average errors for other stellar parameters of interest are 1.02 $R_\odot$ and 4% for stellar radii, 5985 K and 3.72% for effective temperature, 4.41 and 1.41% for surface gravity $\log g$, −0.27 dex, and 95% for metallicity. In order to compare the distributions of the binary sample with those of the larger CORALIE sample, we performed a Kolmogorov-Smirnov test for each stellar parameter derived from the SED fits, finding p-values <0.05 for $M_\star$ (p = 0.008), $R_\star$ (p = 0.009), and $\log g$ (p = 0.014), suggesting that the underlying population of the binary sample is not the same as the overall CORALIE sample. Indeed, we find the median values of stellar mass, radius, and surface gravity in the CORALIE sample to be 0.91 $M_\odot$, 0.95 $R_\odot$, and 4.45, suggesting that the underlying population of our binary sample consists of slightly more massive and larger stars than the underlying population of the overall exoplanetary search sample.

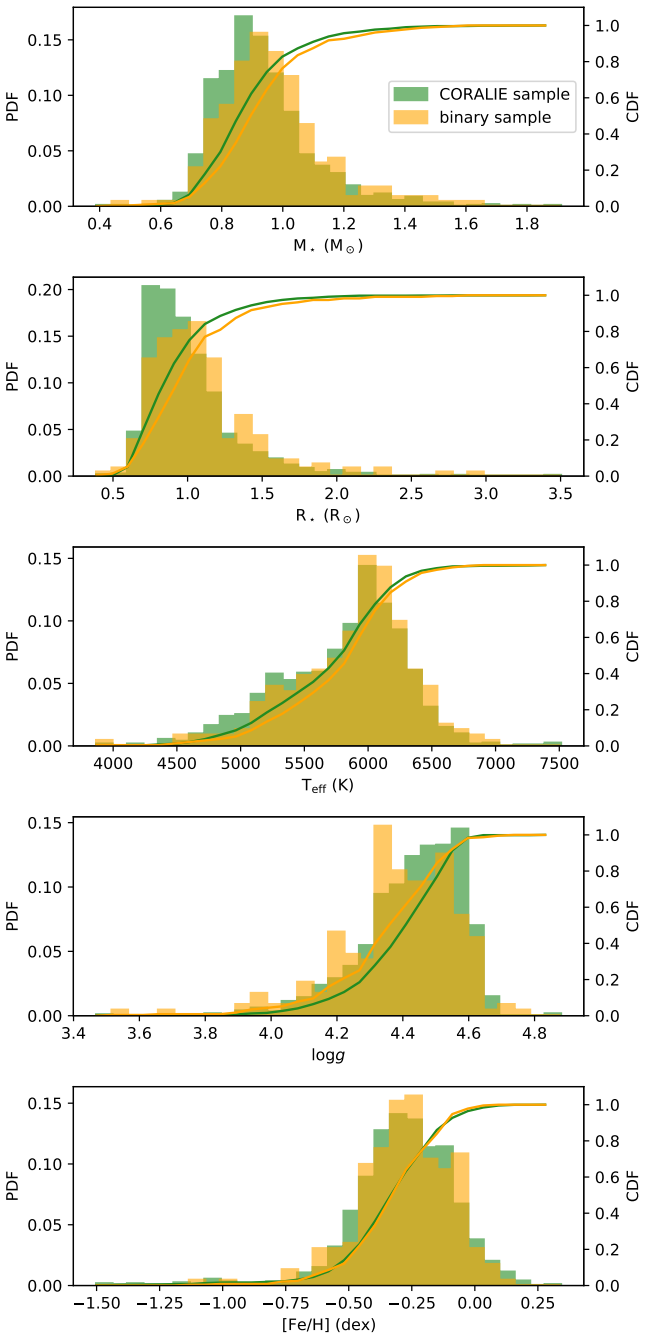

Fig. 1. Distributions of stellar mass, radius, effective temperature, surface gravity and metallicity of the 218 stars composing the sample discussed in this work (orange) and for the whole CORALIE exoplanetary search sample (green).

3. Radial velocity observations and analysis

Since its first observations in June 1998, the CORALIE spectrograph has gone through two significant upgrades, in June 2007 and in November 2014, to increase the overall efficiency and accuracy of the instrument. Specifically, the 2007 upgrade consisted of the replacement of CORALIE's fiber link and cross-disperser optics (Ségransan et al. 2010), while the 2014 upgrade consisted in replacing CORALIE's fiber link with octagonal fibers (Chazelas et al. 2012) and adding a Fabry-Pérot calibration unit (Cersullo et al. 2017). Both interventions on the instrument introduced small offsets between the radial velocity measurements collected before and after each upgrade, depending on such parameters as the spectral type and systemic velocity of the observed star; over the course of the time series analysis, we therefore considered CORALIE as three different instruments, each marked by the different upgrades. Here, we refer to the original CORALIE dataset as CORALIE-98 (C98), to the dataset

Table 1. Stellar parameters for the sample discussed in this work, derived by the SED fits described in Sect. 2 except spectral types, retrieved from Simbad.

Name	α(J2000)	δ(J2000)	SpType	$M_\star$ [$M_\odot$]	$R_\star$ [$R_\odot$]	$L_\star$ [$L_\odot$]	$\rho_\star$ [cgs]	log g [cgs]	$T_{\rm eff}$ [K]	[Fe H] [dex]
HD 225155	$00^h03^m53.37^s$	-28°23′37.70″	G5IV	$1.15^{+0.15}_{-0.16}$	1.41 ± 0.10	$2.78^{+0.75}_{-0.59}$	$0.59^{+0.16}_{-0.13}$	$4.21^{+0.08}_{-0.09}$	6290^{+370}_{-340}	$-0.22^{+0.27}_{-0.28}$
HD 1815	$00^h22^m23.56^s$	–27°01′57.05″	K2V	0.71 ± 0.04	0.67 ± 0.03	$0.24^{+0.04}_{-0.03}$	$3.30^{+0.41}_{-0.36}$	4.63 ± 0.03	4930^{+160}_{-130}	$-0.30^{+0.20}_{-0.21}$
HD 1926	$00^h23^m04.73^s$	–65°07′16.11″	F8/G0V	$1.00^{+0.14}_{-0.12}$	$1.15^{+0.14}_{-0.15}$	$1.90^{+0.64}_{-0.56}$	$0.95^{+0.41}_{-0.28}$	4.33 ± 0.10	6320 ± 260	$-0.49^{+0.29}_{-0.28}$
HD 2070	$00^h24^m44.81^s$	–51°02′37.90″	G0V	$1.15^{+0.14}_{-0.15}$	1.36 ± 0.04	$2.66^{+0.51}_{-0.37}$	$0.65^{+0.12}_{-0.11}$	$4.23^{+0.06}_{-0.07}$	6320^{+330}_{-270}	$-0.23^{+0.24}_{-0.28}$
HD 2098	$00^h25^m01.41^s$	–30°41′51.41″	G2V	$1.01^{+0.15}_{-0.12}$	1.16 ± 0.17	$1.68^{+0.67}_{-0.56}$	$0.94^{+0.47}_{-0.31}$	$4.33^{+0.11}_{-0.12}$	6080^{+310}_{-300}	$-0.22^{+0.32}_{-0.33}$
HD 3222	$00^h35^m02.81^s$	–63°41′42.64″	K2V	$0.78^{+0.05}_{-0.04}$	0.76 ± 0.02	0.46 ± 0.07	$2.54^{+0.25}_{-0.23}$	4.57 ± 0.03	5450^{+200}_{-190}	-0.41 ± 0.21
HD 3277	$00^h35^m34.25^s$	–39°44′46.65″	G8V	$0.94^{+0.11}_{-0.10}$	1.02 ± 0.14	$1.22^{+0.44}_{-0.36}$	$1.28^{+0.55}_{-0.38}$	4.40 ± 0.10	5990 ± 230	$-0.30^{+0.27}_{-0.28}$
HD 3359	$00^h36^m04.40^s$	–49°07′41.28″	G8V	$0.94^{+0.09}_{-0.08}$	0.98 ± 0.07	$1.00^{+0.23}_{-0.20}$	$1.42^{+0.31}_{-0.26}$	4.43 ± 0.06	5830 ± 230	-0.17 ± 0.28
HD 3795	$00^h40^m32.79^s$	–23°48′17.72″	K0V	$1.05^{+0.34}_{-0.17}$	$1.25^{+0.80}_{-0.34}$	$1.76^{+3.90}_{-0.96}$	$0.79^{+0.94}_{-0.57}$	$4.28^{+0.20}_{-0.36}$	5800^{+500}_{-260}	$-0.04^{+0.28}_{-0.35}$
HD 4392	$00^h45^m41.87^s$	–48°18′04.56″	G4V	$0.92^{+0.11}_{-0.09}$	$1.02^{+0.14}_{-0.13}$	$1.30^{+0.44}_{-0.37}$	$1.26^{+0.54}_{-0.38}$	4.40 ± 0.10	6100^{+210}_{-200}	-0.47 ± 0.24
HD 4747	$00^h49^m26.76^s$	–23°12′44.86″	G8V	1.02 ± 0.09	1.70 ± 0.04	$2.45^{+0.26}_{-0.16}$	0.29 ± 0.04	3.98 ± 0.05	5540^{+160}_{-120}	$-0.03^{+0.22}_{-0.24}$
HD 5562	$00^h56^m21.26^s$	–63°57′30.03″	G8IV	$1.19^{+0.22}_{-0.17}$	1.89 ± 0.07	$4.22^{+1.10}_{-0.86}$	$0.25^{+0.07}_{-0.05}$	3.96 ± 0.09	6030^{+430}_{-400}	$-0.14^{+0.25}_{-0.29}$
HD 7320	$01^h13^m18.82^s$	–01°51′43.72″	G5V	0.88 ± 0.06	0.87 ± 0.02	$0.75^{+0.09}_{-0.07}$	$1.87^{+0.19}_{-0.18}$	4.50 ± 0.04	5760^{+180}_{-150}	$-0.30^{+0.19}_{-0.20}$
HD 8129	$01^h20^m30.01^s$	–19°56′56.73″	G7V	$0.94^{+0.11}_{-0.10}$	1.00 ± 0.13	$1.06^{+0.41}_{-0.33}$	$1.36^{+0.55}_{-0.39}$	$4.42^{+0.09}_{-0.10}$	5850 ± 270	$-0.20^{+0.31}_{-0.32}$
HD 9770	$01^h35^m01.00^s$	–29°54′37.34″	K1V	$1.12^{+0.23}_{-0.19}$	$1.40^{+0.26}_{-0.29}$	$2.80^{+1.90}_{-1.30}$	$0.61^{+0.46}_{-0.23}$	$4.22^{+0.15}_{-0.14}$	6290^{+570}_{-460}	$-0.27^{+0.32}_{-0.33}$
HD 9905	$01^h36^m10.09^s$	–29°23′32.47″	K1V	$0.95^{+0.21}_{-0.13}$	$1.11^{+0.75}_{-0.29}$	$1.38^{+2.40}_{-0.73}$	$0.99^{+1.10}_{-0.75}$	$4.33^{+0.20}_{-0.39}$	5830 ± 270	$-0.28^{+0.28}_{-0.29}$
HD 10519	$01^h42^m14.91^s$	–17°53′19.47″	G2V	$1.08^{+0.19}_{-0.15}$	$1.46^{+0.21}_{-0.24}$	$2.77^{+1.10}_{-0.87}$	$0.50^{+0.31}_{-0.17}$	$4.16^{+0.14}_{-0.13}$	6180^{+330}_{-310}	-0.29 ± 0.27
HD 11131	$01^h49^m23.34^s$	–10°42′13.08″	G3V	$0.96^{+0.17}_{-0.12}$	$1.06^{+0.30}_{-0.20}$	$1.30^{+1.00}_{-0.54}$	$1.16^{+0.82}_{-0.57}$	$4.38^{+0.14}_{-0.19}$	5960 ± 260	$-0.27^{+0.32}_{-0.33}$
HD 11264	$01^h49^m35.56^s$	–46°46′07.19″	G5V	$1.02^{+0.14}_{-0.13}$	1.17 ± 0.14	$2.10^{+0.73}_{-0.59}$	$0.92^{+0.37}_{-0.25}$	$4.32^{+0.09}_{-0.10}$	6430^{+310}_{-270}	$-0.57^{+0.30}_{-0.31}$
HD 11352	$01^h51^m31.19^s$	–07°44′23.57″	G5V	0.89 ± 0.07	$0.89^{+0.06}_{-0.05}$	$0.91^{+0.18}_{-0.16}$	$1.79^{+0.32}_{-0.29}$	$4.49^{+0.05}_{-0.06}$	5990 ± 200	$-0.45^{+0.23}_{-0.24}$
HD 13945	$02^h15^m16.20^s$	–23°16′52.93″	G6IV	$1.03^{+0.10}_{-0.11}$	1.12 ± 0.03	$1.63^{+0.23}_{-0.20}$	1.04 ± 0.14	$4.35^{+0.05}_{-0.06}$	6170^{+230}_{-220}	$-0.25^{+0.24}_{-0.27}$
HD 14629	$02^h20^m42.92^s$	–39°02′01.44″	K3V	0.74 ± 0.04	0.71 ± 0.02	$0.36^{+0.05}_{-0.04}$	$2.88^{+0.23}_{-0.21}$	4.60 ± 0.03	5270^{+180}_{-170}	$-0.40^{+0.19}_{-0.20}$
HD 14802	$02^h22^m32.59^s$	–23°49′00.47″	G0V	$1.46^{+0.20}_{-0.23}$	1.84 ± 0.07	$6.20^{+2.70}_{-1.40}$	$0.33^{+0.09}_{-0.07}$	4.07 ± 0.09	6730^{+750}_{-510}	$-0.12^{+0.25}_{-0.28}$
HD 15064	$02^h24^m33.88^s$	–40°50′25.64″	G1V	$1.29^{+0.15}_{-0.20}$	1.66 ± 0.05	$3.70^{+0.84}_{-0.54}$	0.40 ± 0.08	$4.11^{+0.07}_{-0.09}$	6210^{+390}_{-290}	$-0.03^{+0.23}_{-0.27}$
HD 16287	$02^h36^m41.76^s$	–03°09′22.09″	K1V	0.81 ± 0.05	0.78 ± 0.04	$0.41^{+0.07}_{-0.06}$	$2.38^{+0.29}_{-0.28}$	$4.56^{+0.03}_{-0.04}$	5220^{+170}_{-160}	-0.09 ± 0.20
HD 17155	$02^h43^m34.21^s$	–46°27′17.51″	K4V	0.75 ± 0.04	0.71 ± 0.02	$0.27^{+0.04}_{-0.03}$	$2.96^{+0.23}_{-0.22}$	4.61 ± 0.03	4960^{+150}_{-140}	$-0.14^{+0.15}_{-0.16}$
HD 17289	$02^h43^m35.47^s$	–62°55′09.10″	G0V	$1.10^{+0.18}_{-0.16}$	$1.37^{+0.21}_{-0.24}$	$2.65^{+1.30}_{-1.00}$	$0.62^{+0.40}_{-0.21}$	4.22 ± 0.13	6290^{+410}_{-380}	$-0.29^{+0.28}_{-0.27}$
HD 17152	$02^h44^m28.95^s$	–24°24′56.33″	G8V	0.92 ± 0.08	0.96 ± 0.06	$0.98^{+0.19}_{-0.16}$	$1.49^{+0.28}_{-0.24}$	$4.44^{+0.05}_{-0.06}$	5870^{+210}_{-200}	$-0.26^{+0.24}_{-0.25}$
HD 18168	$02^h54^m02.78^s$	–35°54′16.87″	K3V	$0.91^{+0.08}_{-0.07}$	0.94 ± 0.06	$0.91^{+0.17}_{-0.16}$	$1.56^{+0.29}_{-0.26}$	$4.46^{+0.05}_{-0.06}$	5790 ± 210	$-0.20^{+0.25}_{-0.27}$
HD 18809	$03^h00^m19.71^s$	–37°27′16.16″	G4V	0.93 ± 0.08	0.96 ± 0.03	$1.03^{+0.15}_{-0.13}$	1.50 ± 0.19	$4.45^{+0.04}_{-0.05}$	5940^{+200}_{-190}	$-0.31^{+0.24}_{-0.25}$
HD 18907	$03^h01^m37.62^s$	–28°05′29.37″	G9V	$0.48^{+0.52}_{-0.33}$	$0.48^{+0.66}_{-0.30}$	$0.05^{+1.40}_{-0.04}$	$6.30^{+32.00}_{-5.40}$	$4.77^{+0.35}_{-0.46}$	3990^{+2000}_{-650}	$-0.23^{+0.32}_{-0.30}$
HD 20916	$03^h20^m11.75^s$	–52°01′54.67″	K0V	0.81 ± 0.05	0.80 ± 0.02	$0.59^{+0.08}_{-0.07}$	$2.25^{+0.21}_{-0.20}$	4.54 ± 0.03	5670 ± 190	$-0.44^{+0.21}_{-0.22}$
HD 22705	$03^h36^m53.40^s$	–49°57′28.87″	G2V	$1.01^{+0.11}_{-0.12}$	1.11 ± 0.06	$1.94^{+0.43}_{-0.35}$	$1.05^{+0.21}_{-0.20}$	$4.36^{+0.06}_{-0.07}$	6470^{+310}_{-300}	$-0.61^{+0.28}_{-0.29}$
HD 24492	$03^h40^m48.90^s$	–81°47′20.65″	G6V	$0.95^{+0.11}_{-0.10}$	1.02 ± 0.12	$1.23^{+0.41}_{-0.34}$	$1.28^{+0.47}_{-0.35}$	$4.41^{+0.08}_{-0.09}$	6010 ± 250	$-0.30^{+0.29}_{-0.30}$
HD 23308	$03^h42^m09.85^s$	–45°57′28.39″	F7V	$1.16^{+0.33}_{-0.25}$	$1.35^{+0.50}_{-0.39}$	$2.70^{+3.80}_{-1.70}$	$0.67^{+0.87}_{-0.36}$	4.25 ± 0.21	6340^{+530}_{-500}	-0.23 ± 0.29
HD 23576	$03^h44^m45.42^s$	–38°49′05.05″	G1V	$1.03^{+0.10}_{-0.11}$	1.12 ± 0.03	$1.65^{+0.21}_{-0.16}$	1.03 ± 0.14	$4.35^{+0.05}_{-0.06}$	6170^{+220}_{-180}	$-0.26^{+0.23}_{-0.25}$
HD 25874	$04^h02^m26.97^s$	–61°21′25.16″	G2V	$1.00^{+0.12}_{-0.11}$	1.11 ± 0.11	$1.50^{+0.41}_{-0.35}$	$1.05^{+0.34}_{-0.26}$	$4.36^{+0.08}_{-0.09}$	6060^{+240}_{-230}	-0.22 ± 0.27
...	...	...	...	...	...	...	...	...	...	...

Notes. Full table is available at the CDS. A portion is shown here for guidance regarding its form and content.

collected after the first upgrade as CORALIE-07 (C07), and to the one collected after the most recent upgrade as CORALIE-14 (C14). For selected stars in our sample, we additionally include in the analysis the measurements collected at a lower precision ($\sim$300 ms^{-1}) with the CORrelation-RAdial-VELocities (CORAVEL) spectrometer (Baranne et al. 1979) between 1981 and 1998, especially when the CORAVEL data are plentiful enough to help identify long-period signals and constrain the orbital parameters of the companions found.

At the time of writing, over nearly 25 yr of observations based on the CORALIE sample, we collected a total of 62 600 radial velocity measurements for the 1647 stars in the sample, averaging 38 datapoints per star, with median photon-noise uncertainty and time span of 5.21 ms^{-1} and 7698 d, respectively. In order to search for Doppler signals consistent with the presence of stellar companions in the CORALIE radial velocity timeseries, we followed an iterative process of investigation of successive dominant peaks in the radial velocity periodogram, as described in Delisle et al. (2016). As mentioned in Sect. 2, we note again that stars found to be SB2s in the CORALIE sample are excluded from the following analysis.

First of all, in our analysis, we considered only the 1497 stars, for which a total of at least ten CORALIE measurements have been collected over the years, to ensure the robust identification of significant signals. We modelled instrumental offsets, noise, and stellar jitter for each star in the CORALIE sample, following the formalism detailed in Díaz et al. (2016) and Delisle et al. (2018), and computing false alarm probabilities (FAPs) on the periodogram of the residuals, as described in Baluev (2008). The periodogram's main peak is considered significant if characterised by a FAP lower than 0.1% and is modeled as a Keplerian. The new radial velocity residuals obtained in this way are again investigated for significant signals, re-adjusting the jitter, noise, and offsets at each step of the iterative process. This method is, however, valid only when enough measurements are available to compute a value of FAP; for those cases, in which no robust value of FAP is obtained but a clear variation having a scatter in excess of the observation formal errors is present in the radial velocity measurements, we still modelled the data with a Keplerian model, assessing its significance using the difference between the Bayesian information criterion (ΔBIC) of the Keplerian and flat models, computed as:

$$\mathrm{BIC} = \mathrm{k}\log\mathrm{n} - 2\log\mathscr{L}, \quad (1)$$

with k as the number of model parameters, n the number of datapoints, and $\log\mathscr{L}$ the maximised log-likelihood of the model evaluated following Delisle et al. (2020). Additionally, the longer period signals found during this search are also modelled as linear or quadratic trends instead and are included in the final sample that is the main focus of this work, only if $\Delta\mathrm{BIC} > 10$ in favour of the Keplerian solution. Overall, the signal search process is similar to that undertaken in parallel in Unger et al., in prep., focused instead on identifying new giant planets and brown dwarf companions in the CORALIE sample.

At the end of this analysis, we identified a total of 218 stars featuring at least one signal compatible with a companion minimum mass, $M \sin i \gtrapprox 40\,M_{\rm Jup}$, within 1σ – the threshold between giant planets and brown dwarfs we select following the findings reported in Sahlmann et al. (2011a). This comprises the binary sample that represents the main focus of this work. The CORALIE radial velocity dataset for this sample is comprised of a total of 7226 CORALIE measurements, averaging 33 datapoints per star and featuring a median radial velocity uncertainty of 5.31 ms^{-1} as well as an observational time span of 7581 d. We note that all data products are publicly available at the Data and Analysis Center for Exoplanets (DACE)[1]. We ran a Markov chain Monte Carlo (MCMC) analysis for each star in our sample based on the algorithm described in Díaz et al. (2016) and Delisle et al. (2016, 2018) to obtain the posterior distribution of the model parameters, using initial conditions drawn from the orbital solutions we obtained during our preliminary iterative signal search and computing each parameter's confidence intervals for a 68.27% confidence level.

A summary of the best-fit radial velocity orbital solutions for all companions found in the sample is listed in the left portion of Table 2. The distributions of selected orbital parameters and mass ratio are plotted in the histograms shown in Fig 2, while the companions distribution in the $M \sin i$-a parameter space is shown in Fig 3. Finally, the phase-folded radial velocity curves for every companion in the sample are collected in Appendix A.

It can be seen that the population of the companions having $M \sin i > 40\,M_{\rm Jup}$, identified by radial velocity in the sample peaks at $\sim$5.92 au and $\sim$290 $M_{\rm Jup}$ (around 0.27 $M_\odot$). It can also be seen that the orbital elements cover a large variety, with periods ranging from 4 d (for HD 196998B) to 65213 d (HD 3795B), semimajor axes from 0.045 au (HD 196998B) to 36.40 au (HD 3795B), minimum masses from 41.60 $M_{\rm Jup}$ ($\sim$0.04 $M_\odot$, HD 30774B) to $\sim$0.71 $M_\odot$ (HD 181199B), and eccentricities values from fully circular (HD 207450B) to 0.95 (HD 137763B). All the companions in the sample have a minimum mass below the solar mass.

Another point of interest is the distinction between single–lined binaries (SB1) and double–lined spectroscopic binaries (SB2) in the sample. Following Halbwachs et al. (2003), we can use the minimum mass ratio parameter $q_{\rm min}$ between the secondary and primary component to identify possible SB2s as those having $q > 0.8$. In doing so, we find no binary systems in the sample with such high value of q as characterised by our radial velocity solutions.

To search for differences in the properties of inner ($a < 5$ au) and outer ($a \geq 5$ au) companions we again perform a Kolmogorov-Smirnov test of the orbital elements of the detected companions, finding p-values only marginally lower than 0.05 for minimum mass ($p = 0.03$) and an eccentricity ($p = 0.04$) that is suggestive of a possible difference in the respective distributions for inner and outer companions. Indeed, as shown in Fig. 2, more companions are found on low-eccentricity inner orbits than outer ones, likely to be the result of orbit circularisation effects.

Finally, we found three stars in the sample hosting more than one companion. As described by our radial velocity solution, HD 94340 is a triple star system in which the 1.28 $M_\odot$ primary is orbited by a $M \sin i \sim 0.08\,M_\odot$ companion on a 6.84 d orbit and by a $M \sin i \sim 0.07\,M_\odot$ body with an orbital period of $\sim$1123 d, HD 206276 hosting a $M \sin i \sim 0.09\ M_\odot$ companion on a 32 d orbit and a $M \sin i \sim 0.16\,M_\odot$ at 1374 d, and HD 196885 hosting both an inner giant planet with minimum mass of 1.95 $M_{\rm Jup}$ and orbital period of 1330 d and an outer stellar companion with $M \sin i \sim 0.26\,M_\odot$ on a 14912 d orbit. Two of these systems are already known in the literature (see Tokovinin et al. 2006, 2012 for HD 94340 and Correia et al. 2008 for HD 196885), but in the present work, we provide updated orbital parameters for all components, especially with the use of astrometry constrains detailed in Sect. 4, while for HD 206276, we provide an updated solution for the outer stellar companion, whose presence was already hinted at by astrometric observations and we present a

[1] https://dace.unige.ch

Table 2. Best-fit orbital solutions for the binary systems identified in the sample, left side reporting the results from the radial velocity fits (see Sect. 3) and right side referring to the simultaneous radial velocities and proper motions fits (see Sect. 4).

	RV only solution										RV+$\Delta\mu$ solution								
Name	P [d]	K [$\mathrm{km\,s^{-1}}$]	e	λ_0 [deg]	ω [deg]	$M \sin i$ [$M_{\rm Jup}$]	$M \sin i$ [$M_\odot$]	a [au]	$t_{\rm span}/P$	$q_{\rm min}$	M [$M_{\rm Jup}$]	M [$M_\odot$]	a [au]	P [d]	e [deg]	i [deg]	ω	q	Previous publication
HD 225155	$2276.36^{+0.30}_{-0.23}$	4.137 ± 0.003	0.321 ± 0.001	79.91 ± 0.05	$295.24^{+0.13}_{-0.15}$	$278.39^{+25.14}_{-26.40}$	$0.27^{+0.02}_{-0.03}$	$3.80^{+0.16}_{-0.17}$	3.44	0.23	336^{+28}_{-28}	0.32 ± 0.03	$3.85^{+0.15}_{-0.16}$	2276.23 ± 0.24	$0.32004^{+0.00066}_{-0.00068}$	$77.7^{+5.0}_{-3.9}$	$295.37^{+0.15}_{-0.15}$	0.28	—
HD 1815	1160.40 ± 0.05	$6.624^{+0.002}_{-0.003}$	0.130 ± 0.001	146.15 ± 0.02	$81.03^{+0.19}_{-0.22}$	$269.22^{+10.84}_{-11.00}$	0.26 ± 0.01	2.13 ± 0.04	10.62	0.36	—	—	—	—	—	—	—	—	—
HD 1926	156.33 ± 0.01	$7.904^{+0.001}_{-0.002}$	0.039 ± 0.001	−297.16 ± 0.01	$64.91^{+0.35}_{-0.33}$	$209.34^{+19.07}_{-19.98}$	0.20 ± 0.02	0.60 ± 0.03	69.73	0.20	—	—	—	—	—	—	—	—	Tokovinin (2014)
HD 2070	115.20 ± 0.01	15.110 ± 0.001	0.347 ± 0.001	191.37 ± 0.01	$355.98^{+0.02}_{-0.01}$	$372.55^{+31.61}_{-33.19}$	0.36 ± 0.03	0.53 ± 0.02	118.79	0.31	—	—	—	—	—	—	—	—	Tokovinin (2014)
HD 2098	$2693.21^{+0.47}_{-0.50}$	4.909 ± 0.002	0.141 ± 0.001	$-319.46^{+0.07}_{-0.10}$	$317.56^{+0.39}_{-0.44}$	$334.97^{+32.36}_{-34.00}$	0.32 ± 0.03	$4.17^{+0.18}_{-0.20}$	5.20	0.32	528^{+48}_{-49}	0.50 ± 0.05	$4.33^{+0.18}_{-0.20}$	$2690.29^{+1.57}_{-2.37}$	$0.1509^{+0.0087}_{-0.0057}$	$55.7^{+1.7}_{-1.6}$	$315.5^{+1.3}_{-1.7}$	0.50	Tokovinin (2014)
HD 3222	$15676.93^{+2.18}_{-2.37}$	1.771 ± 0.002	0.321 ± 0.001	$222.25^{+0.10}_{-0.07}$	$162.19^{+0.38}_{-0.27}$	$175.00^{+6.95}_{-7.08}$	0.17 ± 0.01	$12.04^{+0.22}_{-0.23}$	0.74	0.21	$218.0^{+8.0}_{-8.2}$	0.21 ± 0.01	$12.21^{+0.22}_{-0.23}$	15675.43 ± 9.86	$0.3202^{+0.0022}_{-0.0021}$	$109.57^{+0.80}_{-0.83}$	$162.43^{+0.62}_{-0.61}$	0.27	—
HD 3277	46.15 ± 0.01	4.071 ± 0.002	0.285 ± 0.001	132.80 ± 0.02	320.50 ± 0.07	$66.17^{+5.04}_{-5.25}$	0.06 ± 0.01	0.25 ± 0.01	231.47	0.07	—	—	—	—	—	—	—	—	Sahlmann et al. (2011b)
HD 3359	22.14 ± 0.01	$22.295^{+0.016}_{-0.006}$	0.342 ± 0.001	$102.46^{+0.09}_{-0.11}$	$5.87^{+0.16}_{-0.30}$	$277.39^{+17.27}_{-17.81}$	0.26 ± 0.02	0.16 ± 0.01	529.05	0.28	—	—	—	—	—	—	—	—	—
HD 3795	$65213.79^{+1409.42}_{-4386.49}$	$2.844^{+0.061}_{-0.103}$	$0.495^{+0.009}_{-0.017}$	$20.15^{+0.53}_{-0.55}$	$32.80^{+0.83}_{-0.76}$	$504.25^{+107.02}_{-116.63}$	$0.48^{+0.10}_{-0.11}$	$36.41^{+3.74}_{-4.27}$	0.12	0.46	949^{+159}_{-177}	$0.91^{+0.15}_{-0.17}$	$39.8^{+3.7}_{-4.1}$	66110.25 ± 4017.75	$0.485^{+0.019}_{-0.020}$	$118.4^{+2.1}_{-2.3}$	$34.4^{+1.6}_{-1.5}$	0.86	—
HD 4392	$548.84^{+0.06}_{-0.08}$	$3.706^{+0.004}_{-0.008}$	0.615 ± 0.001	$148.17^{+0.05}_{-0.06}$	$226.43^{+0.17}_{-0.18}$	$111.20^{+8.69}_{-9.06}$	0.11 ± 0.01	1.32 ± 0.05	22.16	0.12	573^{+88}_{-83}	0.55 ± 0.08	$1.488^{+0.051}_{-0.057}$	$548.73^{+0.05}_{-0.07}$	$0.61518^{+0.0010}_{-0.00088}$	$15.2^{+1.8}_{-1.4}$	$226.21^{+0.11}_{-0.12}$	0.60	Tokovinin (2014)
HD 4747	$12196.71^{+295.98}_{-231.17}$	0.703 ± 0.005	0.732 ± 0.001	55.33 ± 1.10	266.93 ± 0.25	$54.81^{+3.28}_{-3.36}$	0.05 ± 0.01	$10.60^{+0.35}_{-0.36}$	0.69	0.05	$70.5^{+4.8}_{-4.6}$	0.07 ± 0.01	$9.81^{+0.32}_{-0.33}$	$10782.18^{+255.67}_{-237.41}$	$0.651^{+0.032}_{-0.023}$	$41.2^{+2.1}_{-2.4}$	$282.3^{+2.9}_{-4.6}$	0.07	Peretti et al. (2019)
HD 5562	$3968.53^{+0.80}_{-0.67}$	4.605 ± 0.004	0.336 ± 0.001	266.55 ± 0.03	$354.46^{+0.15}_{-0.12}$	$379.31^{+45.32}_{-48.29}$	$0.36^{+0.04}_{-0.05}$	$5.68^{+0.30}_{-0.34}$	2.03	0.30	480^{+48}_{-50}	0.46 ± 0.05	$5.82^{+0.28}_{-0.31}$	$3968.37^{+0.62}_{-0.58}$	$0.33599^{+0.00052}_{-0.00056}$	$97.5^{+1.7}_{-1.8}$	$354.43^{+0.14}_{-0.14}$	0.39	—
HD7320	$13476.31^{+4.81}_{-1.13}$	10.277 ± 0.001	0.950 ± 0.001	$265.41^{+0.37}_{-0.41}$	$91.74^{+0.54}_{-0.61}$	$344.50^{+15.56}_{-15.93}$	$0.33^{+0.01}_{-0.02}$	$11.79^{+0.24}_{-0.25}$	0.97	0.38	333^{+86}_{-129}	$0.32^{+0.08}_{-0.12}$	$11.75^{+0.37}_{-0.57}$	13475.94 ± 2.05	$0.90^{+0.08}_{-0.10}$	$90.28^{+0.79}_{-1.1}$	$100.5^{+1.7}_{-16}$	0.36	Latham et al. (2002)
HD8129	$5269.10^{+145.40}_{-5.90}$	$9.054^{+0.708}_{-1.216}$	$0.949^{+0.007}_{-0.043}$	$83.40^{+3.17}_{-5.96}$	$281.18^{+2.99}_{-4.77}$	$239.88^{+86.78}_{-89.67}$	$0.23^{+0.08}_{-0.09}$	$6.23^{+0.29}_{-0.30}$	1.33	0.24	—	—	—	—	—	—	—	—	Tokovinin (2014)
HD 9770	$1673.32^{+0.08}_{-0.09}$	2.562 ± 0.001	0.312 ± 0.001	$351.33^{+0.03}_{-0.04}$	$292.65^{+0.10}_{-0.09}$	$153.31^{+20.34}_{-21.74}$	0.15 ± 0.02	$2.98^{+0.18}_{-0.21}$	3.97	0.13	—	—	—	—	—	—	—	—	Watson et al. (2001)
HD 9905	$10126.26^{+122.66}_{-156.35}$	$1.608^{+0.021}_{-0.018}$	$0.298^{+0.007}_{-0.008}$	$272.30^{+0.44}_{-0.58}$	$355.47^{+1.18}_{-1.42}$	$157.80^{+22.61}_{-24.24}$	0.15 ± 0.02	$9.46^{+0.63}_{-0.73}$	0.96	0.16	178^{+24}_{-25}	0.17 ± 0.02	$9.57^{+0.62}_{-0.71}$	$10212.39^{+80.36}_{-76.70}$	$0.3032^{+0.0043}_{-0.0042}$	$86.8^{+2.3}_{-2.0}$	$354.35^{+0.88}_{-0.88}$	0.18	—
HD 10519	$7731.73^{+0.98}_{-1.24}$	6.793 ± 0.001	0.765 ± 0.001	172.69 ± 0.04	155.68 ± 0.04	$448.35^{+51.11}_{-54.22}$	0.43 ± 0.05	$8.78^{+0.44}_{-0.50}$	1.90	0.40	600^{+58}_{-63}	0.57 ± 0.06	$9.05^{+0.42}_{-0.49}$	7737.46 ± 9.50	$0.76442^{+0.00081}_{-0.00081}$	$95.4^{+3.3}_{-4.6}$	$155.76^{+0.19}_{-0.19}$	0.53	Tokovinin (2014)
HD 11131	$3358.89^{+1.48}_{-1.45}$	$5.333^{+0.010}_{-0.009}$	0.676 ± 0.001	$92.10^{+0.05}_{-0.06}$	52.60 ± 0.11	$281.96^{+32.38}_{-34.27}$	0.27 ± 0.03	$4.70^{+0.24}_{-0.27}$	3.49	0.28	418^{+42}_{-44}	0.40 ± 0.04	$4.86^{+0.24}_{-0.26}$	$3358.80^{+2.30}_{-2.34}$	$0.6756^{+0.0010}_{-0.0010}$	$58.2^{+1.1}_{-1.1}$	$52.59^{+0.12}_{-0.12}$	0.42	—
HD 11264	$15530.07^{+7.65}_{-7.74}$	$3.200^{+0.007}_{-0.005}$	0.288 ± 0.001	$297.94^{+0.08}_{-0.10}$	$237.76^{+0.32}_{-0.33}$	$381.16^{+34.04}_{-35.71}$	0.36 ± 0.03	$13.58^{+0.54}_{-0.59}$	0.80	0.36	551^{+42}_{-44}	0.53 ± 0.04	$14.08^{+0.53}_{-0.58}$	15529.70 ± 9.86	$0.2889^{+0.0022}_{-0.0022}$	$65.69^{+0.27}_{-0.27}$	$237.65^{+0.44}_{-0.45}$	0.52	Boffin & Pourbaix (2003)
HD 11352	$464.75^{+0.14}_{-0.09}$	8.412 ± 0.001	0.232 ± 0.001	$123.01^{+0.11}_{-0.19}$	$178.44^{+0.22}_{-0.34}$	$287.70^{+15.59}_{-16.01}$	$0.27^{+0.01}_{-0.02}$	1.23 ± 0.03	23.78	0.31	387^{+50}_{-28}	$0.37^{+0.05}_{-0.03}$	$1.270^{+0.031}_{-0.033}$	464.80 ± 0.16	$0.239^{+0.014}_{-0.013}$	107^{+14}_{-14}	$171.4^{+4.6}_{-4.2}$	0.42	—
HD 13945	8.36 ± 0.01	8.147 ± 0.003	0.097 ± 0.001	349.19 ± 0.07	281.55 ± 0.43	$82.43^{+5.77}_{-5.98}$	0.08 ± 0.01	0.08 ± 0.01	967.35	0.08	—	—	—	—	—	—	—	—	Tokovinin (2014)
HD 14629	512.16 ± 0.02	$6.923^{+0.134}_{-0.103}$	$0.887^{+0.002}_{-0.001}$	$110.94^{+0.27}_{-0.34}$	$29.86^{+0.18}_{-0.23}$	$103.27^{+4.20}_{-4.16}$	0.10 ± 0.01	1.18 ± 0.02	14.81	0.13	$117.7^{+5.3}_{-4.0}$	0.11 ± 0.01	$1.198^{+0.017}_{-0.016}$	512.15 ± 0.02	$0.8875^{+0.0020}_{-0.0015}$	88^{+12}_{-13}	$29.83^{+0.20}_{-0.27}$	0.15	—
HD 14802	$9699.95^{+0.46}_{-0.36}$	5.457 ± 0.001	0.331 ± 0.001	$211.55^{+0.01}_{-0.02}$	$261.94^{+0.02}_{-0.03}$	$695.52^{+70.96}_{-75.03}$	0.66 ± 0.07	$11.44^{+0.51}_{-0.57}$	1.43	0.45	—	—	—	—	—	—	—	—	—
HD 15064	142.56 ± 0.01	$18.327^{+0.014}_{-0.010}$	0.247 ± 0.001	$74.14^{+0.04}_{-0.03}$	$195.43^{+0.08}_{-0.09}$	$540.92^{+54.46}_{-57.40}$	0.52 ± 0.05	0.65 ± 0.03	80.07	0.40	—	—	—	—	—	—	—	—	Tokovinin (2014)
HD 16287	14.84 ± 0.01	10.699 ± 0.003	0.208 ± 0.001	328.08 ± 0.13	10.61 ± 0.11	$110.32^{+4.65}_{-4.74}$	0.11 ± 0.01	0.11 ± 0.01	1077.29	0.13	—	—	—	—	—	—	—	—	—
HD 17155	$1426.20^{+0.05}_{-0.04}$	$2.581^{+0.004}_{-0.001}$	0.774 ± 0.001	$50.71^{+0.04}_{-0.07}$	276.62 ± 0.04	$74.44^{+2.43}_{-2.49}$	0.07 ± 0.01	2.32 ± 0.04	8.18	0.10	$87.2^{+3.0}_{-3.0}$	0.08 ± 0.01	$2.330^{+0.036}_{-0.038}$	1426.01 ± 0.69	$0.7751^{+0.0065}_{-0.0056}$	$66.2^{+1.3}_{-1.3}$	$275.9^{+1.0}_{-1.1}$	0.11	—
HD 17289	$561.68^{+0.09}_{-0.07}$	1.395 ± 0.005	$0.528^{+0.002}_{-0.003}$	86.54 ± 0.23	$51.66^{+0.39}_{-0.43}$	$51.26^{+5.45}_{-5.74}$	0.05 ± 0.01	$1.40^{+0.07}_{-0.08}$	17.08	0.04	$63.4^{+21}_{-8.7}$	$0.06^{+0.02}_{-0.01}$	$1.429^{+0.063}_{-0.059}$	561.77 ± 0.07	$0.5261^{+0.0025}_{-0.0025}$	96^{+34}_{-41}	$51.61^{+0.58}_{-0.57}$	0.06	Sahlmann et al. (2011b)
HD 17152	65.51 ± 0.01	9.768 ± 0.060	0.611 ± 0.002	299.43 ± 0.24	239.61 ± 0.18	$144.62^{+8.78}_{-9.01}$	0.14 ± 0.01	0.32 ± 0.01	174.21	0.15	—	—	—	—	—	—	—	—	—
HD 18168	9.41 ± 0.01	$45.740^{+0.014}_{-0.013}$	0.114 ± 0.001	331.70 ± 0.02	$268.78^{+0.15}_{-0.17}$	$444.66^{+26.76}_{-27.67}$	0.42 ± 0.03	0.10 ± 0.01	710.19	0.46	—	—	—	—	—	—	—	—	—
HD 18809	115.17 ± 0.01	9.283 ± 0.001	0.121 ± 0.001	506.30 ± 0.07	$243.00^{+0.73}_{-0.68}$	$209.41^{+11.75}_{-12.08}$	0.20 ± 0.01	0.48 ± 0.01	104.50	0.22	—	—	—	—	—	—	—	—	—
HD 18907	$9860.58^{+68.11}_{-38.37}$	$2.414^{+0.015}_{-0.014}$	$0.218^{+0.003}_{-0.004}$	$-246.47^{+0.36}_{-0.27}$	$306.98^{+0.94}_{-0.90}$	$159.91^{+89.41}_{-86.87}$	$0.15^{+0.09}_{-0.08}$	$8.21^{+1.63}_{-2.21}$	1.27	0.32	274^{+101}_{-98}	$0.26^{+0.10}_{-0.09}$	$8.7^{+1.5}_{-1.7}$	$9880.01^{+40.18}_{-36.52}$	$0.2165^{+0.0029}_{-0.0029}$	$122.44^{+0.33}_{-0.32}$	$307.28^{+0.85}_{-0.87}$	0.54	Jenkins et al. (2015)
HD 20916	$2234.53^{+0.93}_{-0.96}$	$1.616^{+0.007}_{-0.003}$	$0.520^{+0.002}_{-0.003}$	$210.60^{+0.28}_{-0.41}$	$350.60^{+0.35}_{-0.32}$	$77.33^{+3.41}_{-3.47}$	0.07 ± 0.01	3.21 ± 0.07	3.75	0.09	160^{+13}_{-12}	0.15 ± 0.01	$3.305^{+0.068}_{-0.071}$	$2233.72^{+2.96}_{-2.81}$	$0.529^{+0.029}_{-0.025}$	$140.8^{+7.7}_{-111}$	$350.0^{+1.7}_{-1.6}$	0.19	—
HD 22705	204.29 ± 0.01	$7.885^{+0.026}_{-0.022}$	0.182 ± 0.002	74.91 ± 0.26	$358.68^{+0.95}_{-0.91}$	$226.19^{+17.56}_{-18.28}$	0.22 ± 0.02	0.73 ± 0.03	54.00	0.21	—	—	—	—	—	—	—	—	Makarov (2007)
HD 24492	$1566.84^{+0.16}_{-0.17}$	$4.680^{+0.007}_{-0.006}$	0.157 ± 0.001	$230.82^{+0.10}_{-0.09}$	$250.96^{+0.21}_{-0.20}$	$254.68^{+19.35}_{-20.17}$	0.24 ± 0.02	$2.80^{+0.10}_{-0.11}$	5.18	0.26	482^{+37}_{-36}	$0.46^{+0.04}_{-0.03}$	$2.960^{+0.093}_{-0.10}$	$1566.78^{+0.44}_{-0.47}$	$0.1568^{+0.0014}_{-0.0015}$	$136.5^{+1.6}_{-1.7}$	$250.91^{+0.40}_{-0.42}$	0.49	—
HD 23308	4.47 ± 0.01	13.003 ± 0.002	0.001 ± 0.001	237.89 ± 0.01	24.01 ± 14.35	$116.40^{+21.12}_{-23.26}$	0.11 ± 0.02	0.06 ± 0.01	1436.19	0.10	—	—	—	—	—	—	—	—	—
HD 23576	$17109.11^{+3.05}_{-2.97}$	3.834 ± 0.002	0.439 ± 0.001	$322.37^{+0.12}_{-0.15}$	$44.24^{+0.18}_{-0.19}$	$444.53^{+31.23}_{-32.30}$	0.42 ± 0.03	$14.71^{+0.46}_{-0.49}$	0.78	0.41	766^{+43}_{-44}	0.73 ± 0.04	$15.68^{+0.44}_{-0.46}$	17109.77 ± 9.86	$0.4395^{+0.0015}_{-0.0014}$	$123.89^{+0.20}_{-0.19}$	$44.19^{+0.48}_{-0.46}$	0.71	—
HD 25874	$4469.97^{+4.72}_{-3.31}$	$2.207^{+0.005}_{-0.006}$	0.473 ± 0.002	$230.86^{+0.16}_{-0.18}$	$95.86^{+0.21}_{-0.20}$	$157.59^{+12.33}_{-12.89}$	0.15 ± 0.01	$5.56^{+0.20}_{-0.22}$	2.77	0.15	201^{+15}_{-15}	0.19 ± 0.01	$5.63^{+0.21}_{-0.22}$	4475.04 ± 5.84	$0.4730^{+0.0023}_{-0.0023}$	$61.82^{+0.55}_{-0.54}$	$96.14^{+0.21}_{-0.20}$	0.19	—
HD 26491	$9517.81^{+4.90}_{-4.09}$	4.439 ± 0.003	0.564 ± 0.001	58.41 ± 0.12	$221.36^{+0.08}_{-0.09}$	$382.04^{+51.71}_{-55.59}$	0.36 ± 0.05	$9.75^{+0.58}_{-0.67}$	1.32	0.36	498^{+59}_{-64}	0.48 ± 0.06	$9.98^{+0.57}_{-0.66}$	$9521.70^{+8.40}_{-8.04}$	$0.5642^{+0.0011}_{-0.0011}$	$97.7^{+1.4}_{-15}$	$221.34^{+0.14}_{-0.14}$	0.48	—
HD 27019	$6810.51^{+4.14}_{-2.80}$	$3.144^{+0.039}_{-0.012}$	$0.740^{+0.004}_{-0.002}$	$310.68^{+0.25}_{-0.20}$	$157.82^{+0.30}_{-0.26}$	$187.96^{+16.12}_{-16.67}$	0.18 ± 0.02	$7.28^{+0.28}_{-0.31}$	1.73	0.19	1828^{+177}_{-172}	$1.74^{+0.17}_{-0.16}$	$9.77^{+0.30}_{-0.32}$	6817.76 ± 9.86	$0.924^{+0.012}_{-0.015}$	$29.9^{+3.3}_{-3.0}$	$170.3^{+1.2}_{-1.4}$	0.53	Gomez et al. (2016)
HD 28454	6.29 ± 0.01	$7.162^{+0.002}_{-0.001}$	0.001 ± 0.001	142.75 ± 0.03	$213.27^{+44.24}_{-37.04}$	$78.13^{+4.68}_{-4.82}$	0.07 ± 0.01	0.07 ± 0.01	1105.73	0.06	—	—	—	—	—	—	—	—	—
HD 29813	$4488.14^{+2.66}_{-1.06}$	$2.908^{+0.003}_{-0.004}$	0.254 ± 0.001	$179.29^{+0.11}_{-0.05}$	$24.90^{+0.27}_{-0.11}$	$223.72^{+16.61}_{-17.23}$	0.21 ± 0.02	$5.63^{+0.19}_{-0.21}$	2.61	0.22	336^{+23}_{-23}	0.32 ± 0.02	$5.80^{+0.19}_{-0.21}$	$4488.41^{+1.94}_{-2.01}$	$0.2542^{+0.0015}_{-0.0015}$	$53.71^{+0.67}_{-0.66}$	$25.08^{+0.27}_{-0.27}$	0.33	Tokovinin (2014)
HIP22059	$13855.08^{+16.54}_{-15.13}$	0.624 ± 0.004	$0.100^{+0.006}_{-0.007}$	$350.51^{+0.37}_{-0.47}$	$303.34^{+3.36}_{-3.83}$	$57.90^{+2.05}_{-2.08}$	0.06 ± 0.01	$10.29^{+0.17}_{-0.18}$	0.50	0.08	$182.7^{+6.1}_{-6.2}$	0.17 ± 0.01	$10.80^{+0.17}_{-0.18}$	13855.76 ± 14.98	$0.0977^{+0.0088}_{-0.0086}$	$158.42^{+0.27}_{-0.28}$	$303.1^{+4.7}_{-5.6}$	0.25	Rickman et al. (2022)
HD 30501	$2076.27^{+2.81}_{-2.97}$	$1.756^{+0.011}_{-0.010}$	$0.758^{+0.004}_{-0.005}$	$358.19^{+1.46}_{-1.65}$	$71.79^{+0.55}_{-0.65}$	$62.44^{+3.82}_{-3.92}$	0.06 ± 0.01	3.04 ± 0.09	3.18	0.07	$68.3^{+4.0}_{-4.2}$	0.07 ± 0.01	$3.045^{+0.087}_{-0.093}$	$2075.72^{+3.14}_{-3.10}$	$0.7539^{+0.0041}_{-0.0036}$	$104.5^{+2.5}_{-3.3}$	$71.11^{+0.68}_{-0.77}$	0.08	Sahlmann et al. (2011b)
HD 30517	$29184.35^{+6.42}_{-5.07}$	1.238 ± 0.004	0.001 ± 0.001	$295.44^{+0.21}_{-0.16}$	$33.19^{+277.23}_{-342.19}$	$169.12^{+7.71}_{-7.87}$	0.16 ± 0.01	$18.66^{+0.40}_{-0.42}$	0.26	0.19	359^{+62}_{-60}	0.34 ± 0.06	$19.71^{+0.48}_{-0.49}$	29183.48 ± 9.86	$0.21^{+0.11}_{-0.13}$	$120.6^{+8.8}_{-18}$	88^{+12}_{-17}	0.40	—
HD 30774	4.93 ± 0.01	5.000 ± 0.002	0.003 ± 0.001	217.67 ± 0.04	310.85 ± 6.78	$41.59^{+3.30}_{-3.42}$	0.04 ± 0.01	0.06 ± 0.01	1349.68	0.04	—	—	—	—	—	—	—	—	Tokovinin (2014)
HD 31143	$8669.86^{+662.20}_{-755.93}$	$3.319^{+0.041}_{-0.035}$	$0.472^{+0.009}_{-0.011}$	$149.51^{+5.41}_{-6.02}$	$125.46^{+5.34}_{-5.47}$	$260.50^{+18.58}_{-18.63}$	0.25 ± 0.02	8.46 ± 0.57	0.97	0.30	372^{+25}_{-24}	0.36 ± 0.02	$7.89^{+0.21}_{-0.23}$	$7436.49^{+58.44}_{-47.48}$	$0.4047^{+0.0093}_{-0.0091}$	$95.6^{+2.9}_{-2.8}$	$148.0^{+2.3}_{-2.5}$	0.43	—
HD 32778	$5248.65^{+1.18}_{-2.37}$	$1.774^{+0.003}_{-0.002}$	0.346 ± 0.001	$426.36^{+0.14}_{-0.09}$	$168.75^{+0.28}_{-0.21}$	$131.69^{+8.92}_{-9.24}$	0.13 ± 0.01	$5.94^{+0.19}_{-0.20}$	2.28	0.14	$145.3^{+9.3}_{-10}$	0.14 ± 0.01	$5.97^{+0.19}_{-0.20}$	$5247.91^{+4.02}_{-4.38}$	$0.3440^{+0.0026}_{-0.0027}$	$92.2^{+1.5}_{-1.5}$	$169.07^{+0.53}_{-0.52}$	0.16	—
HD 33487	$1366.25^{+0.11}_{-0.09}$	$5.661^{+0.001}_{-0.002}$	0.155 ± 0.001	234.97 ± 0.05	$161.92^{+0.17}_{-0.20}$	$259.17^{+9.60}_{-9.80}$	0.25 ± 0.01	2.43 ± 0.04	4.77	0.32	331^{+11}_{-11}	0.32 ± 0.01	$2.487^{+0.040}_{-0.041}$	1366.25 ± 0.15	$0.15496^{+0.00072}_{-0.00075}$	$100.4^{+2.0}_{-2.0}$	$162.02^{+0.25}_{-0.23}$	0.40	—
HD 34101	803.63 ± 0.01	3.601 ± 0.001	0.084 ± 0.001	$269.82^{+0.03}_{-0.02}$	$273.99^{+0.20}_{-0.29}$	$160.85^{+14.01}_{-14.68}$	0.15 ± 0.01	$1.76^{+0.07}_{-0.08}$	14.58	0.16	205^{+20}_{-14}	$0.20^{+0.02}_{-0.01}$	$1.862^{+0.053}_{-0.061}$	803.62 ± 0.02	$0.08388^{+0.00050}_{-0.00049}$	79^{+13}_{-13}	$274.32^{+0.48}_{-0.48}$	0.20	Nidever et al. (2002)
HD 34540	$696.52^{+0.07}_{-0.09}$	$8.391^{+0.020}_{-0.013}$	0.033 ± 0.002	3430.25 ± 0.19	$149.29^{+2.98}_{-1.48}$	$361.11^{+23.40}_{-24.27}$	0.34 ± 0.02	1.69 ± 0.05	15.71	0.35	—	—	—	—	—	—	—	—	—
HD 39012	$3313.56^{+0.28}_{-0.54}$	3.565 ± 0.001	0.166 ± 0.001	$470.13^{+0.02}_{-0.03}$	$264.19^{+0.19}_{-0.22}$	$235.18^{+11.59}_{-11.82}$	0.22 ± 0.01	$4.48^{+0.10}_{-0.11}$	2.86	0.26	741^{+37}_{-37}	0.71 ± 0.04	$5.06^{+0.10}_{-0.10}$	3311.61 ± 1.79	$0.1634^{+0.0015}_{-0.0014}$	$151.86^{+0.65}_{-0.67}$	$263.21^{+0.55}_{-0.55}$	0.81	—
HD 40107	$4166.79^{+1.30}_{-1.81}$	$2.824^{+0.002}_{-0.003}$	$0.692^{+0.001}_{-0.002}$	$-251.00^{+0.20}_{-0.13}$	$93.02^{+0.14}_{-0.11}$	$134.37^{+4.56}_{-4.62}$	0.13 ± 0.01	4.87 ± 0.08	1.76	0.17	462^{+29}_{-27}	0.44 ± 0.03	$5.393^{+0.086}_{-0.087}$	$4173.35^{+9.86}_{-10.59}$	$0.705^{+0.017}_{-0.016}$	$24.1^{+132}_{-1.2}$	$94.6^{+2.0}_{-1.9}$	0.58	—
HD 42286	$9449.67^{+4.28}_{-2.97}$	3.754 ± 0.003	0.531 ± 0.001	$67.87^{+0.04}_{-0.05}$	17.08 ± 0.04	$274.86^{+13.87}_{-14.23}$	0.26 ± 0.01	$8.80^{+0.20}_{-0.21}$	1.24	0.35	358^{+16}_{-16}	0.34 ± 0.02	$9.02^{+0.20}_{-0.20}$	9447.92 ± 9.50	$0.53078^{+0.00056}_{-0.00056}$	$99.9^{+1.0}_{-1.1}$	$17.08^{+0.12}_{-0.12}$	0.45	—
HD 43848	$2345.72^{+2.00}_{-3.78}$	$2.537^{+0.003}_{-0.065}$	$0.916^{+0.001}_{-0.002}$	$-178.73^{+0.41}_{-0.29}$	$203.12^{+0.35}_{-0.25}$	$61.17^{+3.52}_{-3.51}$	0.06 ± 0.01	3.38 ± 0.08	3.11	0.07	$135.8^{+7.4}_{-7.2}$	0.13 ± 0.01	$3.463^{+0.081}_{-0.084}$	$2343.63^{+3.21}_{-3.36}$	$0.9746^{+0.0020}_{-0.0041}$	82^{+18}_{-17}	$192.27^{+1.0}_{-0.45}$	0.15	Sahlmann et al. (2011b)
HD 45701	$18709.40^{+12.78}_{-13.20}$	2.691 ± 0.006	0.166 ± 0.002	$63.47^{+0.21}_{-0.26}$	$118.33^{+0.46}_{-0.41}$	$389.21^{+38.22}_{-40.29}$	0.37 ± 0.04	$16.00^{+0.71}_{-0.78}$	0.80	0.31	688^{+59}_{-62}	0.66 ± 0.06	$16.89^{+0.71}_{-0.78}$	18708.84 ± 13.15	$0.1646^{+0.0048}_{-0.0047}$	$49.15^{+0.27}_{-0.27}$	$118.29^{+0.59}_{-0.59}$	0.55	—
HD 46569	$9335.06^{+2.66}_{-2.51}$	$1.712^{+0.001}_{-0.002}$	0.585 ± 0.001	$58.31^{+0.05}_{-0.07}$	$278.71^{+0.07}_{-0.08}$	$195.13^{+14.52}_{-15.08}$	0.19 ± 0.01	$10.49^{+0.37}_{-0.40}$	1.21	0.12	310^{+22}_{-23}	0.30 ± 0.02	$10.69^{+0.37}_{-0.40}$	9334.33 ± 9.50	$0.5848^{+0.0010}_{-0.0010}$	$44.74^{+0.66}_{-0.62}$	$278.55^{+0.22}_{-0.23}$	0.19	—
HD 48189	254.33 ± 0.01	10.383 ± 0.024	0.590 ± 0.002	12.25 ± 0.26	196.92 ± 0.21	$263.17^{+20.44}_{-21.24}$	0.25 ± 0.02	0.85 ± 0.03	56.17	0.25	—	—	—	—	—	—	—	—	Zúñiga-Fernández et al. (2021)
HD 52698	$3013.66^{+0.46}_{-0.43}$	$4.947^{+0.007}_{-0.005}$	0.763 ± 0.001	$116.65^{+0.03}_{-0.04}$	$181.31^{+0.06}_{-0.07}$	$203.58^{+8.84}_{-9.05}$	0.19 ± 0.01	$4.14^{+0.08}_{-0.09}$	3.91	0.23	248^{+10}_{-10}	0.24 ± 0.01	$4.197^{+0.082}_{-0.086}$	3013.75 ± 0.66	$0.7630^{+0.0010}_{-0.0010}$	$104.1^{+1.1}_{-1.2}$	$181.339^{+0.085}_{-0.085}$	0.28	—
HD 53680	$1685.20^{+0.37}_{-0.38}$	$1.252^{+0.001}_{-0.002}$	0.481 ± 0.001	$147.86^{+0.06}_{-0.08}$	$226.17^{+0.13}_{-0.17}$	$51.33^{+1.95}_{-1.99}$	0.05 ± 0.01	2.53 ± 0.05	3.46	0.07	—	—	—	—	—	—	—	—	Sahlmann et al. (2011b)
HD 58696	345.28 ± 0.01	$18.545^{+0.010}_{-0.007}$	0.899 ± 0.001	231.34 ± 0.02	$336.05^{+0.03}_{-0.02}$	$337.58^{+34.91}_{-36.75}$	$0.32^{+0.03}_{-0.04}$	$1.14^{+0.05}_{-0.06}$	35.17	0.24	228^{+65}_{-28}	$0.22^{+0.06}_{-0.03}$	$1.176^{+0.062}_{-0.083}$	$362.59^{+0.04}_{-17.17}$	$0.9823^{+0.0077}_{-0.051}$	88^{+30}_{-21}	310^{+26}_{-36}	0.16	Tokovinin (2014)
HD 59099	2312.88 ± 0.54	$5.515^{+0.003}_{-0.005}$	0.598 ± 0.001	$50.04^{+0.13}_{-0.10}$	$64.21^{+0.09}_{-0.10}$	$339.17^{+29.36}_{-30.83}$	0.32 ± 0.03	$4.01^{+0.16}_{-0.17}$	3.30	0.25	603^{+54}_{-57}	0.58 ± 0.05	$4.18^{+0.16}_{-0.17}$	$2311.52^{+2.89}_{-43.83}$	$0.5968^{+0.0036}_{-0.041}$	$134.3^{+1.2}_{-86}$	$64.02^{+0.35}_{-6.0}$	0.45	Tokovinin (2014)
HD 59380	998.45 ± 0.06	2.966 ± 0.003	$0.560^{+0.002}_{-0.001}$	$150.62^{+0.13}_{-0.34}$	$358.22^{+0.12}_{-0.28}$	$145.43^{+10.79}_{-11.23}$	0.14 ± 0.01	2.22 ± 0.08	8.05	0.11	—	—	—	—	—	—	—	—	Fekel et al. (2018)
...	...	...	...	...	...	...	...	...	...	...	...	...	...	...	...	...	...	...	...

Notes. We note that systems with mass ratio $q > 0.6$ could in principle be affected by photocenter bias leading to underestimating the barycentric semimajor axis at most by 5-9%. Full table is available at the CDS. A portion is shown here for guidance regarding its form and content.

new inner stellar companion (see Sects 5.2–5.4 for more details on the specific systems).

4. Astrometric constraints

To achieve a more complete characterisation of the orbital parameters of the stellar companions of the CORALIE sample identified in our radial velocity analysis, we used the variations in the proper motion measurements, $\delta\mu$, in conjunction with the radial velocity data we previously analysed separately in Sect. 3 to derive precise dynamical mass and orbits for the massive companions in the sample. Specifically, we used the proper motion anomalies between the HIPPARCOS (Perryman et al. 1997) and *Gaia* (Gaia Collaboration 2016) epochs, which have been shown to be able to detect accelerations as small as a few μas yr^{-2} (Sahlmann 2016; Brandt 2018). Such an approach has been used more and more often in recent years to characterise both stellar and substellar companions successfully (see e.g. Calissendorff & Janson 2018; Snellen & Brown 2018; Kervella et al. 2019a,b,c, 2020, 2022; Brandt et al. 2019, 2020, 2021a; Damasso et al. 2020a,b; Makarov et al. 2021a,b; Venner et al. 2021; Feng et al. 2021; Llop-Sayson et al. 2021), especially with the advent of more and more precise proper motion measurements provided by the different *Gaia* Data Releases.

In this work, we use the proper motion measurements provided by *Gaia* EDR3, which are (on average) about three to four times more precise than those provided by the previous *Gaia* DR2 (Gaia Collaboration 2021; Lindegren et al. 2021; Brandt 2021). More specifically, we use the variations $\Delta\mu_{\alpha,\delta}$ from a purely linear motion as reported in the HIPPARCOS-*Gaia* Catalog of Accelerations (HGCA, Brandt 2018, 2021), where the HIPPARCOS and *Gaia* EDR3 catalogues have been cross-calibrated to account for systematics and shift all proper motions in the *Gaia* EDR3. For this purpose, we used the open source code `orvara` (Brandt et al. 2021b), an MCMC orbit-fitting code that is able to fit Keplerian orbits to any combination of HGGA proper motion variations, absolute astrometry, relative astrometry, and radial velocities to obtain precise dynamical masses and orbital elements. We used a version of `orvara` that has been especially modified to accept priors on orbital periods and semi-major axes[2], in addition to the priors on primary mass and stellar jitter already included in the original version of the code, to help in achieving better convergence and more constrained orbital elements, especially for intermediate-separation binaries.

We found that there are 40 stars in our binary sample not included in the HGCA, leaving us with 178 stars for which the simultaneous use of proper motion anomalies and radial velocity is (in principle) viable. For each of them, we imposed priors on the primary mass equal to the stellar masses obtained with the SED fits (see Sect. 2) and on orbital periods equal to the periods retrieved from the radial velocity analysis (see Sect. 3).

As the use of proper motion anomaly is based on two measurements separated by almost 25 yr, the method is clearly more efficient for long orbital periods (Kervella et al. 2019a); when analysing the entirety of our sample in such a manner, which (as discussed in Sect. 3) features a large variety of orbital periods, special precautions must be taken. This is particularly evident when comparing the semimajor axes for the companions in the sample, as characterised by radial velocities alone with those resulting from the `orvara` simultaneous fit of proper motion variations and radial velocities. Such a comparison, shown in Fig. 4, highlights a broad discrepancy between the values obtained by the two methods for the companions whose radial velocities were characterised as having shorter separations; in addition, it shows that `orvara` typically overestimates the orbital periods of such close-in stellar companions. For the purposes of this work, we identified $a_{\rm RV} \sim 1$ au as a reasonable threshold above which astrometry constraints are indeed helpful in constraining the orbital elements of the stellar companions in our sample. We decided to focus our following analysis only on the 132 stars in our sample for which our radial velocity analysis

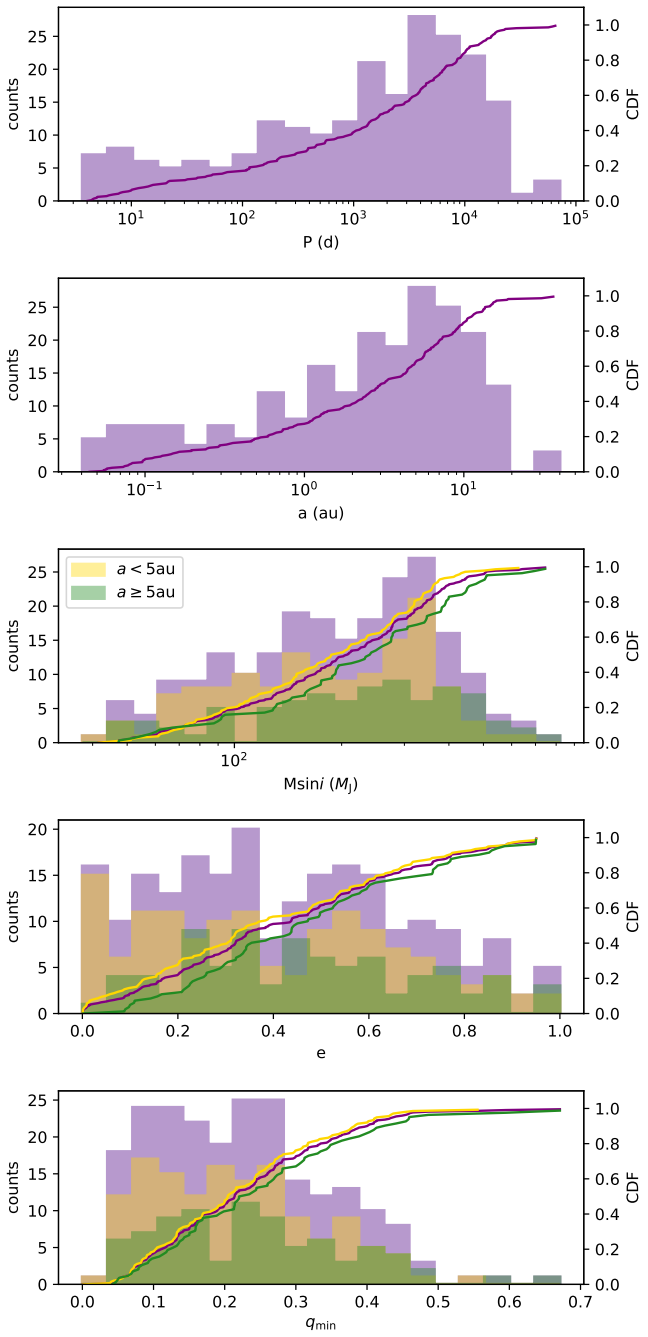

Fig. 2. Distributions of orbital period, semimajor axis, minimum mass, eccentricity, and mass ratio q of the $M \sin i > 40\ M_{\rm Jup}$ companions identified in the sample and characterised via radial velocity analysis. The minimum masses, eccentricity, and q distributions for inner ($a < 5$ au) and outer ($a \geq 5$ au) companions found in the sample are shown in yellow and green, respectively.

[2] https://github.com/nicochunger/orvara/tree/period-prior

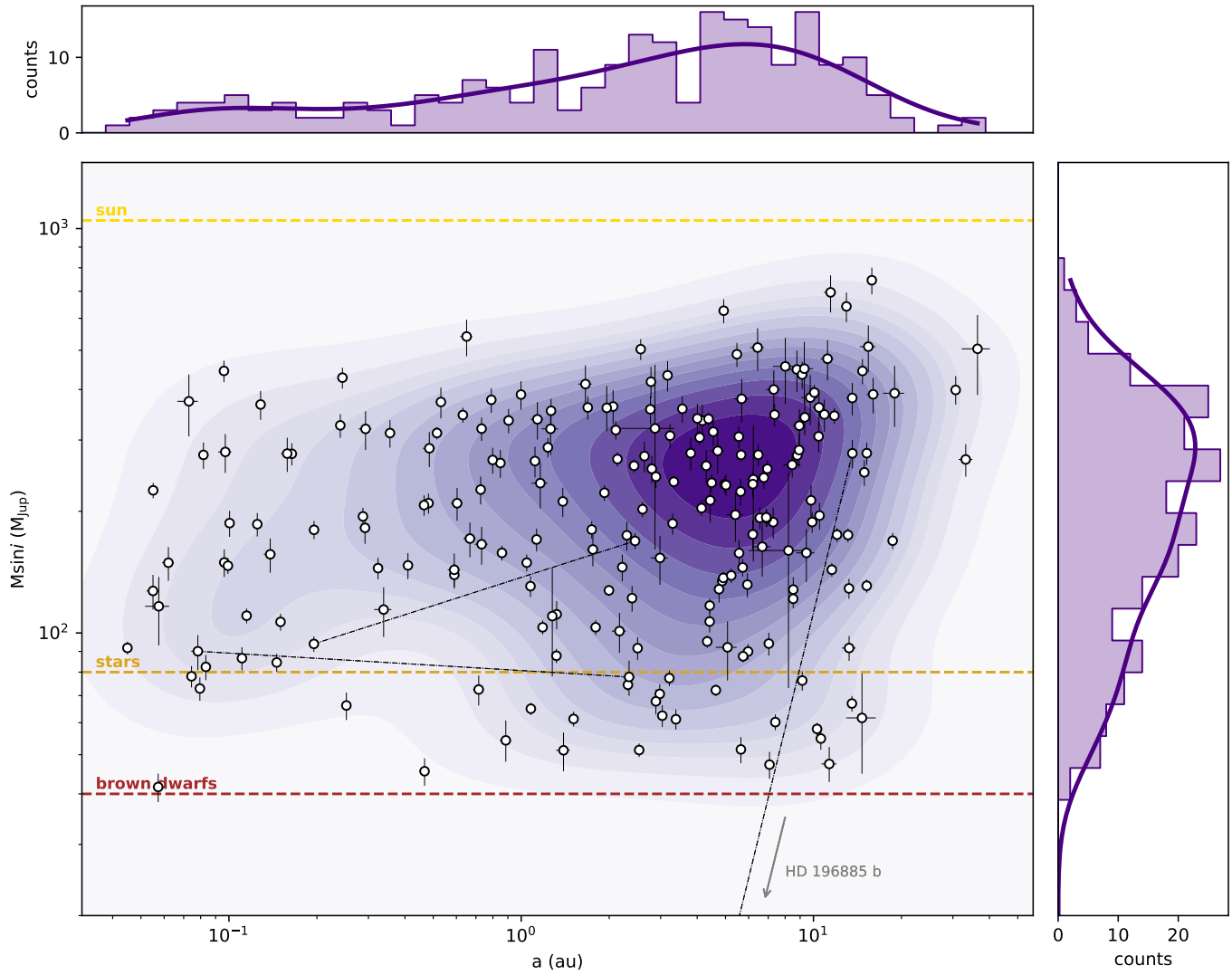

Fig. 3. Distribution in the M sin i-a parameter space of the M sin $i > 40\ M_{Jup}$ companions identified in the sample and characterised via radial velocity analysis. In the main plot, the kernel density estimation of the population is plotted as contour levels, the components of multiple systems are connected by black dash-dotted lines, while the horizontal dashed brown, orange and yellow lines respectively indicate the brown dwarf ($40\ M_{Jup}$), dwarf star ($80\ M_{Jup}$), and solar-mass thresholds. The top-left and right-hand histograms show the distribution and kernel density estimation of the semimajor axes and minimum mass of the companions, respectively.

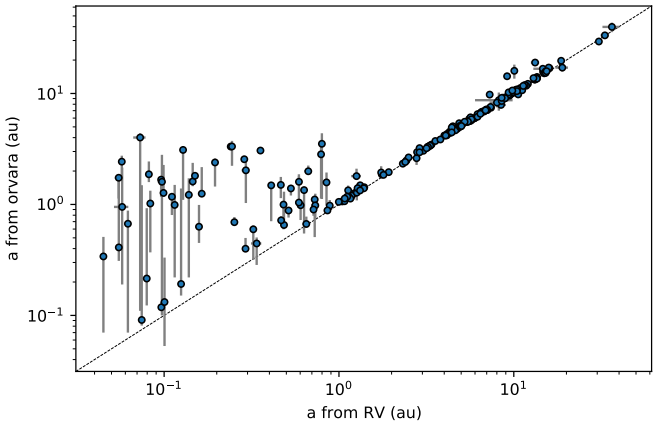

Fig. 4. Comparison between the best-fit semimajor axes obtained by the simultaneous fitting of radial velocity timeseries and proper motions variations and those obtained by the fitting of radial velocities alone.

identified a companion with semimajor axis greater than 1 au. In the cases of HD 206276 and HD 94340, both being triple star systems hosting one companion below 1 au, we performed the `orvara` analysis using, as the radial velocity time series, the residuals obtained after subtracting the Keplerian signal of the inner stellar companion at 0.19 and 0.08 au, respectively, so that the time series used for the simultaneous fit contain (in principle) only the contribution of the outer companions in the systems. Lastly, we must note that binary systems with mass ratios $q > 0.6$ could (in principle) be affected by the luminosity of the secondary companion shifting the photocenter orbit from the primary orbit. To account for this, we analysed all the CCFs for the systems having such mass ratios, failing to detect any secondary peak; this corresponds to a lower limit on magnitude ratio of 2.5–3.0, which would lead (at most) to a barycentric semimajor axis underestimation of 5–9%.

A summary of the best-fit solutions obtained for these 132 systems using `orvara` is listed in Table 2, while Fig. 5 compares the distributions of the stellar companions, as characterised by radial velocity alone as well as the simultaneous use of

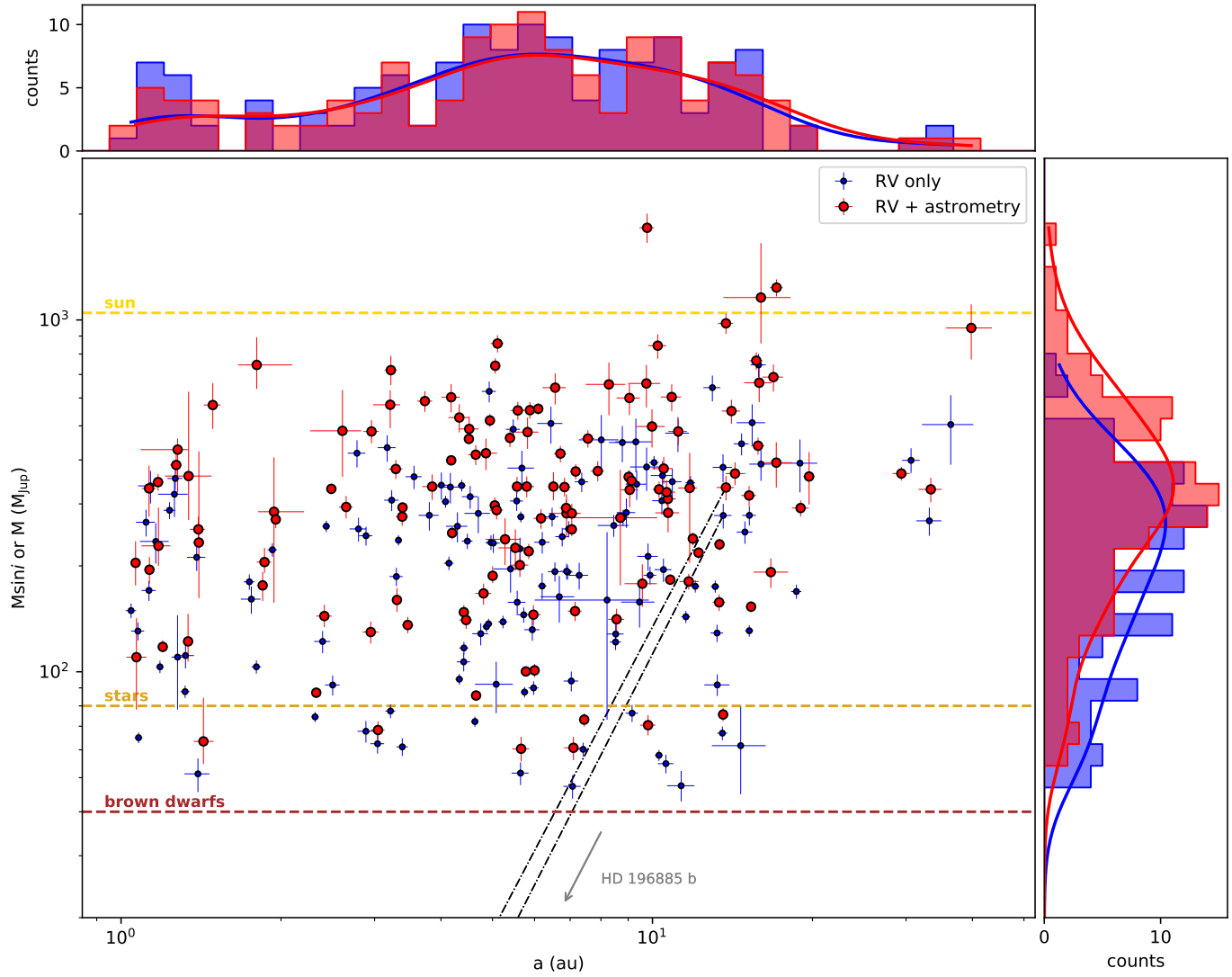

Fig. 5. Comparison between the distributions in the $M \sin i$-a parameter space of the $M \sin i > 40\,M_{\rm Jup}$ companions orbiting the 132 stars in the sample for which we performed simultaneous radial velocity and proper motion anomaly fits. The blue dots and histogram show the parameter space position and distribution of semimajor axes and minimum mass, respectively, as retrieved by the radial velocity analysis alone, while the respective red plot elements refer instead to the results of the simultaneous astrometry and radial velocity fits, and, therefore, true dynamical mass instead of minimum mass. The components of multiple systems are connected by gray dash-dotted lines, while the horizontal dashed brown, orange, and yellow lines respectively indicate the brown dwarf (40 $M_{\rm Jup}$), dwarf star (80 $M_{\rm Jup}$), and solar-mass (1047.58 $M_{\rm Jup}$) thresholds.

radial velocity and proper motion anomaly. Generally speaking, this plot shows again the good agreement in orbital separations for the companions in the sample between the two different solutions, with the semimajor axis distribution from the radial velocity fits alone and the one obtained with the addition of proper motion anomalies peaking both at ∼6.30 au. Another item of clear interest is the comparison between the mass distributions obtained by the two solutions, as the determination of orbital inclinations derived from the use of astrometry permits the derivation of the true dynamical mass of the stellar companions, shifting the peak of the mass distribution upwards to ∼343 $M_{\rm Jup}$ (∼0.33 $M_\odot$), from the peak value of ∼262 $M_{\rm Jup}$ (∼0.25 $M_\odot$) for the $M \sin i$ distribution derived from radial velocity alone. Figure 6 shows a comparison between the values of selected orbital parameters of $M \sin i > 40\,M_{\rm Jup}$ companions, as obtained by radial velocities and those obtained using also astrometry constraints, while Fig. 7 shows the distribution of the same parameters as obtained by the simultaneous radial velocity and proper motion anomaly fits. Once again, we generally find a good agreement between the orbital separations found from the two solutions and between the eccentricities as well. As done for the orbital parameters obtained from the radial velocity solutions (see Sect. 3) we again performed Kolmogorov–Smirnov tests to search for significant differences in the distributions of the properties of inner ($1 \le a < 5$ au) and outer ($a \ge 5$ au) companions, this time finding no significant difference between the respective distributions of true mass ($p = 0.39$) and eccentricities ($p = 0.66$).

The true masses derived from the simultaneous fit once again show that the majority of the companions found in the sample lie below the solar mass value within the respective uncertainties, although the precise estimate of orbital inclination provided by the astrometry measurements allow some companions to reveal themselves to have a true mass greater than 1 $M_\odot$. Specifically, these are the ones found orbiting HD 27019 ($M = 1.74 \pm 0.17\,M_\odot$), HD 223084 ($M = 0.93 \pm 0.06\,M_\odot$), HD 173872

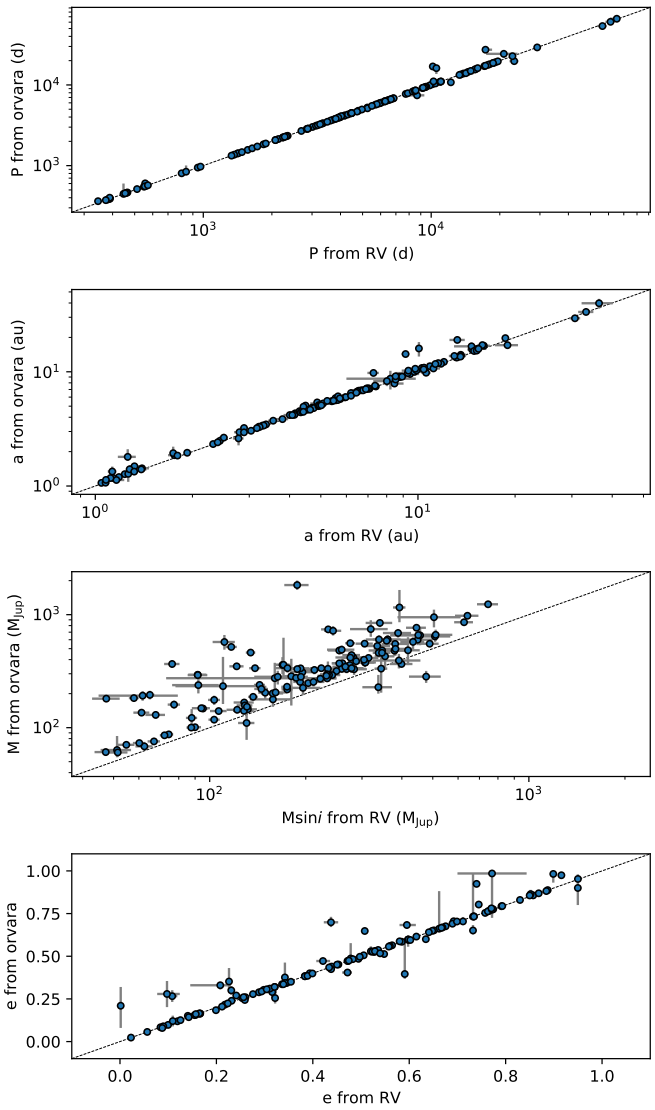

Fig. 6. Comparison between the best-fit orbital period, semimajor axis, minimum (or true) mass and eccentricity values of $M \sin i > 40\,M_{\rm Jup}$ companions as obtained by the simultaneous fitting of radial velocity time series and proper motion variations and those obtained by the fitting of radial velocities alone for the 132 stars considered in Sect. 4.

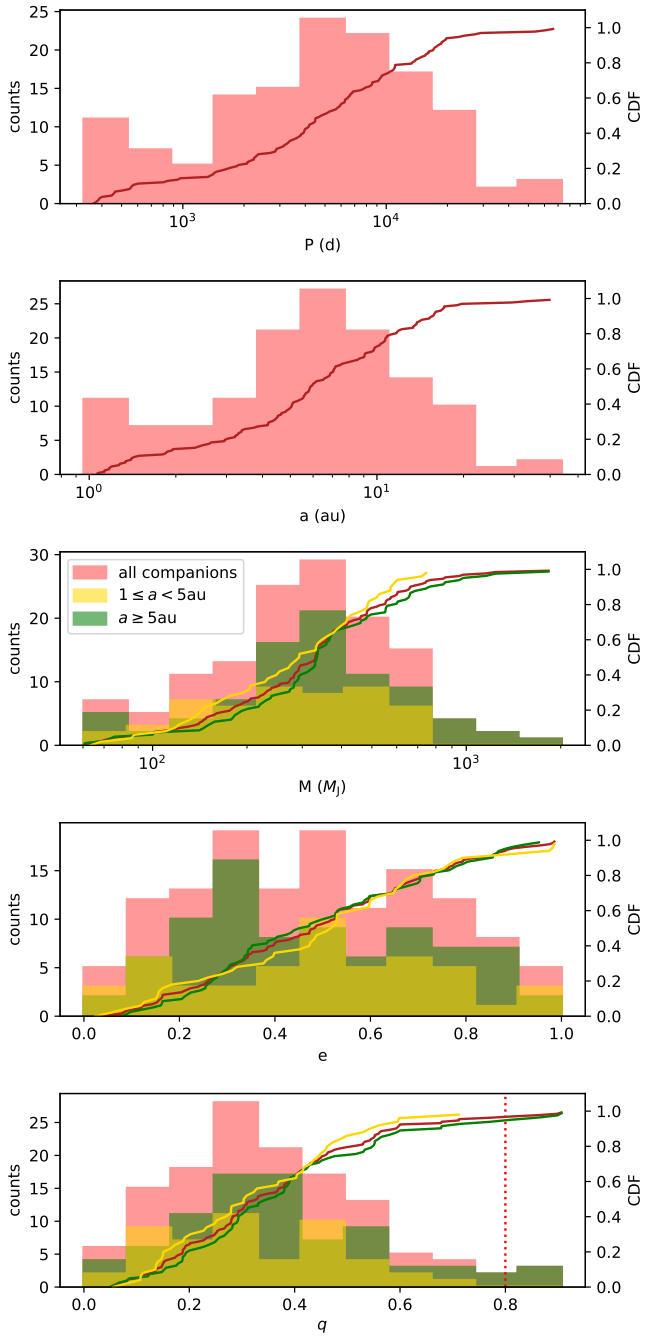

Fig. 7. Distributions of orbital period, semimajor axis, minimum mass, eccentricity, and mass ratio q of $M \sin i > 40\,M_{\rm Jup}$ companions as obtained by the simultaneous radial velocity and proper motion anomaly fits for the 132 stars considered in Sect. 4. The minimum masses, eccentricity, and q distributions for inner ($1 \leq a < 5$ au) and outer ($a \geq 5$ au) companions found in the sample are shown in yellow and green, respectively.

($M = 1.10^{+0.47}_{-0.29}\,M_\odot$), HD 181199A ($M = 1.18 \pm 0.06\,M_\odot$), and HD 3795 ($M = 0.90^{+0.15}_{-0.17}\,M_\odot$).

As previously described in Sect. 3, we followed Halbwachs et al. (2003) and selected a threshold of mass ratio $q > 0.8$ for SB2s in the sample, this time using the companion true mass values obtained by the joint radial velocity and proper motion anomalies analysis. By virtue of the true masses derived, this time we found four systems to have $q > 0.8$, namely, HD 3795 ($q = 0.86$), HD 39012 ($q = 0.81$), HD 181199A ($q = 0.90$), and HD 223084 ($q = 0.90$), which are therefore possible undetected blended binaries.

In addition to the companions detected in this sample we also report some results from Unger et al. (in prep.) in which a similar joint analysis of radial velocity and astrometric measurements is performed on the planetary companions detected in the CORALIE sample. Specifically, the possible brown dwarf companions found to be orbiting stars HD 162020 and HD 112758, having respective minimum masses of $14.96 \pm 0.53\,M_{\rm Jup}$ and $32.7 \pm 1.9\,M_{\rm Jup}$ are found to have true masses of $0.392 \pm 0.005\,M_\odot$ and $0.245 \pm 0.001\,M_\odot$. While we shall not go into the details of the orbital solutions of these two companions in the present work, as they are thoroughly analysed in Unger et al. (in prep.), here these additional stellar objects in the CORALIE sample are considered in the analysis of occurrence rates detailed in Sect. 13.

5. A few notable cases

5.1. Brown dwarfs in the sample

Following the radial velocity analysis detailed in Sect. 3, we find 28 companions in the sample to have a minimum mass between 40 and 80 $M_{\rm Jup}$ which are therefore describable as possible brown dwarfs. While the low number of such companions found in the sample does not allow for robust statistical analysis, it is possible to note that most of them are found at orbital separations larger than 0.5 au from the primary star, in a further example of the brown dwarfs desert observed around solar-type stars (Grether & Lineweaver 2006; Shahaf & Mazeh 2019; Kiefer et al. 2019). As the simultaneous fit of radial velocities and proper motion anomalies performed and discussed in Sect. 4 allows for the determination of orbital inclination and, therefore, the true mass of the companions, it is of clear interest to discuss how many and which of these possible brown dwarfs are confirmed to be as such by this analysis – and which would instead be revealed as stellar companions.

Firstly, it is important to note that the primary stars hosting three of these possible brown dwarf companions (i.e. those found orbiting HD 53680, HD 153284, and HD 184860A) are not included in the HGCA and, therefore, no astrometric analysis is possible for these stars; in addition, seven additional possible brown dwarf companions (HD 3277, HD 28454, HD 30774, HD 89707, HD 151528, HD 164427A, and HD 219709) are found to be on orbits tighter than the 1 au threshold that we have set for reliable analysis with `orvara`. Thus, this leaves us with 18 such companions for which we are able to determine true masses and confirm or reject their nature as brown dwarfs.

Of these 18 objects, our use of proper motion anomalies confirmed 7 companions (those orbiting HD 4747, HD 17289, HD 30501, HD 74014, HD 112863, HD 167665, and HD 206505) to remain in the brown dwarf mass range, while the remaining 11 (orbiting HIP 22059, HD 17155, HD 20916, HD 43848, HD 78746, HD 87359, HD 94340, HD 119559, HD 154697, HD 195010, and HD 217580) are found to have a true mass above 80 $M_{\rm Jup}$ and are therefore revealed to be stellar companions. Of the latter, the companion characterised by the larger difference in minimum and true mass is the one found orbiting star HD 119559, which starting from a minimum mass of $76.267^{+4.149}_{-4.274}$ $M_{\rm Jup}$ is revealed by astrometric constraints to have a true mass of 0.35 ± 0.02 $M_\odot$.

Finally, we report further results from Unger et al. (in prep.), as done in Sect. 4, where the usage of *Gaia* DR3 astrometric measurements allow for 4 of the aforementioned 11 possible brown dwarf companions to be revealed as stellar companions, having a true mass above 80 $M_{\rm Jup}$. These are: the ones found around HD 3277 ($0.468^{+0.023}_{-0.005}$ $M_\odot$), HD 89707 (0.100 ± 0.001 $M_\odot$), HD 151528 ($0.1403^{+0.0001}_{-0.0030}$ $M_\odot$), and HD 164427A ($0.3369^{+0.003}_{-0.002}$ $M_{\rm Jup}$). As mentioned before, we refer to Unger et al. (in prep.) for further details on the respective orbital solution, in the present work, we consider them as stellar companions in the occurrence rates analysis detailed in Sect. 6.2.

5.2. A new triple star system: HD206276 (HIP107143)

The possible presence of a long-period massive companion around K3 V star HD 206276 was first noted in Goldin & Makarov (2007), in which the use of a genetic optimisation-based algorithm allowed for obtain additional orbital solutions for a subsample of HIPPARCOS stars with previous stochastic solutions. In the cited work, HD 206276 was reported as possibly hosting a massive companion on a 1338^{+171}_{-73} d orbit with a $0.14^{+0.21}_{-0.11}$ eccentricity and an orbital inclination of 40 ± 6 deg. However, no radial velocity measurements have been published since, nor used to confirm that companion or to provide a better orbital solution for the system.

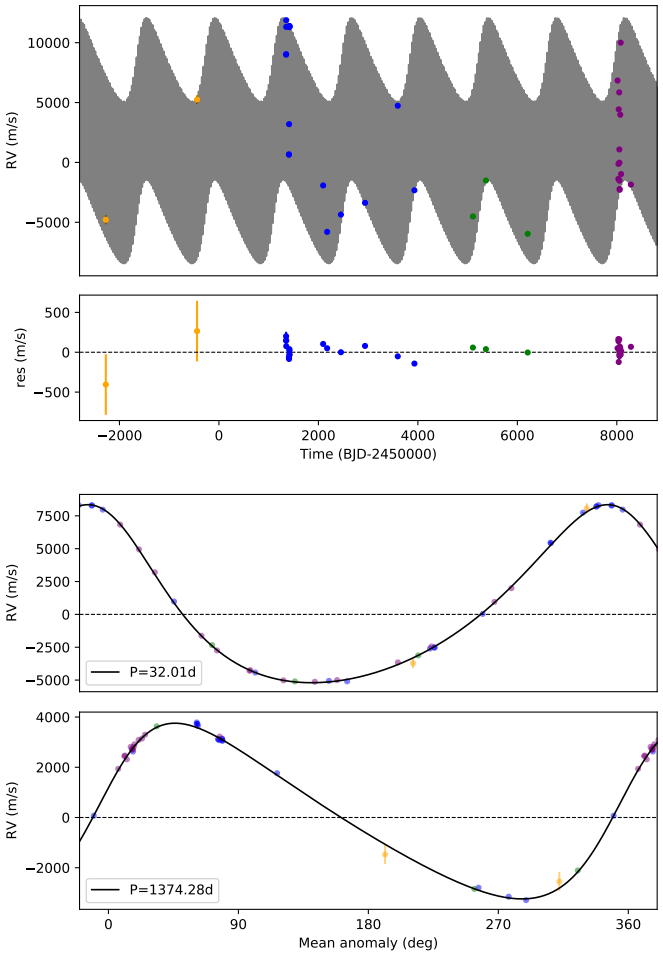

Fig. 8. Radial velocity best-fit solution and phase folded model curves for triple stellar system HD 206276, with CORAVEL, CORALIE98, CORALIE07, and CORALIE14 measurements shown in orange, blue, green, and purple, respectively.

Within the scope of the CORALIE exoplanetary search, we have observed HD 206276 over a total of 6932 d collecting 35 radial velocity measurements (divided as 18 C98, 3 C07, and 14 C14); the additional usage of two CORAVEL measurements brings the total of data points available for our analysis to 37 over the course of 10584 d. We identify, in the time series periodogram, a highly significant peak (FAP = 4.3×10^{-6}) at 32 d, with an one-Keplerian residual peak present at 1363 d with FAP = 3.1×10^{-4} corresponding to the astrometric signal reported in Goldin & Makarov (2007), with no further significant signals present in the two-Keplerian residuals. We therefore present our two-Keplerian best-fit model (shown in Fig. 8) with which we confirm the presence of the outer companions having an orbital period of $P_{\rm C} = 1374.27 \pm 0.97$ d, semiamplitude of $K_{\rm C} = 3.50 \pm 0.03$ kms^{-1}, and eccentricity of $e_{\rm C} = 0.275 \pm 0.008$. We also report the detection of an inner companion with $P_{\rm B} = 32.005 \pm 0.0002$ d, $K_{\rm B} = 6.8 \pm 0.03$ kms^{-1} and eccentricity of $e_{\rm B} = 0.255 \pm 0.003$. By virtue of the primary star having a mass of $0.88^{+0.06}_{-0.05}$ $M_\odot$ (see Sect. 2), we derived values for the minimum masses and semimajor axes of $168.89^{+7.59}_{-7.66}$ $M_{\rm Jup}$ (corresponding

to $0.161 \pm 0.007\,M_{\odot}$) and 2.45 ± 0.05 au for the outer companion and of $93.96^{+4.09}_{-4.19}\,M_{\rm Jup}$ (corresponding to $0.089 \pm 0.004\,M_{\odot}$) and 0.195 ± 0.004 au for the inner one.

As mentioned in Sect. 4, when performing the simultaneous fit of radial velocities and proper motion anomaly with `orvara`, we first subtracted the Keplerian signal of the inner companion, since its short period of 32 d is not detectable through the use of proper motion measurements at the two HIPPARCOS and *Gaia* epochs, thereby using, for the joint analysis, a radial velocity time series containing (in principle) only the contribution of the outer companion. However, we find the joint `orvara` to be unable to converge, failing to constrain the orbital elements of the outer stellar companions, likely due to the 32 d stellar companion still producing a significant astrometric contribution to the proper motion anomalies. The same failure to converge is obtained when trying to model the triple system by jointly fitting our radial velocity with the HIPPARCOS epoch astrometric time series via the kepmodel python package (see Delisle et al. 2016; Delisle & Ségransan 2022) and the samsam MCMC sampler (e.g. Delisle et al. 2018). We additionally note that this triple system is not listed amongst the *Gaia* DR3 astrometric orbital solutions validated in Holl et al. (2023), further highlighting the difficulties in disentagling the astrometric signature of the inner stellar companion. For this system, we are therefore able to provide only the orbital solutions resulting from the radial velocity fit alone.

5.3. An updated triple star system: HD 94340 (HIP53217)

First hints of the multiple nature of the G4 V star HD 94340 were reported in Makarov & Kaplan (2005), where the presence of a stellar companion to the primary star is suggested by the detection of a large proper motion acceleration between HIPPARCOS and *Tycho*-2 measurements. More specifically, using preliminary results from the CORALIE survey, Tokovinin et al. (2006) reported the presence of a stellar companion with an orbital period of 6.8 d and hints of a possible second massive companion at 1200 d; a joint analysis of HIPPARCOS proper motion anomaly, adaptive optics, and speckle interferometry presented in Tokovinin et al. (2012) confirm the triple nature of the system, with an inner companion of 6.8 d and an outer one with an estimated orbital period of 3.3 yr period and 40 mas axis unresolved by speckle interferometry.

Over the course of our survey, we collected a total of 63 radial velocity measurements (17 CORAVEL, 10 C98, 20 C07, and 16 C14) with an observational time span of 11772 d. The timeseries periodogram features a high significance (FAP = 1.8×10^{-45}) peak at 6.84 d and the one-Keplerian solution residuals show an additionally highly significant (FAP = 9.6×10^{-19}) signal at 1120 d, both signals clearly consistent with literature values, with no further residual significant peak and no correspondence between the identified significant peaks and stellar activity signals among the activity indicators analysed. According to our two-Keplerian best-fit model (shown in the top two rows of Fig. 9), we find the inner companion to have an orbital period $P_{\rm B} = 6.84 \pm 0.01$ d, semiamplitude $K_{\rm B} = 8.182 \pm 0.003\,{\rm kms}^{-1}$ and eccentricity $e_{\rm B} = 0.009 \pm 0.001$; while for the outer companion, we find $P_{\rm C} = 1122.96^{+0.60}_{-0.48}$ d, $K_{\rm C} = 1.356^{+0.008}_{-0.010}\,{\rm kms}^{-1}$ and $e_{\rm C} = 0.305 \pm 0.004$; having obtained from the SED fit of the primary star (see Sect. 2) a stellar mass of $1.28^{+0.15}_{-0.19}\,M_{\odot}$ we derive values of minimum masses and semimajor axes of $90.08^{+8.71}_{-9.13}\,M_{\rm Jup}$ and 0.08 ± 0.01 au for the inner companion and of $77.85^{+7.54}_{-7.93}\,M_{\rm Jup}$ and $2.34^{+0.11}_{-0.12}$ au for the outer companion.

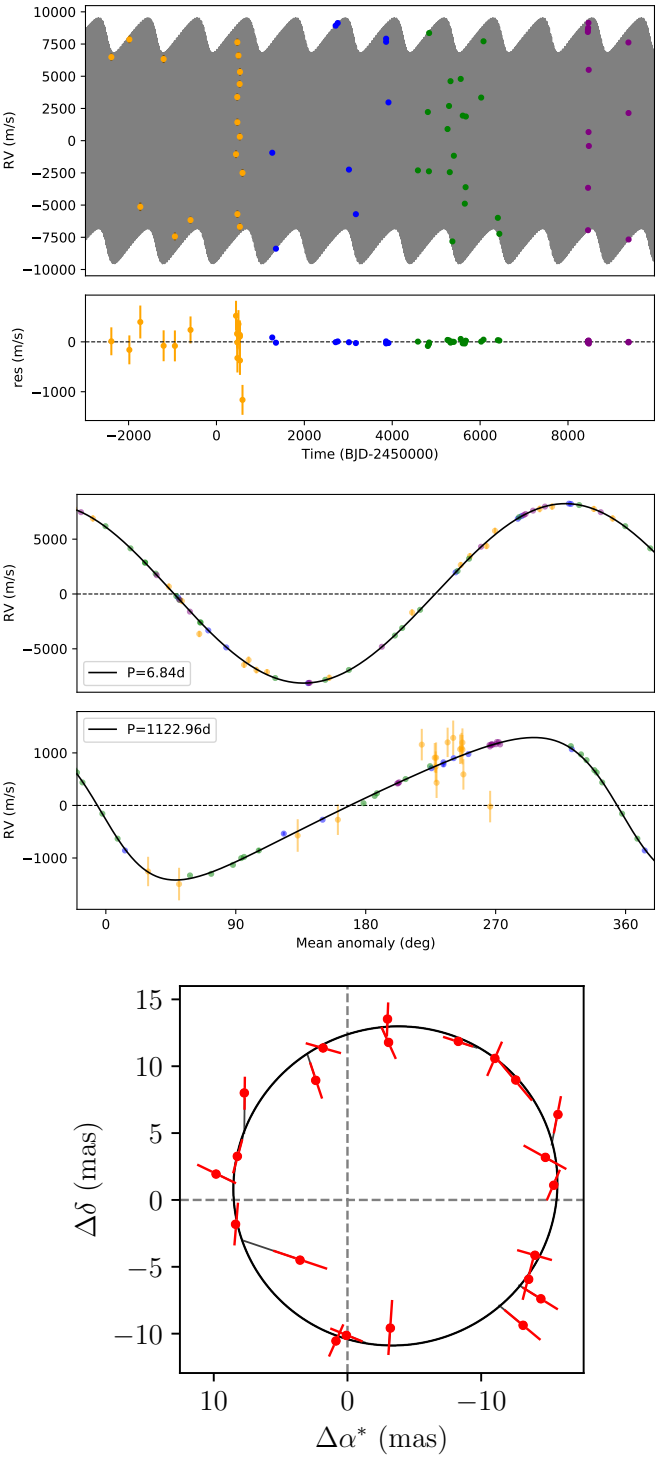

Fig. 9. Top two rows: radial velocity best-fit solution and phase folded model curves for triple stellar system HD 94340, with CORAVEL, CORALIE98, CORALIE07, and CORALIE14 measurements shown in orange, blue, green, and purple, respectively. Bottom panel: best-fit solution astrometric orbit induced by HD 94340C. HIPPARCOS intermediate astrometric data shown in red.

As mentioned in Sect. 4 and done previously for HD 206276, we subtract from the radial velocity timeseries the Keplerian signal of the 6.84 d inner companion, performing the `orvara` fit using the obtained residuals. From the results of this simultaneous radial velocity and proper motion anomaly fit we find

for the outer companion a true mass of $M_C = 269^{+51}_{-45}\,M_{\rm Jup}$ (corresponding to $0.26^{+0.05}_{-0.04}\,M_\odot$), inclination $i_C = 18.2^{+2.8}_{-2.3}$ deg, with values of semimajor axis ($a_C = 2.44^{+0.11}_{-0.12}$ au), and eccentricity ($e_C = 0.332^{+0.023}_{-0.022}$) showing good agreement with those derived from fitting the radial velocity measurements alone.

We additionally note that the outer stellar companion in this system is part of the *Gaia* DR3 astrometric orbital solutions validated in Holl et al. (2023), where it is characterised by an orbital period of 1213.8 ± 22.0 d and eccentricity of 0.30 ± 0.01. The inclination corresponding to this solution is $i_C = 20.9^{+1.1}_{-1.3}$ deg, the companion's true mass is $M_C = 0.37 \pm 0.03\,M_\odot$, and the relative semi-major axis is $a_C = 2.63^{+0.12}_{-0.13}$ au. This astrometric-only solution would correspond to a minimum-mass of $M_C \sin i_C = 137 \pm 15\,M_{\rm Jup}$ or $0.131 \pm 0.015\,M_\odot$, which we note is larger by a factor 1.75 than the radial velocity solution. The parallax is 22.508 ± 0.036 instead of 19.72 ± 0.56 for the *Gaia* DR3 single-star solution.

Moreover, we additionally carried out a joint analysis of the radial velocity and HIPPARCOS epoch astrometric time series, using the kepmodel python package (see Delisle et al. 2016; Delisle & Ségransan 2022) and the samsam MCMC sampler (e.g. Delisle et al. 2018). While the inclination of the inner 6.8 d companion remains, as expected, unconstrained, the outer 1100 d companion is detected by HIPPARCOS and its inclination and true mass are constrained. We find an inclination of $i_C = 13.2 \pm 0.8$ deg, corrsponding to a true mass of $M_C = 0.39 \pm 0.04\,M_\odot$. The relative semi-major axis is $a_C = 2.5 \pm 0.1$ au (53.8 ± 2.7mas) and we found an orbital period for the outer companion of 1122.9 ± 0.4 d, an eccentricity of $0.305^{+0.004}_{-0.003}$, $\omega_C = 98.9^{+0.7}_{-0.8}$ deg, $\Omega = 8.6 \pm 4.0$ deg, and a revised parallax of $21.4^{+0.7}_{-0.8}$ mas instead of the 19.58 ± 1.46 mas reported for the HIPPARCOS single-star solution.

We find some discrepancy between the joint HIPPARCOS and radial velocity solution, the `orvara` solution, and the *Gaia* DR3 astrometric orbit solution, in particular between the respective outer companion orbital inclination values. We note that the orbital period is slightly longer than the *Gaia* DR3 timespan, which typically makes the *Gaia* DR3 solution less accurate. Moreover, the errorbars of the *Gaia* DR3 solution are probably underestimated, which is confirmed by the poor matching between the *Gaia* DR3 period and the well determined RV period (about 4σ). Finally, in this regime of period, the `orvara` solution is expected to be more sensitive to the *Gaia* scanning-law, which could lead to inaccurate results. We therefore adopted the joint HIPPARCOS and radial velocity solution for this system.

5.4. A planet-hosting system: HD196885 (HIP 101966)

The presence of a possible stellar companion to the F8 V star HD196885 was first reported in Chauvin et al. (2006, 2007) as the result of a near-infrared adaptive optics survey, while Correia et al. (2008) additionally detected a planetary companion of having minimum mass of $3\,M_{\rm Jup}$ and orbital period of 1349 d using CORAVEL, CORALIE, and ELODIE radial velocity measurements. Follow-up relative astrometry and radial velocity observations (Fischer et al. 2009; Chauvin et al. 2011) confirmed the binary nature of the system as well as the orbital parameters of the planetary body found around the primary star.

In the scope of this work, we analyse 18 CORAVEL and 41 CORALIE radial velocity measurements (divided as 33 C98, 1 C07, and 7 C14), over a total of 14574 d of and we are able to provide yet another update on the HD 196885 multiple system. The time series periodogram features a highly significant region (FAP = 1.08×10^{-8}) at a periodicity higher than 16 800 d, indicating either a Keplerian signal longer than our observational timespan or a long-term drift trend, and a residual peak at 1323 d with a FAP level of 1×10^{-3} after subtracting a one-Keplerian solution, with no further significant residual signals. In our two-Keplerian solution, shown in the top row of Fig. 10, we find the outer stellar companion to have orbital period of $P_B = 14\,912.14^{+1.13}_{-1.16}$ d, semiamplitude, $K_B = 2.102^{+0.001}_{-0.001}$ kms^{-1}, and eccentricity, $e_B = 0.322^{+0.001}_{-0.003}$. We then derive, using a primary mass of $1.24^{+0.12}_{-0.15}\,M_\odot$ (see Sect. 2), values of minimum mass, $M_B \sin i_B = 278.19^{+21.98}_{-22.84}\,M_{\rm Jup}$, and semimajor axis, $a_B = 13.59^{+0.50}_{-0.54}$ au. Similarly, we characterise the inner planetary companion as having orbital period $P_b = 1330.64^{+0.07}_{-0.43}$ d, semiamplitude $K_c = 36.94^{+1.24}_{-1.67}$ ms^{-1}, and eccentricity of $e_b = 0.521^{+0.325}_{-0.085}$. We also derive a minimum mass of $M_b \sin i_b = 1.96^{+0.34}_{-0.53}\,M_{\rm Jup}$ and semimajor axis of $a_b = 2.54^{+0.10}_{-0.11}$ au.

As both companions of the primary star orbit beyond our 1 au threshold, we performed the `orvara` fit on the original radial velocity time series instead of removing one of the companions. As a result, we find, for the outer companion, a true mass of $M_B = 334^{+26}_{-27}\,M_{\rm Jup}$ (corresponding to $0.32 \pm 0.02\,M_\odot$) and inclination of $i_B = 101.9^{+1.6}_{-1.5}$ deg; while for the inner one, we have $M_b = 2.67^{+1.4}_{-0.63}\,M_{\rm Jup}$ and inclination of $i_C = 89^{+42}_{-44}$ deg. The best-fit solutions for the proper motion anomaly curves are shown in the bottom row of Fig. 10.

The simultaneous usage of radial velocity and proper motion measurements allowed us to therefore confirm the planetary and stellar nature of the inner and outer companion, respectively. Following Tokovinin (1993), we additionally computed the relative orientation of angular momenta φ to try to provide further information on the system's configuration. However, due to the highly unconstrained value of the longitude of the ascending node of the inner planetary companion ($\Omega_b = 169^{+142}_{-121}$ deg), we obtained a relative orientation of $\varphi = 87$ deg, a value that is too close to the 90 deg threshold proposed in Tokovinin (1993) to provide any further robust statement on the configuration of the HD 196855 system components.

6. Prospects for exoplanetary search

As discussed in Sect. 1, the binarity of a stellar system has a deep influence on the formation and evolution of planetary companions, especially when the orbital separations between the stellar components of the systems is below a few hundreds au. In that case, most studies in the literature suggest that the formation and survival of more massive and close-in exoplanets is more likely than for those found around single stars (see e.g. Fontanive et al. 2019; Fontanive & Bardalez Gagliuffi 2021; Cadman et al. 2022). Additionally (and more closely related to the present work), different studies have highlighted how planetary formation and evolution is especially affected by binary separations less than 100 au (see e.g. Mayer et al. 2005; Moe & Kratter 2021). Fontanive et al. (2019) derives a binary fraction of $79.0^{+13.2}_{-14.7}$% for stars hosting giant planets and brown dwarfs on orbits shorter than 1 au, again supporting the critical influence that the presence of stellar companions have on the formation and evolution of such planetary systems. Similarly, based on a literature search for binary companions to exoplanet-hosting stars within 200 pc, Fontanive & Bardalez Gagliuffi (2021) finds that while exoplanets found on circumprimary orbits in very wide binary systems show similar physical properties than those around single stars,

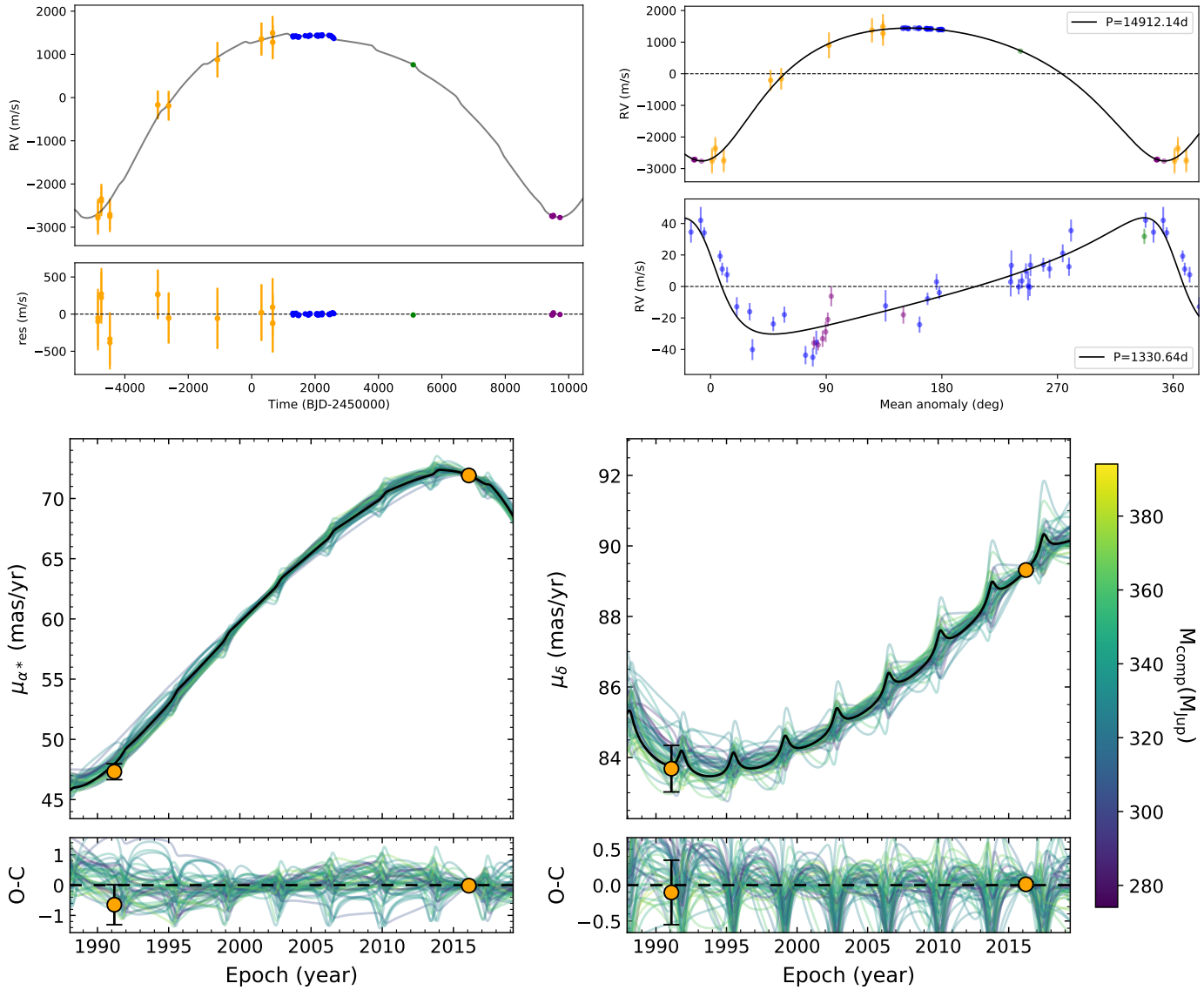

Fig. 10. Best-fit orbital solutions for HD 196885. Top row: radial velocity solution and phase folded model curves, with CORAVEL, CORALIE98, CORALIE07, and CORALIE14 measurements shown in orange, blue, green, and purple, respectively. Bottom row: observed and fitted proper motions in right ascension and declination. The thick black line is the best-fit orbit obtained by the simultaneous fit of radial velocities and proper motion anomalies, with 50 orbits randomly drawn from the posterior distributions and color-coded according to the mass of the outer massive companion, and the proper motion measurements from HIPPARCOS and *Gaia* EDR3 are shown in orange. Note: in the radial velocity phase folded plot for HD 196885 b, the low-precision CORAVEL data are not shown in order to better display the radial velocity curve of the low-amplitude inner companion.

tighter binary systems with separations up to a few hundred astronomical units tend to promote instead the formation and survival of more massive giant planets and brown dwarfs with shorter orbital periods and typically in single-planet configurations. The same work also suggests that the properties of close-in exoplanets in wide binary systems are consistent with them being the result of formation via fragmentation in a gravitationally unstable disc. This result is further supported by the simulations detailed in Cadman et al. (2022), which find that intermediate separations between the component of a binary stellar system promoting fragmentation is consistent with those featured in the systems displaying an excess of close-in giant planets and brown dwarfs (Wang et al. 2014; Kraus et al. 2016; Ngo et al. 2016).

Even though we detected no new robust exoplanetary signal in the radial velocity analysis of our binary sample, the low-to-intermediate range of orbital separations we derived for the stellar companions in this work, ranging from ~0.045 au to ~36.40 au, makes our sample a significant opportunity for the search of exoplanetary companions in binary systems. It is also a suitable testing field for planetary formation theoretical models, provided a larger number of radial velocity measurements with high enough density and precision are collected to successfully disentangle the stellar companion's radial velocity signal from that of any lower-mass body that can orbit the system.

6.1. Planetary stability in the binary sample

In order to provide a first assessment of the regions in which exoplanets could be found on stable orbits in the systems of our sample, we use the analytical stability criteria provided in Ballantyne et al. (2021) and based on the numerical simulations performed in Holman & Wiegert (1999).

Considering a planet on a circumprimary (or S-type) orbit in a binary system, Ballantyne et al. (2021) defines the critical semimajor axis $a_{\rm cS}$ as the maximum stable distance from the primary star as:

$$a_{\rm cS} = a_{\rm bin}\Big(0.464 - 0.38\mu - 0.631e + 0.586\mu e + 0.15e^2 - 0.198\mu e^2\Big), \quad (2)$$

with $a_{\rm bin}$ and e as the semimajor axis and eccentricity of the binary, respectively, and where:

$$\mu = \frac{m_s}{m_p + m_s}, \quad (3)$$

with m_p and m_s as the masses of the primary and secondary stellar components of the binary. Similarly, for a circumbinary (or P-type) orbit the critical semimajor axis, $a_{\rm cP}$, being the minimum stable distance from the binary system, is given by:

$$a_{cP} = a_{\rm bin}\Big(1.6 + 5.1e - 2.22e^2 + 4.12\mu - 4.27\mu e - 5.09\mu^2 + 4.61\mu^2 e^2\Big). \quad (4)$$

While finally considering a planet on a circumsecondaty orbit, the maximum stable distance from the secondary star $a_{\rm cS,sec}$ is given by using again Eq. (2), instead with:

$$\mu = \frac{m_p}{m_p + m_s}. \quad (5)$$

As noted in Ballantyne et al. (2021), these stability criteria are to be taken as a first-order indication of the circumprimary or circumbinary stability of a planet, since there is a variety of mechanisms that can further enhance or disrupt the stability of such orbits (see e.g. Pilat-Lohinger & Dvorak 2002; Pilat-Lohinger et al. 2003; Parker & Quanz 2013; Lam & Kipping 2018; Quarles et al. 2018, 2020; Kong et al. 2021, and references therein). However, since a full dynamical characterisation of the binary systems in our sample is beyond the scope of the present work, we assume the validity of the defined stability criteria for the purpose of producing a first estimate of the stability regions of the considered systems.

Additionally, we consider the minimum stable distance from the primary star the Roche limit of the host star as:

$$d_{\rm Roche} = 2.423\, R_\star \sqrt[3]{\frac{\rho_\star}{\rho_{\rm pl}}}, \quad (6)$$

where $R_\star$ and $\rho_\star$ are the radius and density of the primary star and $\rho_{\rm pl}$ is the density of the orbiting planet. We used, for each primary component, the stellar parameters derived from the SED fits detailed in Sect. 2. For the planetary density used to compute the Roche limits, we used the Earth density, $\rho_\oplus$, as a lower-limit scenario. The values of stability limits $d_{\rm Roche}$, $a_{\rm cS}$, and $a_{\rm cP}$ computed for the systems in the sample are listed in Table 3.

We first focussed our attention on the binary systems for which we obtained true mass values from the simultaneous fit of radial velocities and proper motion anomalies performed with `orvara` (detailed in Sect. 4), ignoring for the moment the 40 systems absent from the HGCA and the 44 systems with orbital period too short to be detected by proper motion anomalies. We therefore consider, in the following analysis, only the 132 systems for which we have derived values of companion true dynamical mass. Additionally, we note that the dynamical stability of a planet in the triple systems HD 206276 and HD 94340 is likely beyond the validity of the Ballantyne et al. (2021) criteria and therefore warrants further study and focused analysis such as numerical simulations, and that the stability assessments presented here for these two systems should then be interpreted as first-order estimates. Figure 11 shows the system architectures compared with that of the Solar System, with the stability regions represented by green bands.

From our stability estimates, we note that only four systems in our sample do not allow for stable S-type orbits, namely, the HD 58696, HD 43848, HD 139696, and HD 118598 systems, due to the high eccentricities (0.98, 0.97, 0.98, and 0.95, respectively) of their secondary components as derived by the simultaneous radial velocity and proper motion analysis. Additionally, we find both triple systems HD 206276 and HD 94340 to have a very narrow stable region for S-type orbits, spanning below 0.05 au and therefore unlikely to host circumprimary planetary companions, especially by virtue of the presence of the two stellar companions discussed in Sects. 5.2–5.3. The system featuring the widest S-type stability region in the sample is HD 30517, with this region spanning 5.16 au. Then, the system for which the secondary companion has the larger impact on planetary stability is, rather, HD 3795, where no planetary orbits appear to be stable from an orbital separation of 5.07 au–144.91 au from the primary star. The latter system is also the one in the sample characterised by the wider minimum P-type stable orbit in the sample, while the system with the tighter circumbinary stable orbit is HD 120559, having a $a_{\rm cP}$ of 2.58 au. Finally focussing on planetary companions orbiting the secondary component of our binary systems, the largest stable circumsecondary region in our sample is found in the HD 3795 system with a $a_{\rm cS,sec}$ of 4.65 au.

Table 3. Boundaries of the circumprimary, circumbinary and circumsecondary stability regions of the systems in the binary sample as described in Sect. 6.1.

Name	$d_{\rm Roche}$ [au]	$a_{\rm cS}$ [au]	$a_{\rm cP}$ [au]	$a_{\rm cS,sec}$ [au]	Note
HD 225155	0.008	0.889	13.035	0.428	$M_{\rm true}$
HD 1815	0.006	0.646	6.016	0.340	$M \sin i$
HD 1926	0.007	0.229	1.396	0.086	$M \sin i$
HD 2070	0.008	0.115	1.843	0.058	$M \sin i$
HD 2098	0.007	1.185	12.659	0.756	$M_{\rm true}$
HD 3222	0.007	2.839	41.274	1.336	$M_{\rm true}$
HD 3277	0.007	0.071	0.766	0.021	$M \sin i$
HD 3359	0.007	0.036	0.566	0.018	$M \sin i$
HD 3795	0.007	5.067	144.914	4.650	$M_{\rm true}$
HD 4392	0.007	0.145	5.935	0.109	$M_{\rm true}$
HD 4747	0.007	1.096	39.734	0.387	$M_{\rm true}$
HD 5562	0.008	1.233	20.116	0.702	$M_{\rm true}$
HD 7320	0.007	0.166	51.340	0.095	$M_{\rm true}$
HD 8129	0.007	-	27.509	-	$M \sin i$
HD 9770	0.008	0.766	9.656	0.269	$M \sin i$
HD 9905	0.007	2.421	31.232	0.951	$M_{\rm true}$
HD 10519	0.007	0.477	38.102	0.345	$M_{\rm true}$
HD 11131	0.007	0.410	20.108	0.260	$M_{\rm true}$
HD 11264	0.007	3.054	46.823	2.032	$M_{\rm true}$
HD 11352	0.007	0.315	4.046	0.183	$M_{\rm true}$
...	...	...	...	...	

Notes. Note column indicates the value of the detected companion mass used for the stability estimation. Full table is available at the CDS. A portion is shown here for guidance regarding its form and content.

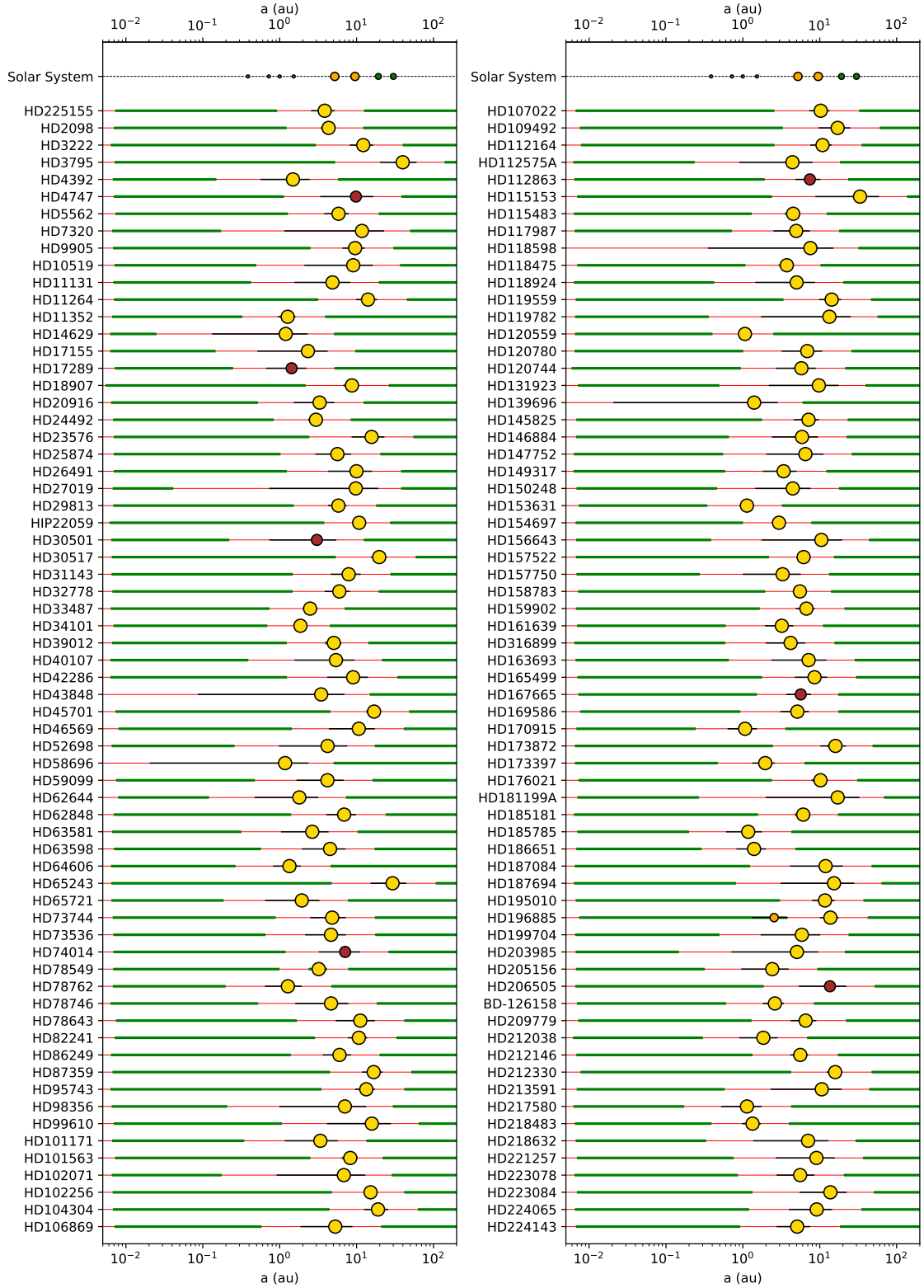

Fig. 11. Overview of the architectures of the 132 binary systems for which true masses were derived using simultaneous radial velocity and proper motion anomaly fits, compared to that of the Solar System. For each system, the companion periastron and apoastron are connected by a thin black line, while the thick green and thin red lines highlight the stable and unstable regions for additional planetary companions, respectively, as detailed in Sect. 6.1; we note that circumbinary stable regions are typically smaller than the companion marker size due to the logarithmic axis used. The mass of each companion is represented by the marker growing size and different color, namely grey for terrestrial ($M < 2\,M_\oplus$), green for Neptune-mass ($10\,M_\oplus < M < 30\,M_\oplus$), orange for giant planets ($30\,M_\oplus < M < 40\,M_{\rm Jup}$), brown for brown dwarfs ($40\,M_{\rm Jup} < M < 80\,M_{\rm Jup}$), and yellow for stellar companions ($M > 80\,M_{\rm Jup}$).

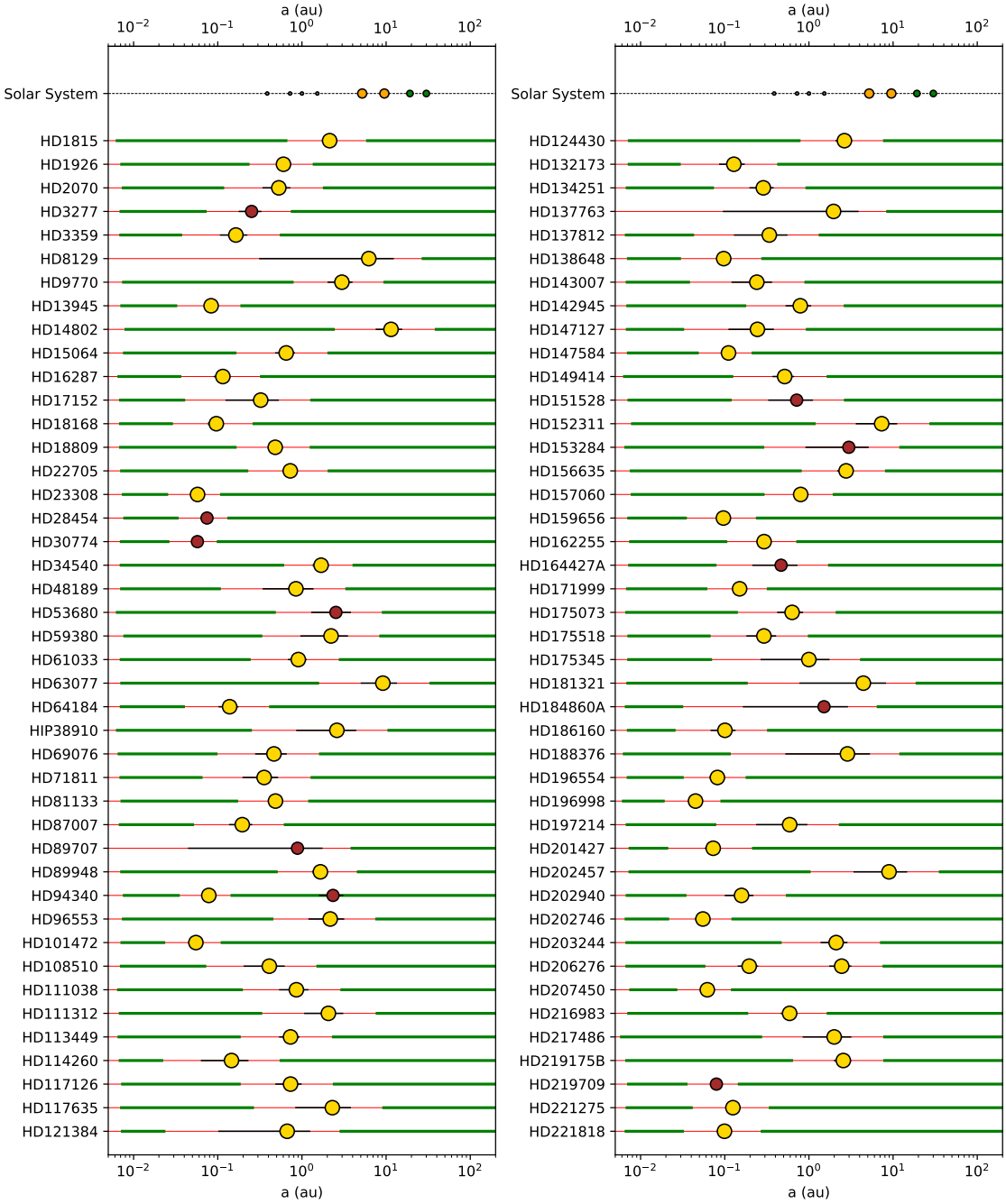

Fig. 12. Overview of the architectures of the 86 systems with only radial velocity solutions available, for which the dynamically stable and unstable regions for additional planetary companions are computed using the $M \sin i$ value of the detected companions, compared to that of the Solar System. For each system, the companion periastron and apoastron are connected by a thin black line, while the thick green and thin red lines highlight the stable and unstable regions for additional planetary companions, respectively, as detailed in Sect. 6.1; we note that circumbinary stable regions are typically smaller than the companion marker size due to the logarithmic axis used. The mass of each companion is represented by the marker growing size and different color, namely grey for terrestrial ($M < 2\,M_{\oplus}$), green for Neptune-mass ($10\,M_{\oplus} < M < 30\,M_{\oplus}$), orange for giant planets ($30\,M_{\oplus} < M < 40\,M_{\rm Jup}$), brown for brown dwarfs ($40\,M_{\rm Jup} < M < 80\,M_{\rm Jup}$), and yellow for stellar companions ($M > 80\,M_{\rm Jup}$).

Considering instead the 86 binary systems in the sample for which we have only radial velocity orbital solution and, therefore, only minimum mass values for the companions detected in these systems, we applied the same stability criterion using the value of $M \sin i$ as the m_s in Eqs. (2)–(4); the stable regions thus obtained are then to be considered estimates of the maximum range of semimajor axes in which stable orbits for planetary companions are possible. The architecture of these systems is shown in Fig. 12, from which it can be noted that three systems (HD 8129, HD 89707, and HD 137763) do not allow for stable S-type orbits – again, by virtue of the large eccentricities (0.95 for all of them) of the detected companions.

6.2. Detection limits

In order to investigate the detection capabilities of the CORAVEL and CORALIE data analysed so far, we computed the detection limits for the binary sample object of the present

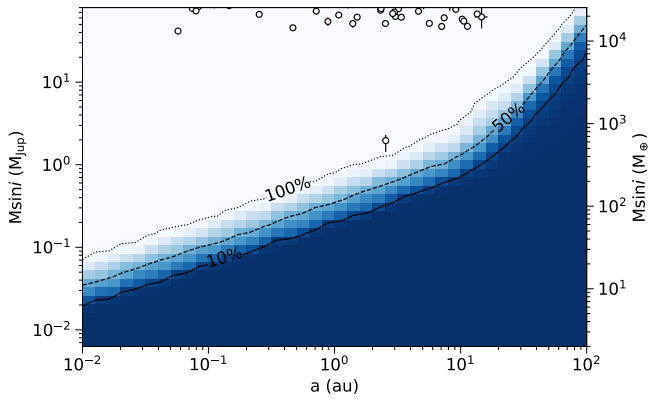

Fig. 13. Completeness map of the binary sample, focused on the substellar ($2\,M_\oplus < M \sin i < 80\,M_{\rm Jup}$) companion regime. Detection frequency contour levels of 10, 50, and 100% are shown as solid, dashed, and dotted curves, respectively, while the companions detected in our search are shown as white circles.

work, with a particular focus on the substellar ($M \sin i < 80\,M_{\rm Jup}$) regime.

To this end, we followed an injection and retrieval scheme similar to the one pursued in Barbato et al. (2018), injecting synthetic companion signals into the radial velocity residuals time series of each star in the sample, obtained by subtracting, from the original radial velocity data, the contribution of the companions detected and characterised as described in Sect. 3. The synthetic signals were generated over a 40×40 grid of semimajor axes $a_{\rm inj}$, evenly spaced in logarithm from 0.01 to 100 au and minimum masses, $M_{\rm inj}$, that were similarly spaced from $2\,M_\oplus$ to $80\,M_{\rm Jup}$. For each of the 1600 ($a_{\rm inj}$, $M_{\rm inj}$) realisations, we generated and injected into the residuals 500 synthetic radial velocity curves with randomly drawn values of mean longitude, $\lambda_{0,\rm inj}$, eccentricity, $e_{\rm inj}$ and argument of periastron, $\omega_{\rm inj}$. Lastly, we added to each synthetic data point generated in this way a random Gaussian noise with an amplitude equal to the standard deviation of the instrumental uncertainties of the original time series. Each of the resulting 8×10^5 synthetic radial velocity time series was then fitted with a flat model and a Keplerian one, and the injected signal was considered as detected only if the ΔBIC between the two models was at least ten points in favour of the Keplerian model. The resulting detection limit maps obtained for each star in our binary sample are collected in Appendix B, highlighting both the dynamically unstable regions estimated in Sect. 6.1 and the parameter space region of additional companions that we can exclude based on the available radial velocity measurements.

We show in Fig. 13 the averaged completeness map for the whole binary sample. Since the CORALIE and CORAVEL measurements collected for the sample do not have the precision and sampling necessary to ensure detection completeness for planetary companion below $10\,M_\oplus$ and because we have only partially completeness for giant companions below the mass of Jupiter in the explored range of orbital separation. On the other hand, the radial velocity measurements are enough to ensure full detection completeness for companions above $1\,M_{\rm Jup}$ within 1.80 au.

7. Occurrence rates for stellar and brown dwarfs companions in the sample

From the detection limit map produced in Sect. 6.2 (and shown in Fig. 13), it is possible to notice that the radial velocity measurements collected for the sample analysed in the present paper allow us to reach full detection completeness for both brown dwarf companions ($40 < M \sin i < 80\,M_{\rm Jup}$) with a semimajor axis below ~62 au and stellar ($M \sin i > 80\,M_{\rm Jup}$) companions within 100 au from the primary stars. The thorough analysis of the detection limits map produced instead for the whole CORALIE sample will be the focus of a future paper in the series, but for the purposes of the present work, it is possible to report that the detection completeness for the aforementioned brown dwarf and stellar companion parameter space is confirmed for the overall CORALIE sample. We excluded from the following analysis the five companions with $q > 0.8$, identified in Sects. 3 and 4.

We can use this information to provide an assessment of the occurrence rate, f, for brown dwarfs and stellar companions using the binomial distribution:

$$p(m; N, f) = \frac{N!}{m!(N-m)!}\, f^m (1-f)^{N-m}, \tag{7}$$

with N being the size of the CORALIE search sample and m the number of detections within the parameter space taken into account here. In order to derive f we follow the approach described in Burgasser et al. (2003), McCarthy & Zuckerman (2004) and previously applied in different occurrence rate sudies (e.g. Sozzetti et al. 2009; Faria et al. 2016; Barbato et al. 2018; Santos et al. 2011, to name a few), where the inverse binomial function $p'(f; m, N) \propto p(m; N, f)$ is normalised to 1 over a range of f values bound between 0 and 1. This yields the result:

$$\int_0^1 p'(f; m, N)\, {\rm d}f = 1 \rightarrow p' = (N+1)p, \tag{8}$$

and the occurrence rate, f, is then found as the value corresponding to the mode of p'. Lastly, the upper and lower uncertainty limits, $f_{\rm U}$, $f_{\rm L}$, corresponding to 1σ confidence limits are computed by finding the range covering 68% of the p' distribution by numerically solving the relation:

$$\sum_{i=0}^{m} \frac{(N+1)!}{i!(N+1-i)!} x^i (1-x)^{N+i-1} = \begin{cases} 0.84, & x = f_{\rm L} \\ 0.16, & x = f_{\rm U} \end{cases}. \tag{9}$$

Firstly, considering the 209 stellar companions detected (203 from this work and 6 from Unger et al., in prep.), we find an occurrence rate for stellar companions of $f_\star = 12.69^{+0.87}_{-0.77}$%. If again we distinguish between the 127 inner and 82 outer stellar companions setting the threshold at 5 au, we find occurrence rate values of $7.71^{+0.71}_{-0.60}$% and $4.98^{+0.59}_{-0.48}$%, respectively. It can be noted that these occurrence rates are much lower than the ~50% computed for the CORAVEL survey presented in Duquennoy & Mayor (1991), but it is important to underline not only the fact that the sample analysed in the cited work was composed of 164 stars (and therefore much smaller in size than the whole CORALIE sample we have instead considered in the present study), but also that the CORAVEL sample also included a number of SB2 that we excluded from our analysis, thereby making a direct comparison between the two studies non-trivial.

Considering the 13 detections with $40 < M \sin i < 80\,M_{\rm Jup}$ for which the astrometric analysis has either confirmed the brown dwarf nature of the object or where confirmation was not possible (see Sect. 5.1 and Unger et al., in prep.), we obtained an occurrence rate for brown dwarf companions in the CORALIE sample of $f_{\rm BD} = 0.79^{+0.29}_{-0.16}$%; considering only those 8 such companions found within 5 au from the primary star, we obtained an

occurrence rate of close-in brown dwarfs of $0.49^{+0.24}_{-0.12}$%, while for the 5 wider brown dwarf companions we obtained an occurrence rate of $0.30^{+0.21}_{-0.07}$%, values that we noted to be compatible within 1σ. While this apparent surplus of brown dwarfs on closer orbits might be interpreted as in opposition with the known brown dwarf desert, it is important to remember that, while the CORALIE survey is certainly able to detect the large amplitude signals of brown dwarf companions on wide orbits (as evident from Fig. 13), its 25 yr timespan allows only for the robust identification of Keplerian signals corresponding to an orbital separation up to ∼7 au; whereas wider companions would be instead detected as radial velocity trends that have not been considered for analysis in the present work (see Sect. 3). Thus, a number of possible long-period brown dwarf companions in the CORALIE sample are possibly yet to be detected, leading to an larger difference in the occurrence rates between the two population and the same applies to the stellar companions in the sample.

By instead considering only the seven brown dwarfs in the sample confirmed as such by the joint radial velocity and proper motion analysis, we obtained an occurrence rate of $f_{\rm BD} = 0.43^{+0.23}_{-0.11}$%, which we therefore propose as a lower limit on the occurrence rate of brown dwarfs in the sample. Selecting again a threshold of 5 au between inner and outer brown dwarfs, we find occurrence rate values of $0.12^{+0.17}_{-0.03}$% and $0.30^{+0.21}_{-0.07}$%, respectively. While we now find a lower occurrence rate of inner brown dwarfs, we must again note that these two values are compatible within 1σ.

8. Discussion and conclusions

In this paper, we present the results of the homogeneous analysis performed in search for brown dwarf and stellar companions to the 1647 stars within the long-term CORALIE exoplanetary survey, in order to produce an updated catalog of binary objects in the sample using a combination of radial velocity and astrometry measurements. As a result, we found 218 stars in the CORALIE sample to host at least one stellar or brown dwarf companion, 88 of which are already known in the literature and for which we present updated orbital solutions, and 130 of which are have not been known thus far and for which we therefore provide first assessment of the orbital parameters.

Furthermore, by combining radial velocity measurements and astrometric accelerations, as computed between the HIPPARCOS and *Gaia* EDR3, we were able to derive precise dynamical masses of 132 stellar and brown dwarf companions with an orbital separation down to 1 au. Notably, we were also able to confirm the planetary nature of HD 196885 b as well as the brown dwarf nature of 7 companions with $40 \leq M \sin i \leq 80\,M_{\rm Jup}$, while we found 11 companions with minimum masses within this range to be revealed as stellar-mass companions – again stressing the power of joint usage of radial velocity and astrometric measurements in painting a full picture of system characterisation.

The detection completeness analysis we performed on the sample also allow us to derive occurrence rates of $f_\star = 12.69^{+0.87}_{-0.77}$% and $f_{\rm BD} = 0.43^{+0.23}_{-0.11}$% for stellar and brown dwarf companions, respectively. While our occurrence rates also show an apparent overabundance of stellar and brown dwarf companions below 5 au, compared to those found on wider orbits, it is imperative to stress that in the present work we have considered only those companions that are found to be best characterised by Keplerian models instead of linear or parabolic trends; therefore, a possibly large number of wide massive companions are yet to be found and fully characterised by continuous observations by spectrographs and, especially, direct imaging instruments. This will be the subject of future papers in this series.

The binary sample presented and characterised in this work does not only represent an important element for follow-up studies on binary statistics and comparison with formation and evolution theoretical models for both stellar and brown dwarf companions, but it also offers an unparalleled opportunity in the search of exoplanetary bodies in binary systems. This is based on the fact that theoretical models have shown that planetary formation and survival is deeply influenced by stellar companions within ∼100 au, such as those detailed in the present study. Both the dynamical stability assessment and detection-limit maps we produced show that there is still significant space for the further discovery of exoplanets on circumprimary and circumbinary orbits around the stars analysed here. Continued follow-up observations will allow for deep probes of the exoplanetary discovery space in the sample in the near future, paving the way for this catalogue to be used as testing field for models of planetary formation in binary systems.

Acknowledgements. The authors wish to thank the referee, Dr. F. Kiefer, for the thorough and useful comments which significantly improved the quality of the manuscript. This work has been carried out within the framework of the National Centre of Competence in Research PlanetS supported by the Swiss National Science Foundation under grants 51NF40_182901 and 51NF40_205606. The authors acknowledge the financial support of the SNSF. The 120 cm EULER telescope and the CORALIE spectrograph were funded by the SNSF and the University of Geneva. This publication makes use of the Data & Analysis Center for Exoplanets (DACE), which is a facility based at the University of Geneva (CH) dedicated to extrasolar planets data visualisation, exchange and analysis. DACE is a platform of the Swiss National Centre of Competence in Research (NCCR) PlanetS, federating the Swiss expertise in Exoplanet research. The DACE platform is available at https://dace.unige.ch. N.C.S. acknowledges support from the European Research Council through the grant agreement 101052347 (FIERCE) and by FCT - Fundação para a Ciência e a Tecnologia through national funds and by FEDER through COMPETE2020 - Programa Operacional Competitividade e Internacionalização by these grants: UIDB/04434/2020; UIDP/04434/2020. This work has made use of data from the European Space Agency (ESA) mission *Gaia* (https://www.cosmos.esa.int/gaia), processed by the *Gaia* Data Processing and Analysis Consortium (DPAC, https://www.cosmos.esa.int/web/gaia/dpac/consortium). Funding for the DPAC has been provided by national institutions, in particular the institutions participating in the *Gaia* Multilateral Agreement. This research has made use of the SIMBAD database, operated at CDS, Strasbourg, France. The authors made use of ASTROPY (a community-developed core Python package for Astronomy Astropy Collaboration 2013, 2018), MATPLOTLIB (Hunter 2007), NUMPY (Harris et al. 2020), SCIPY (Jones et al. 2001) and SEABORN (Waskom 2021). DB also wishes to thank N. Gaiman for his inspiring words about the illusion of permanence and stellar transience.

References

Anders, F., Khalatyan, A., Chiappini, C., et al. 2019, A&A, 628, A94
Astropy Collaboration (Robitaille, T. P., et al.) 2013, A&A, 558, A33
Astropy Collaboration (Price-Whelan, A. M., et al.) 2018, AJ, 156, 123
Ballantyne, H. A., Espaas, T., Norgrove, B. Z., et al. 2021, MNRAS, 507, 4507
Baluev, R. V. 2008, MNRAS, 385, 1279
Baranne, A., Mayor, M., & Poncet, J. L. 1979, Vistas Astron., 23, 279
Barbato, D., Sozzetti, A., Desidera, S., et al. 2018, A&A, 615, A175
Boffin, H. M. J., & Pourbaix, D. 2003, The Observatory, 123, 126
Bonnell, I. A. 1994, MNRAS, 269, 837
Brandt, T. D. 2018, ApJS, 239, 31
Brandt, T. D. 2021, ApJS, 254, 42
Brandt, T. D., Dupuy, T. J., & Bowler, B. P. 2019, AJ, 158, 140
Brandt, T. D., Dupuy, T. J., Bowler, B. P., et al. 2020, AJ, 160, 196
Brandt, G. M., Brandt, T. D., Dupuy, T. J., Li, Y., & Michalik, D. 2021a, AJ, 161, 179
Brandt, T. D., Dupuy, T. J., Li, Y., et al. 2021b, AJ, 162, 186
Burgasser, A. J., Kirkpatrick, J. D., Reid, I. N., et al. 2003, ApJ, 586, 512

Cadman, J., Hall, C., Fontanive, C., & Rice, K. 2022, MNRAS, 511, 457
Calissendorff, P., & Janson, M. 2018, A&A, 615, A149
Cersullo, F., Wildi, F., Chazelas, B., & Pepe, F. 2017, A&A, 601, A102
Chauvin, G., Lagrange, A. M., Udry, S., et al. 2006, A&A, 456, 1165
Chauvin, G., Lagrange, A. M., Udry, S., & Mayor, M. 2007, A&A, 475, 723
Chauvin, G., Beust, H., Lagrange, A. M., & Eggenberger, A. 2011, A&A, 528, A8
Chazelas, B., Pepe, F., & Wildi, F. 2012, SPIE, 8450, 845013
Choi, J., Dotter, A., Conroy, C., et al. 2016, ApJ, 823, 102
Correia, A. C. M., Udry, S., Mayor, M., et al. 2008, A&A, 479, 271
Cutri, R. M., Wright, E. L., Conrow, T., et al. 2021, VizieR Online Data Catalog: II/328
Damasso, M., Del Sordo, F., Anglada-Escudé, G., et al. 2020a, Sci. Adv., 6, eaax7467
Damasso, M., Sozzetti, A., Lovis, C., et al. 2020b, A&A, 642, A31
Delisle, J. B., & Ségransan, D. 2022, A&A, 667, A172
Delisle, J. B., Ségransan, D., Buchschacher, N., & Alesina, F. 2016, A&A, 590, A134
Delisle, J. B., Ségransan, D., Dumusque, X., et al. 2018, A&A, 614, A133
Delisle, J. B., Hara, N., & Ségransan, D. 2020, A&A, 638, A95
Díaz, R. F., Ségransan, D., Udry, S., et al. 2016, A&A, 585, A134
Dotter, A. 2016, ApJS, 222, 8
Duquennoy, A., & Mayor, M. 1991, A&A, 248, 485
Eastman, J. D., Rodriguez, J. E., Agol, E., et al. 2019, PASP, submitted [arXiv:1907.09480]
Eggenberger, A., & Udry, S. 2010, Astrophys. Space Sci. Lib., 366, 19
El-Badry, K., Rix, H.-W., Tian, H., Duchêne, G., & Moe, M. 2019, MNRAS, 489, 5822
Faria, J. P., Santos, N. C., Figueira, P., et al. 2016, A&A, 589, A25
Fekel, F. C., Willmarth, D. W., Abt, H. A., & Pourbaix, D. 2018, AJ, 156, 117
Feng, F., Butler, R. P., Jones, H. R. A., et al. 2021, MNRAS, 507, 2856
Fischer, D., Driscoll, P., Isaacson, H., et al. 2009, ApJ, 703, 1545
Fontanive, C., & Bardalez Gagliuffi, D. 2021, Front. Astron. Space Sci., 8, 16
Fontanive, C., Rice, K., Bonavita, M., et al. 2019, MNRAS, 485, 4967
Gaia Collaboration (Prusti, T., et al.) 2016, A&A, 595, A1
Gaia Collaboration (Brown, A. G. A., et al.) 2021, A&A, 649, A1
Gammie, C. F. 2001, ApJ, 553, 174
Goldin, A., & Makarov, V. V. 2007, ApJS, 173, 137
Gomez, J., Docobo, J. A., Campo, P. P., & Mendez, R. A. 2016, AJ, 152, 216
Grether, D., & Lineweaver, C. H. 2006, ApJ, 640, 1051
Grieves, N., Ge, J., Thomas, N., et al. 2017, MNRAS, 467, 4264
Guszejnov, D., & Hopkins, P. F. 2015, MNRAS, 450, 4137
Guszejnov, D., Hopkins, P. F., & Krumholz, M. R. 2017, MNRAS, 468, 4093
Halbwachs, J. L., Mayor, M., Udry, S., & Arenou, F. 2003, A&A, 397, 159
Halbwachs, J. L., Mayor, M., & Udry, S. 2018, A&A, 619, A81
Harris, C. R., Millman, K. J., van der Walt, S. J., et al. 2020, Nature, 585, 357
Harsono, D., Alexander, R. D., & Levin, Y. 2011, MNRAS, 413, 423
Høg, E., Fabricius, C., Makarov, V. V., et al. 2000, A&A, 355, L27
Holl, B., Sozzetti, A., Sahlmann, J., et al. 2023, A&A, in press, https://doi.org/10.1051/0004-6361/202244161
Holman, M. J., & Wiegert, P. A. 1999, AJ, 117, 621
Hunter, J. D. 2007, Comput. Sci. Eng., 9, 90
Jenkins, J. S., Díaz, M., Jones, H. R. A., et al. 2015, MNRAS, 453, 1439
Jones, E., Oliphant, T., Peterson, P., et al. 2001, SciPy: Open source scientific tools for Python
Kervella, P., Arenou, F., Mignard, F., & Thévenin, F. 2019a, A&A, 623, A72
Kervella, P., Gallenne, A., Evans, N. R., et al. 2019b, A&A, 623, A117
Kervella, P., Gallenne, A., Remage Evans, N., et al. 2019c, A&A, 623, A116
Kervella, P., Arenou, F., & Schneider, J. 2020, A&A, 635, L14
Kervella, P., Arenou, F., & Thévenin, F. 2022, A&A, 657, A7
Kiefer, F., Hébrard, G., Sahlmann, J., et al. 2019, A&A, 631, A125
Kong, Z., Jiang, J. H., Zhu, Z.-H., Fahy, K. A., & Burn, R. 2021, ArXiv e-prints [arXiv:1209.3114]
Könyves, V., André, P., Men'shchikov, A., et al. 2015, A&A, 584, A91
Kratter, K. M., Matzner, C. D., Krumholz, M. R., & Klein, R. I. 2010, ApJ, 708, 1585
Kraus, A. L., Ireland, M. J., Huber, D., Mann, A. W., & Dupuy, T. J. 2016, AJ, 152, 8
Lam, C., & Kipping, D. 2018, MNRAS, 476, 5692
Latham, D. W., Stefanik, R. P., Torres, G., et al. 2002, AJ, 124, 1144
Lindegren, L., Klioner, S. A., Hernández, J., et al. 2021, A&A, 649, A2
Llop-Sayson, J., Wang, J. J., Ruffio, J.-B., et al. 2021, AJ, 162, 181
Lucy, L. B., & Ricco, E. 1979, AJ, 84, 401
Ma, B., & Ge, J. 2014, MNRAS, 439, 2781
Makarov, V. V. 2007, ApJ, 654, L81
Makarov, V. V., & Kaplan, G. H. 2005, AJ, 129, 2420
Makarov, V. V., Zacharias, N., & Finch, C. T. 2021a, Res. Notes Am. Astron. Soc., 5, 108
Makarov, V. V., Zacharias, N., & Finch, C. T. 2021b, ArXiv e-prints [arXiv:2107.01090]
Marmier, M., Ségransan, D., Udry, S., et al. 2013, A&A, 551, A90
Marzari, F., & Gallina, G. 2016, A&A, 594, A89
Mayer, L., Wadsley, J., Quinn, T., & Stadel, J. 2005, MNRAS, 363, 641
Mayor, M., Marmier, M., Lovis, C., et al. 2011, ArXiv e-prints, [arXiv:1109.2497]
Mayor, M., Pepe, F., Queloz, D., et al. 2003, The Messenger, 114, 20
McCarthy, C., & Zuckerman, B. 2004, AJ, 127, 2871
Melo, C. H. F. 2003, A&A, 410, 269
Moe, M., & Di Stefano, R. 2017, ApJS, 230, 15
Moe, M., & Kratter, K. M. 2021, MNRAS, 507, 3593
Musielak, Z. E., Cuntz, M., Marshall, E. A., & Stuit, T. D. 2005, A&A, 434, 355
Ngo, H., Knutson, H. A., Hinkley, S., et al. 2016, ApJ, 827, 8
Ngo, H., Knutson, H. A., Bryan, M. L., et al. 2017, AJ, 153, 242
Nidever, D. L., Marcy, G. W., Butler, R. P., Fischer, D. A., & Vogt, S. S. 2002, ApJS, 141, 503
Offner, S. S. R., Moe, M., Kratter, K. M., et al. 2022, ArXiv e-prints [arXiv:2203.10066]
Parker, R. J., & Quanz, S. P. 2013, MNRAS, 436, 650
Pepe, F., Mayor, M., Delabre, B., et al. 2000, SPIE, 4008, 582
Pepe, F., Molaro, P., Cristiani, S., et al. 2014, ArXiv e-prints [arXiv:1401.5918]
Peretti, S., Ségransan, D., Lavie, B., et al. 2019, A&A, 631, A107
Perryman, M. A. C., Lindegren, L., Kovalevsky, J., et al. 1997, A&A, 323, L49
Pilat-Lohinger, E., & Dvorak, R. 2002, Celest. Mech. Dyn. Astron., 82, 143
Pilat-Lohinger, E., Funk, B., & Dvorak, R. 2003, A&A, 400, 1085
Pineda, J. E., Offner, S. S. R., Parker, R. J., et al. 2015, Nature, 518, 213
Quarles, B., Satyal, S., Kostov, V., Kaib, N., & Haghighipour, N. 2018, ApJ, 856, 150
Quarles, B., Li, G., Kostov, V., & Haghighipour, N. 2020, AJ, 159, 80
Queloz, D., Mayor, M., Weber, L., et al. 2000, A&A, 354, 99
Raghavan, D., McAlister, H. A., Henry, T. J., et al. 2010, ApJS, 190, 1
Rickman, E. L., Ségransan, D., Marmier, M., et al. 2019, A&A, 625, A71
Rickman, E. L., Matthews, E., Ceva, W., et al. 2022, A&A, 668, A140
Roell, T., Neuhäuser, R., Seifahrt, A., & Mugrauer, M. 2012, A&A, 542, A92
Sahlmann, J. 2016, IAU Focus Meeting, 29A, 217
Sahlmann, J., Ségransan, D., Queloz, D., & Udry, S. 2011a, IAU Symp., 276, 117
Sahlmann, J., Ségransan, D., Queloz, D., et al. 2011b, A&A, 525, A95
Santos, N. C., Israelian, G., & Mayor, M. 2001, A&A, 373, 1019
Santos, N. C., Mayor, M., Naef, D., et al. 2002, A&A, 392, 215
Santos, N. C., Mayor, M., Bonfils, X., et al. 2011, A&A, 526, A112
Ségransan, D., Udry, S., Mayor, M., et al. 2010, A&A, 511, A45
Shahaf, S., & Mazeh, T. 2019, MNRAS, 487, 3356
Snellen, I. A. G., & Brown, A. G. A. 2018, Nat. Astron., 2, 883
Sozzetti, A., Torres, G., Latham, D. W., et al. 2009, ApJ, 697, 544
Su, X.-N., Xie, J.-W., Zhou, J.-L., & Thebault, P. 2021, AJ, 162, 272
Tamuz, O., Ségransan, D., Udry, S., et al. 2008, A&A, 480, L33
Thebault, P., & Haghighipour, N. 2015, in Planetary Exploration and Science: Recent Results and Advances (Berlin: Springer), 309
Tokovinin, A. A. 1993, Astron. Lett., 19, 383
Tokovinin, A. A. 2000, A&A, 360, 997
Tokovinin, A. 2014, AJ, 147, 87
Tokovinin, A., Thomas, S., Sterzik, M., & Udry, S. 2006, A&A, 450, 681
Tokovinin, A., Hartung, M., Hayward, T. L., & Makarov, V. V. 2012, AJ, 144, 7
Turrini, D., Barbieri, M., Marzari, F., Thebault, P., & Tricarico, P. 2005, Mem. Soc. Astron. Ital. Suppl., 6, 172
Udry, S., & Santos, N. C. 2007, ARA&A, 45, 397
Udry, S., Mayor, M., Naef, D., et al. 2000, A&A, 356, 590
Udry, S., Mayor, M., Naef, D., et al. 2002, A&A, 390, 267
Venner, A., Vanderburg, A., & Pearce, L. A. 2021, AJ, 162, 12
Wang, J., Xie, J.-W., Barclay, T., & Fischer, D. A. 2014, ApJ, 783, 4
Waskom, M. L. 2021, J. Open Source Softw., 6, 3021
Watson, L. C., Pritchard, J. D., Hearnshaw, J. B., Kilmartin, P. M., & Gilmore, A. C. 2001, MNRAS, 325, 143
Zacharias, N., Finch, C. T., Girard, T. M., et al. 2012, VizieR Online Data Catalog: I/322A
Zúñiga-Fernández, S., Bayo, A., Elliott, P., et al. 2021, A&A, 645, A30

Appendix A: RV orbital solutions' phase-folded plots

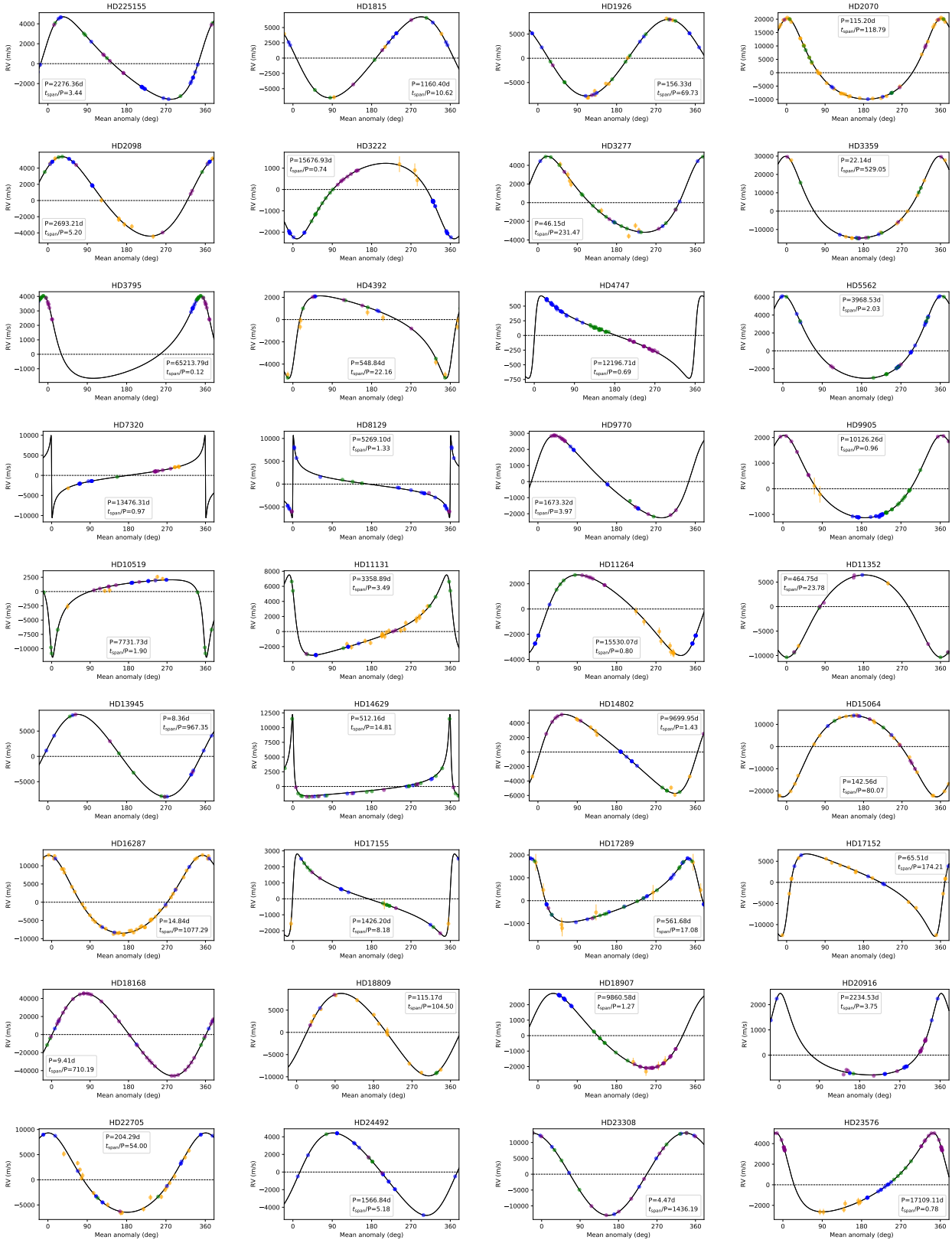

Fig. A.1: Phase-folded radial velocity curves for the companions detected around each star in the binary sample as described in Sect.3. In each plot, the CORAVEL, CORALIE98, CORALIE07, and CORALIE14 measurements are shown in orange, blue, green, and purple, respectively, over the phase-folded model radial velocity curve. Companion orbital period and orbit completeness, indicated as the ratio between observational span and period, are noted in each plot's box.

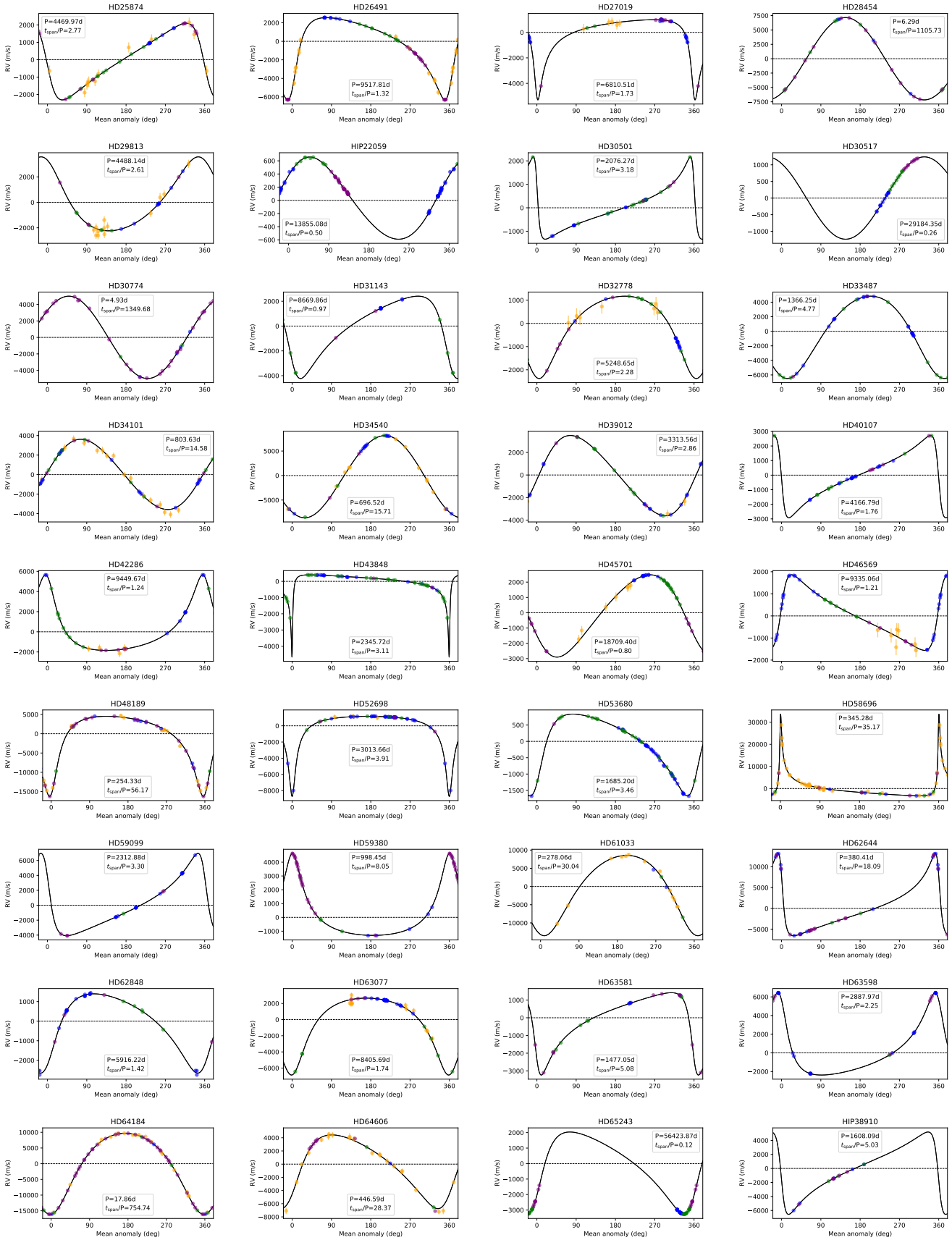

Fig. A.1: Continued

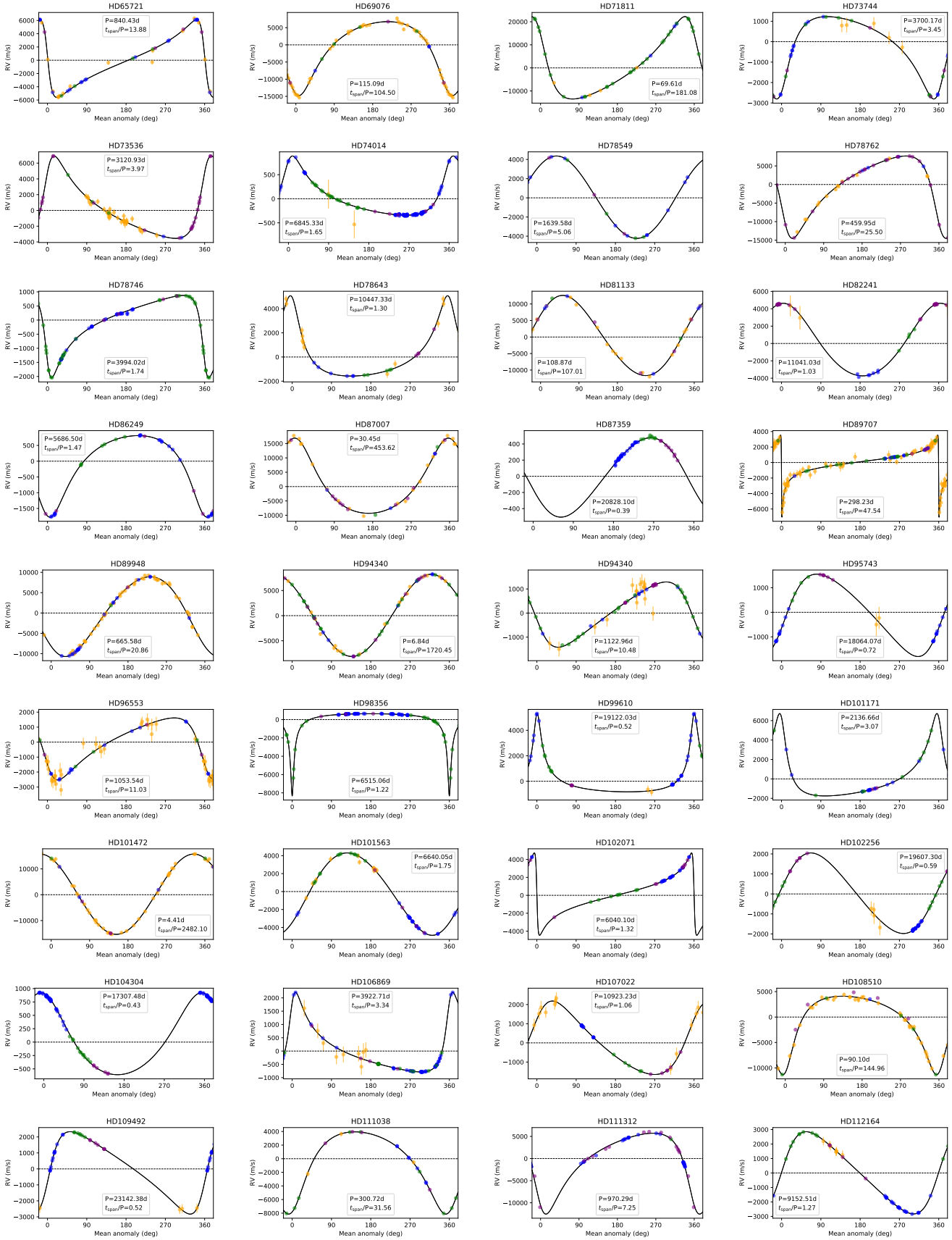

Fig. A.1: Continued

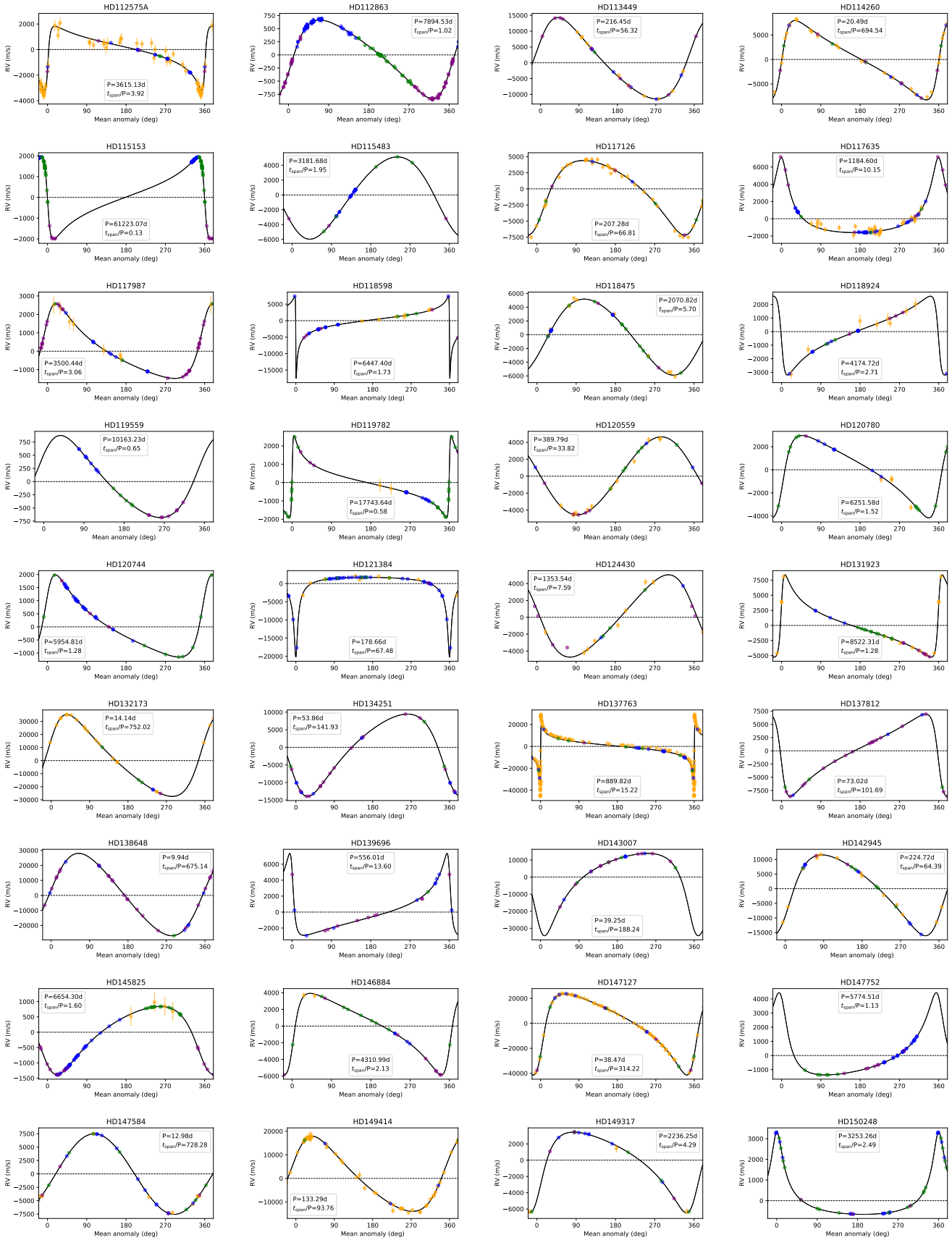

Fig. A.1: Continued

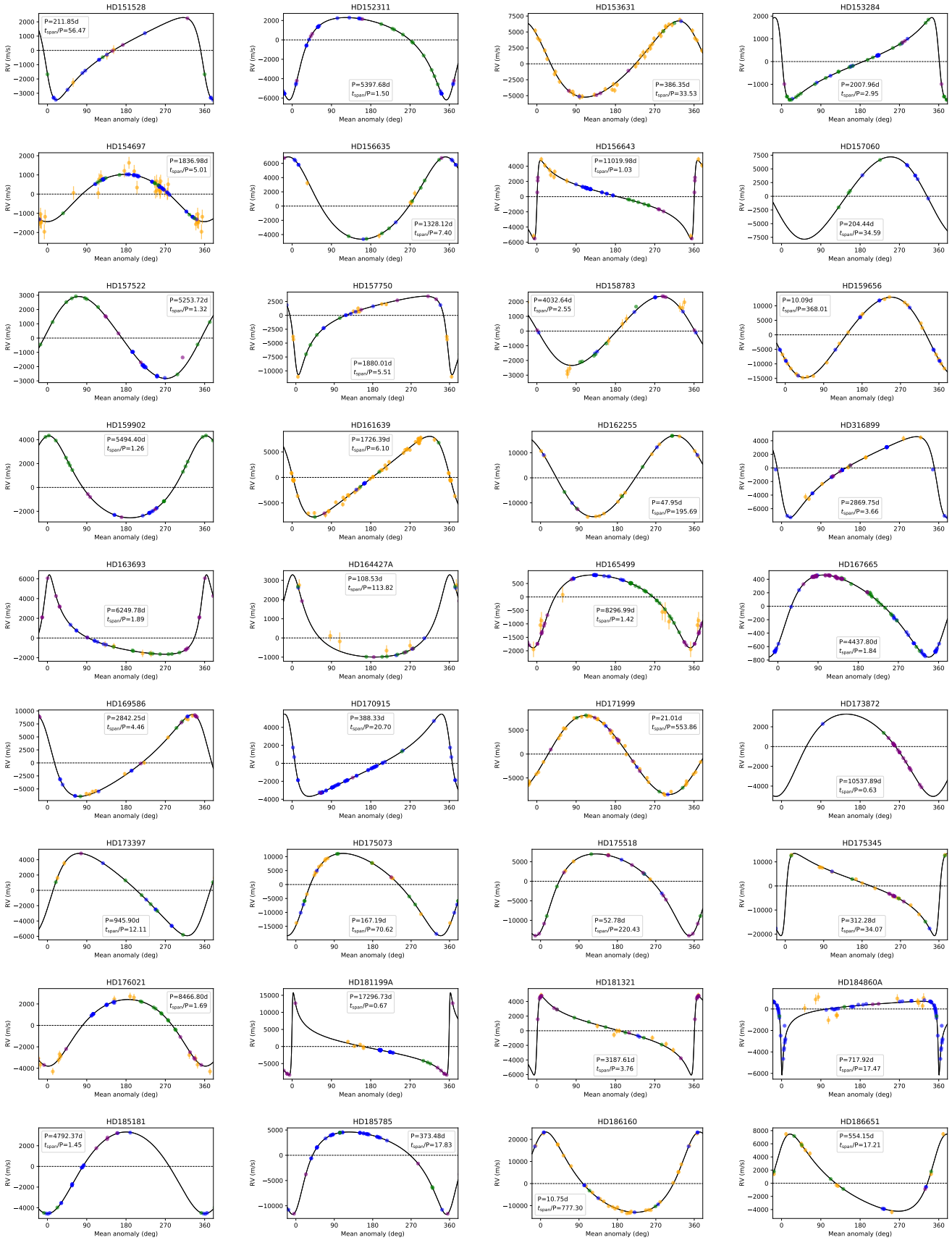

Fig. A.1: Continued

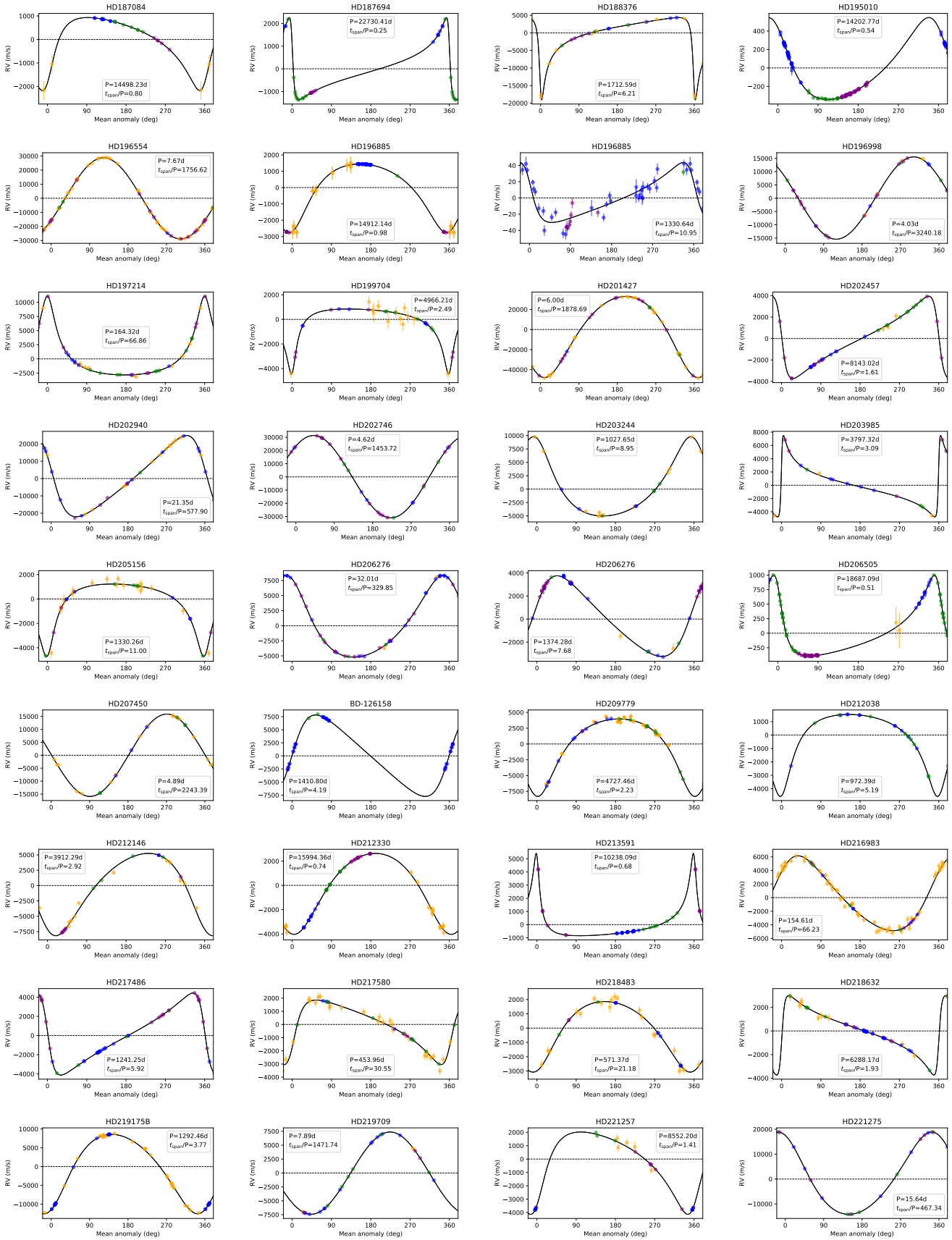

Fig. A.1: Continued

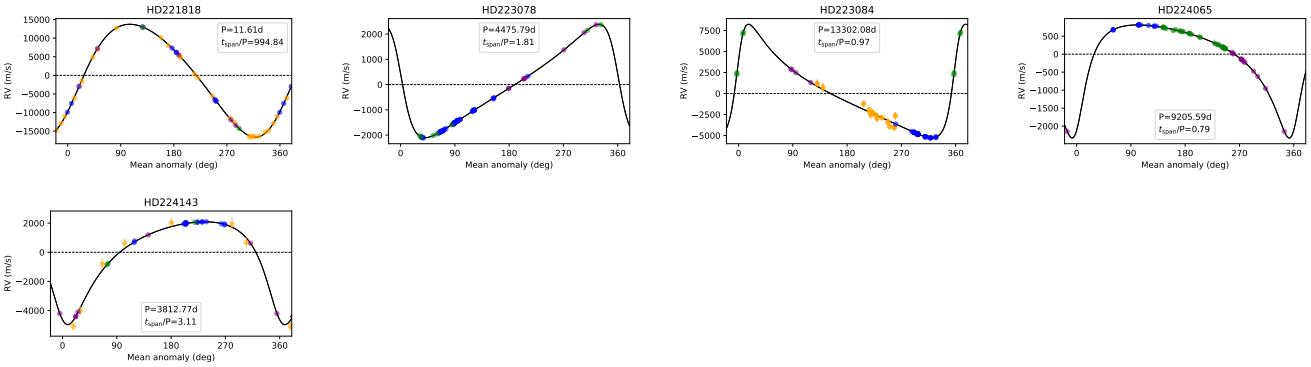

Fig. A.1: Continued

Appendix B: Detection limit maps

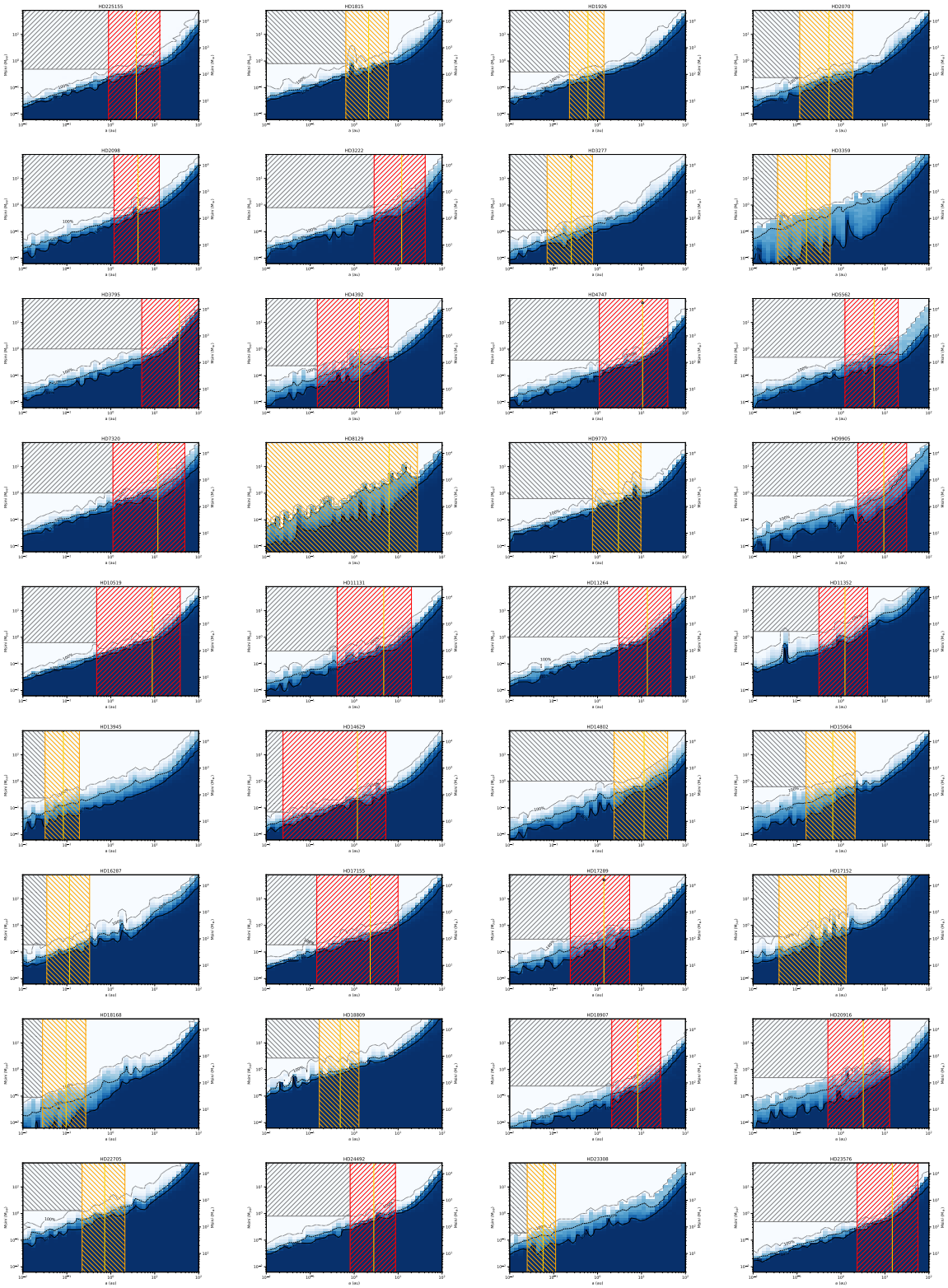

Fig. B.1: Completeness maps of each star in the binary sample, focused on the substellar ($2\,M_{\oplus} < M \sin i < 80\,M_{\rm Jup}$) companion regime. Detection frequency contour levels of 10, 50, and 100% are respectively shown as solid, dashed, and dotted curves, while the companions detected around each star are shown as white circles. In each plot, the hatched red and orange boxes represent the dynamically unstable semimajor axis range for additional substellar companions computed (respectively) using the true mass and minimum mass values of the detected companions in the sample, as described in Sect. 6.1. A vertical yellow line represents the detected companion semimajor axis. Hatched grey boxes show the region of parameter space for which we can exclude the presence of additional circumprimary companions based on the CORAVEL and CORALIE data analysed.

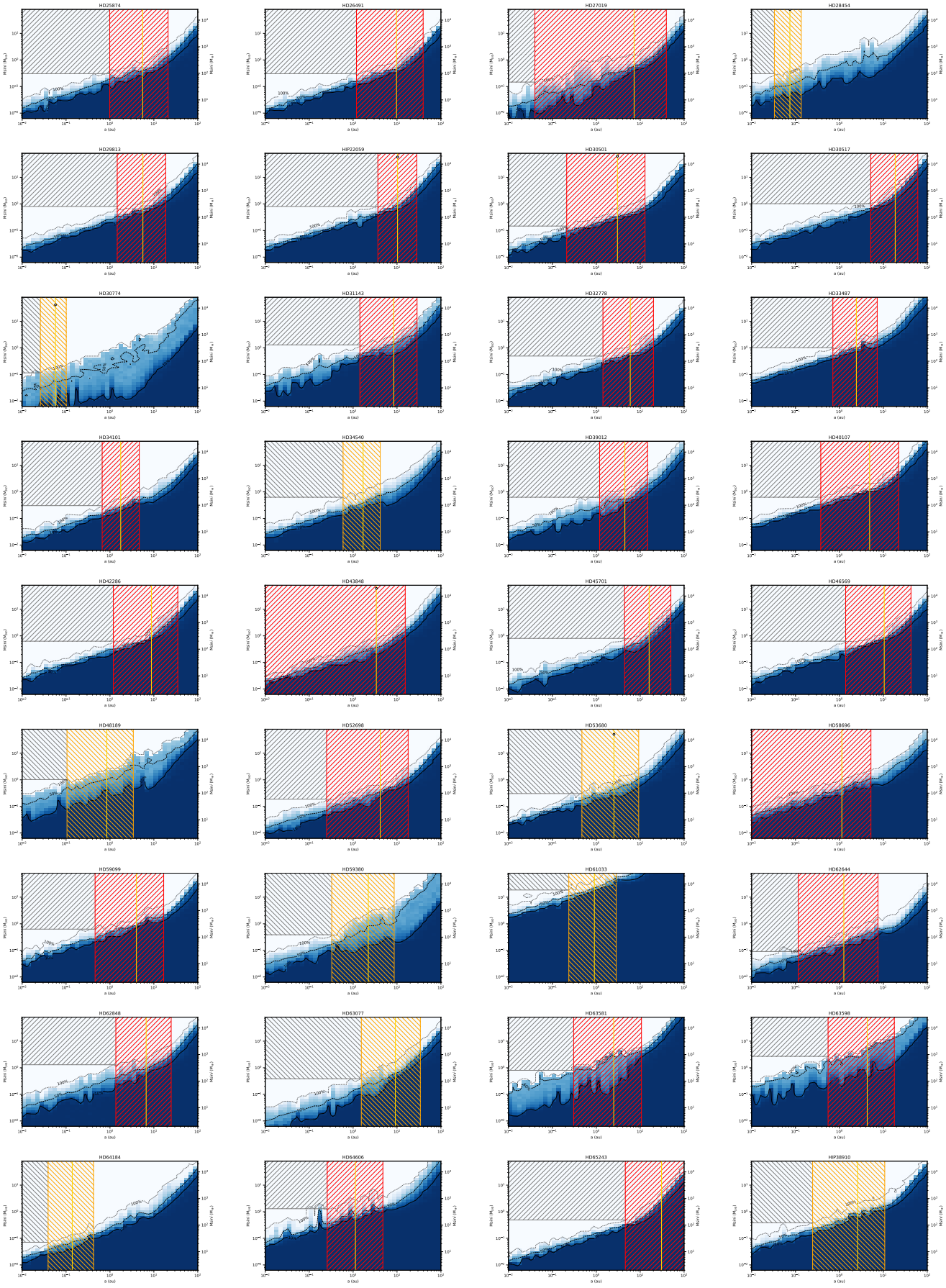

Fig. B.1: Continued

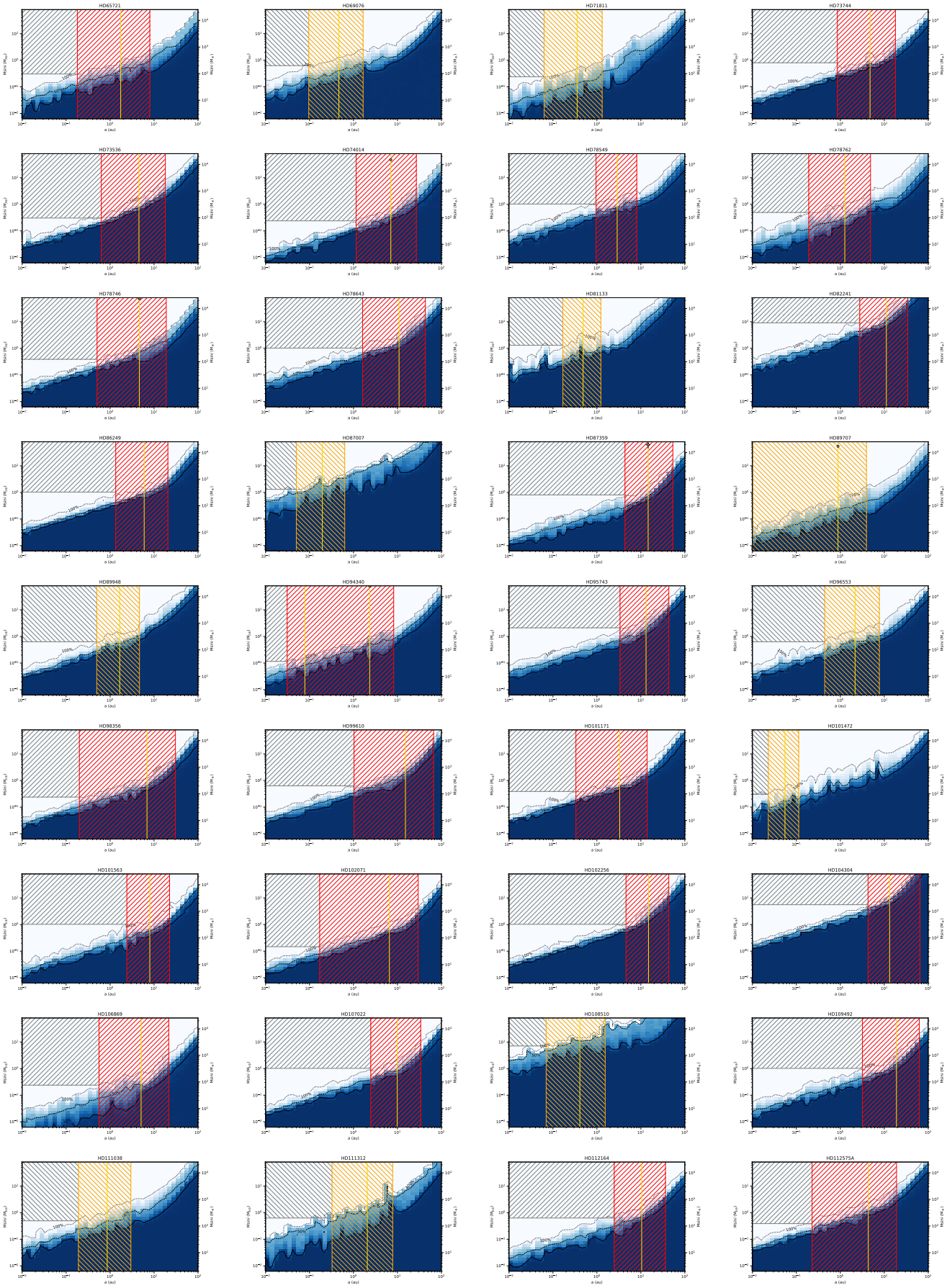

Fig. B.1: Continued

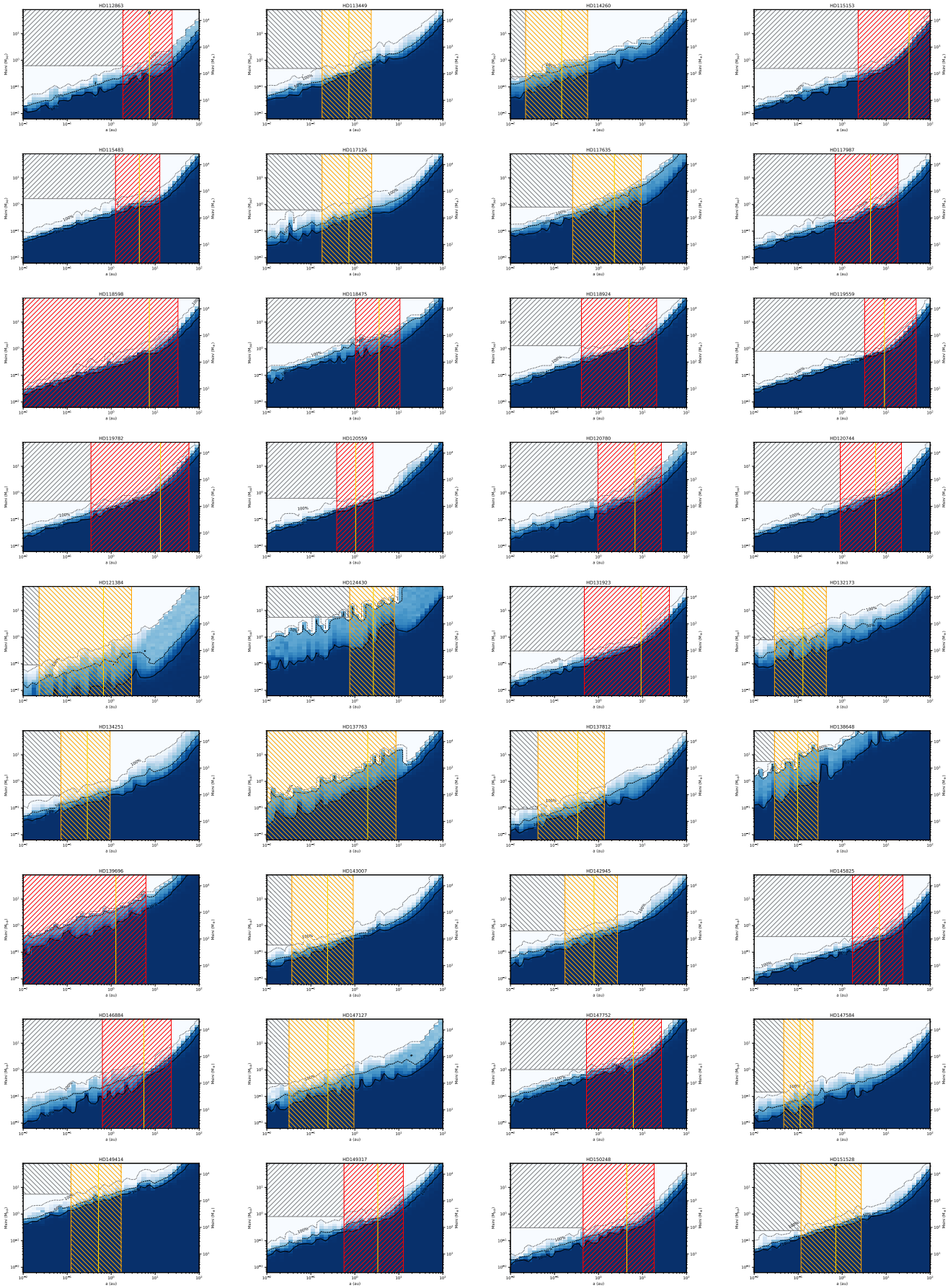

Fig. B.1: Continued

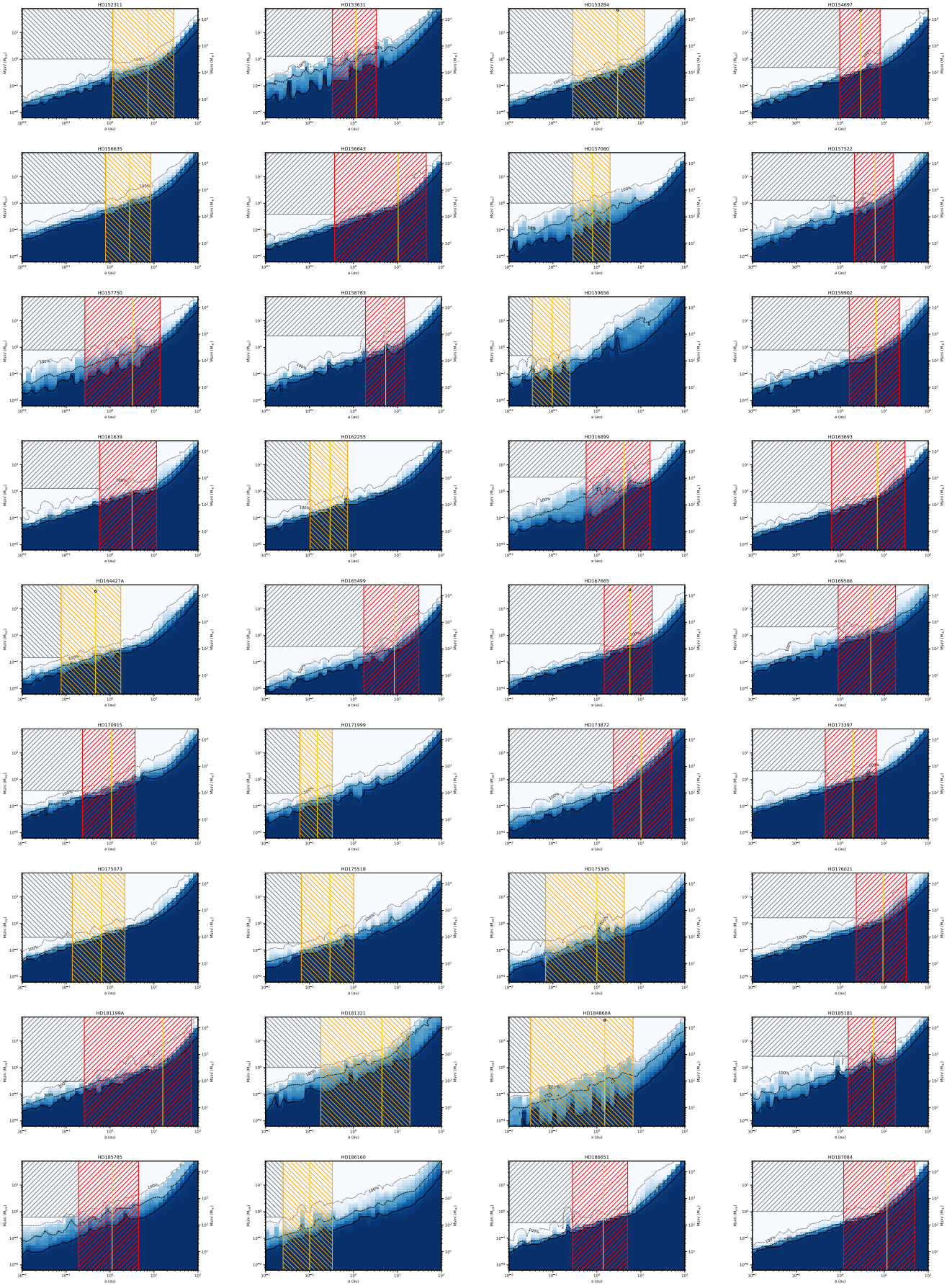

Fig. B.1: Continued

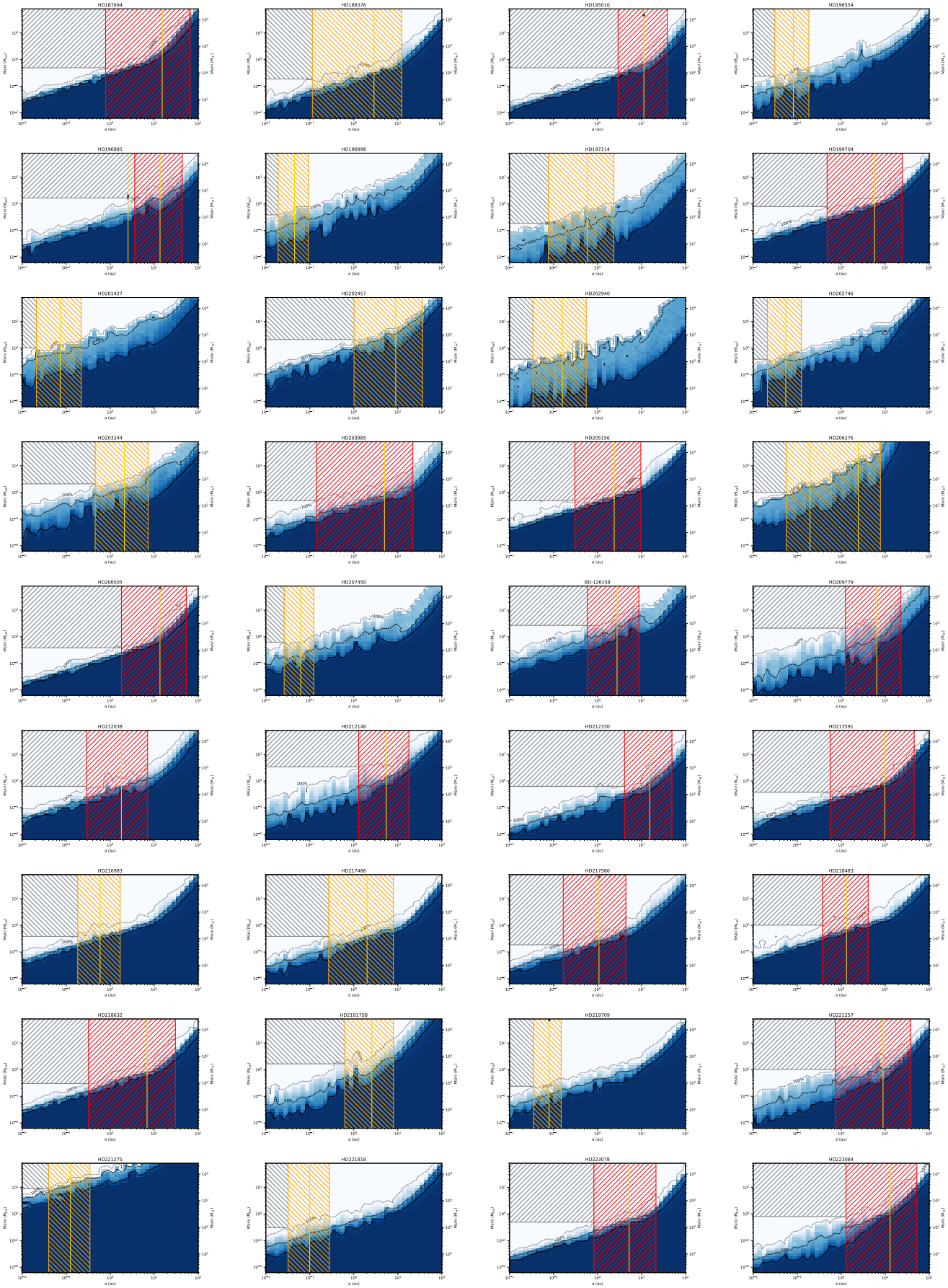

Fig. B.1: Continued

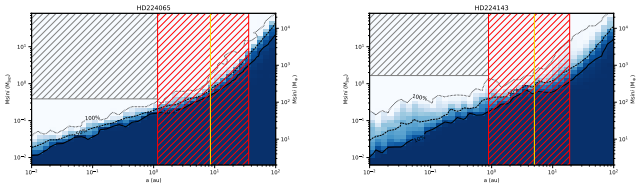

Fig. B.1: Continued